The Dissertation Committee for Cem Okan Kılıç Certifies that this is the approved version of the following dissertation:

Characterization and Quantification of Middle Miocene Reservoirs of Starfak and Tiger Shoal Fields, Offshore Louisiana, Using Genetic Sequence Stratigraphy and Neural-Networks

Committee:

William L. Fisher, Supervisor

Lesli J. Wood

Scott W. Tinker

Sergey Fomel

William E. Galloway

Characterization and Quantification of Middle Miocene Reservoirs of Starfak and Tiger Shoal Fields, Offshore Louisiana, Using Genetic Sequence Stratigraphy and Neural-Networks

by

Cem Okan Kılıç, B.Sc., M.Sc.

Dissertation

Presented to the Faculty of the Graduate School of
The University of Texas at Austin
in Partial Fulfillment
of the Requirements
for the Degree of

Doctor of Philosophy

The University of Texas at Austin
December, 2004

Dedication

This dissertation is dedicated to my wife, Sezin, and daughter, Simay, and to my beloved parents for their support and love, and to my supervisor, Dr. Fisher, for his being a father figure in my life, and for his patience with me.

Acknowledgements

I would like to express my deepest appreciation to and admiration of my supervisor, William L. Fisher, for his support of my education and for believing in me, trusting, that I would to bring this study to a conclusion. He is truly the most patient and wise educator in my life. He raised the bar of high standards that I put in front of myself to achieve to be a better person and to excel in every aspect of life.

Special thanks to Dr. Lesli J. Wood, who has encouraged me to investigate deeper into reservoir geology and who edited this dissertation many times; Dr. Scott W. Tinker and Dr. Sergey Fomel, who kept me in the real world of exploration with their scientific reasoning and practical investigative comments; and Dr. William E. Galloway, who inspired me to implement genetic sequence stratigraphy to study higher orders of geology.

This study would not have been realized without generous support from the Bureau of Economic Geology and Jackson School of Geosciences. Twelve semesters of research assistantships and fellowships allowed me to achieve my master's and doctorate dream, and provided me industry-standard geoscience training with many projects around the world. I would also like to express appreciation to my colleagues in the Offshore SGR team: Lesli J. Wood, Tucker F. Hentz, Hongliu Zeng, Michael V. DeAngelo, Adrian Badescu, and Claudia Rassi, for their help in creating a very well studied and documented project. I relied on the team’s sequence stratigraphic framework and frequency enhanced seismic data. I used the fourth-order flooding-surface picks, interpreted on well logs, and interpreted them on the enhanced seismic data, which allowed me to develop fourth-order genetic sequence of the area.

The research project was generously funded by the U.S. Department of Energy and supported with many types of software by Landmark Graphics Corporation through their University Grants Program. The entire dataset used in this project, consisting of well logs, production data, 3-D seismic data, and sidewall core analyses, was donated by Texaco E&P, New Orleans, Louisiana. I would like to thank the IT (BEG) group for a smooth operating computing platform, and Amanda Masterson for editing this dissertation.

Finally, I would like to thank my two best friends in the U.S., Robert E. Barba and Eric VonLunen, for their encouragements, and my beloved wife Sezin and precious daughter Simay for their love, understanding, support and patience. I will be in their debt forever.

Characterization and Quantification of Middle Miocene Reservoirs of Starfak and Tiger Shoal Fields, Offshore Louisiana, Using Genetic Sequence Stratigraphy and Neural-Networks

Publication No._____________

Cem Okan Kılıç, Ph.D.

The University of Texas at Austin, 2004

Supervisor: William L. Fisher

Gulf of Mexico Outer Continental Shelf (GOM-OCS) is one of the most prolific petroleum systems in the world, but because of stratigraphic and structural complexity, Miocene reservoirs on the shelf are not efficiently drained. A new approach to partitioning and imaging of individual reservoirs is developed, and the effective porosity and volume of clay of the reservoirs were estimated in fourth-order scale sequences by neural-network analysis techniques.

In the Middle Miocene, there are 24 fourth-order (~0.19 my) genetic sequences. These genetic sequences are defined between fourth-order maximum flooding surfaces, which are interpreted on a seismic data volume boosted to improve resolution. Spectral decomposition and balancing of seismic data allows interpretation of these fourth-order maximum-flooding surfaces, and integration of paleontological data confirms the ages and the stratigraphic order during interpretation.

Genetic sequences can be characterized in fourth-order scale by seismic facies classification and interpretation of proportionally sliced genetic sequences. While proportional amplitude slices result in a series of maps of deposition, the trace similarity yields a map of depositional elements of the genetic sequence. Interpretations of these two kinds of maps allow better understanding of reservoir architectures and complexity. A genetic sequence can be quantified in a fourth-order scale by neural-network analysis. Selected seismic attributes derived from the genetic sequences can be linked to, and used to quantify, the petrophysical character of reservoirs.

There are two orders of faults and two different kinds of opportunities in the Middle Miocene; broadly arcuate E-W trending large faults, which create large rollover structures, and N-S trending smaller faults, which create smaller structural traps. Large faults, rooted in the deep halokinetic activity across the region, form a significant topography across which thick, Early Miocene age lowstand deltas are deposited and are later deformed into large rollover structures. Smaller faults cut each other in narrow angles, and usually are cut by a large fault at a high angle. Integration of seismic, log, and production data within a fourth-order scale sequence allows identification of untapped zones, which are readily accessible for production, and bypassed small traps, developed especially among small faults, and between small and large faults.

Table of Contents

List of Tables

List of Figures

Chapter 1: Hypothesis and Objectives

HYPOTHESIS

Thick Gulf of Mexico Miocene and Pliocene sections with structural overprint offer ample stratigraphic and structural traps opportunities. However, the long production history on the shelf and decreasing reservoir size have increased the need for finer stratigraphic control and better quantification models of the reservoir.

There have been numerous exploration strategies and different reservoir imaging techniques used in the Gulf of Mexico shelf to increase hydrocarbon production. Although these techniques were able to image the reservoirs, they usually lacked, ignored, or approximated the stratigraphic correlative units, which are necessary for modeling geological information and documenting depositional history.

Incorporating fourth-order genetic sequences (Galloway, 1989) into seismic stratigraphic analysis, along with paleontological and petrophysical analysis, in a methodical way should yield finer stratigraphic control and allow for better quantification of reservoir porosity and volume of clay from a seismic data.

OBJECTIVES

1) This study develops a new methodology to characterize and quantify Middle Miocene reservoir architectures in the northern Gulf of Mexico.

The study involves integrating the results of petrophysical study, detailed genetic sequence stratigraphy (Galloway, 1989), and seismic attribute analysis into a comprehensive reservoir model of the area. The key aspect, which will make this study unique, is the application of the neural network analysis technique (Russell et al., 1997) as an attribute analysis tool, to supplement the geology driven framework for the final integrated model.

The scope of the study is to visualize the macroscopic heterogeneity (**Figure 1-1**) at the fourth-order sequence system tract level (Tyler, 1988), or "fieldwide scale heterogeneity (Slatt and Galloway, 1992)." The large study area contains considerable stratigraphic heterogeneity and erratically distributed different types of measurements. Recent techniques and methodologies are somewhat heavily weighted toward reliance on a single dataset to provide the bulk of information for model building. This study introduces a more integrated approach of involving attribute analysis, seismic data interpretation, and petrophysical analysis. Seismic data are integrated with petrophysical analysis by neural-network applications, and the results are compared to classic seismic slicing techniques. Seismic facies analysis and attribute analysis are also used to verify the geological history. Although this is not the first attempt to translate attributes to reservoir properties, it is a unique effort to identify and quantify "geobodies" in fourth-order sequence tracts. As is necessary for all neural-network applications, accuracy checks and validations are done at every stage for better transformation and to produce a more realistic geologic model (Kilic, 1998).

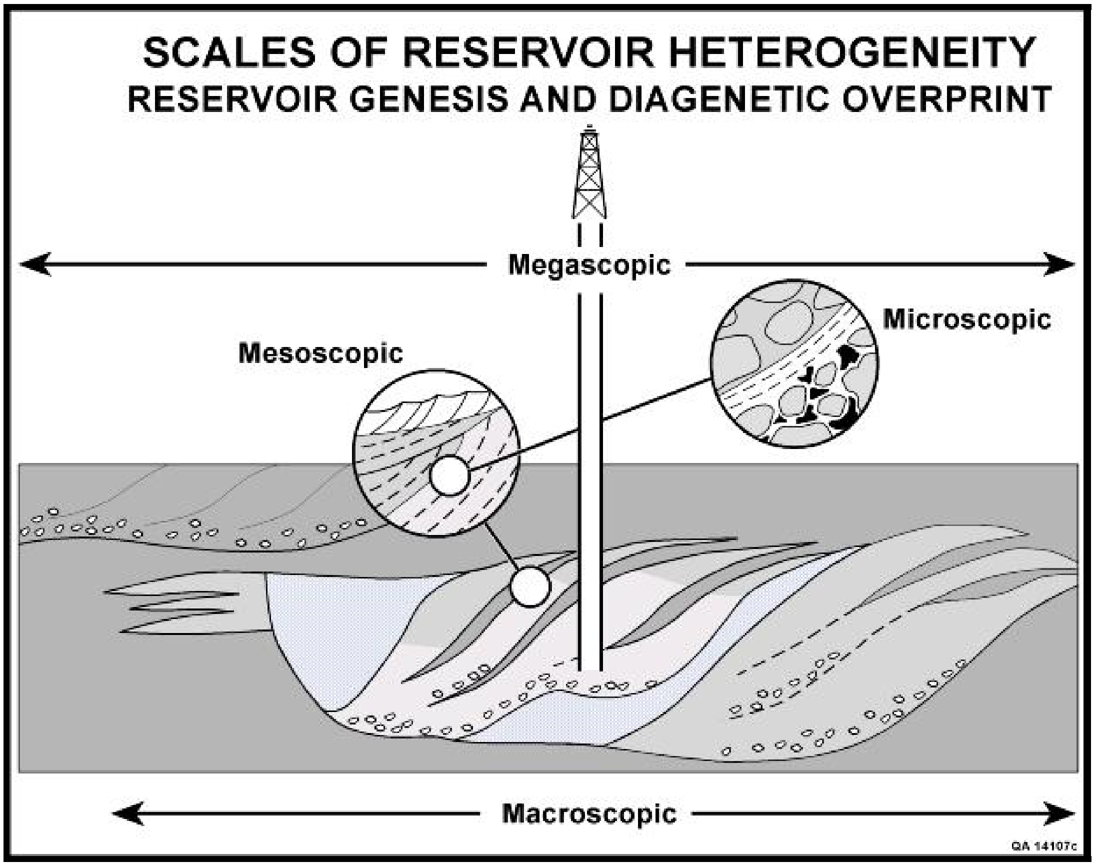

Figure 1-1 Reservoir characterization in macroscopic scale (Modified from Tyler, 1988).

2) A second objective is to determine the best way to correlate seismic attributes to reservoir properties using the petrophysical analysis. A lack of initial input data for generalizations and/or correlation is the main impediment to accuracy in transformation in seismic attribute studies (Hirsche, 1997). Within the area of study for this reservoir analysis there are 300 mi^2 of 3D seismic data, 156 wells with various well logs, and 99 sidewall core analyses from 41 wells.

Detailed explanations regarding data distribution, handling, and processing are given in the “Available database and method of investigation” section (Chapter 2). The interest area is narrowed to the portion of seismic data that has good well coverage. Seismic data allow for imaging approximately every other fourth-order maximum flooding surface, and there are limited amounts of porosity curves (well log measurements).

3) A third objective is to determine if the numerous forms of data being analyzed are genetically (geologically, physically) related and if they provide a meaningful correlation with different variables. Geologically inappropriate usage of geostatistics is an ongoing problem in reservoir modeling. Often the data used for generalization do not sample (represent) every part of the data-range and/or geoscientists try to find relationships between truly unrelated variables (Pennington, 1997). For correlation problems, data-driven (empirical) models work reasonably well in the small range of data, but it is usually unsatisfactory for generalizations. Acquiring a more detailed and accurate answer may not be feasible in all cases, and the error bar is usually quite high (Nur et al., 1998).

The use of neural networks has evolved in response to some of these problems. Unlike empirical methods, neural networks can be used to integrate different types of information and to analyze nonlinear relationships among them. They also allow predicting of approximate results beyond their input/training data. Such models are applicable to different aspects of reservoir characterization. Neural networks can be used to resolve a variety of problems, including interpreting seismic surfaces, defining seismic facies, predicting porosity permeability, water saturation and hydrocarbon presence, and quantifying cement types (Ronen et al., 1994; Schultz et al., 1994a and b; De Groot, 1995, 1999a, 1999b; Gastaldi et al., 1997; Love et al., 1997; Doraisamy et al., 2000; Walls et al., 2000; Hampson et al., 2001).

The accuracy and repeatability of the characterization techniques are always critical criteria to be addressed but are usually ignored. Neural networks are easy to implement and fast, and they allow more repetitions for accuracy and quality checking.

Problems such as poor data resolution, complex geology, lack of data density, or lack of critical data should never be ignored. Like every other technique, results have to make sense within the interpreted geologic framework. Even though transformation of seismic attributes to rock properties is based on measurements of rock itself, statistical analysis may sometimes fail, because analysis is in the end data driven (Ronen et al., 1994).

4) A fourth objective is to segregate the immensely thick Middle Miocene section into geological units in order to analyze and quantify the seismic data, and create an analog of neural networks application with clastic sections in the GOM Miocene.

Interpretation of genetic sequence stratigraphy with high-frequency seismic volume divides the Middle Miocene into smaller genetic units. Seismic attributes are created along the individual horizons and defined in a window relative to those horizons. Classification of attribute types is discussed in chapter

2, and detailed definitions of common attributes types are explained in Taner et al., (1979, 1994). Necessary attributes for characterization of selected geological settings (Chen and Sidney, 1997) are created within this framework of genetically related reservoir sequences.

Detailed geological interpretations of fourth-order sequence boundaries were picked within the limitations of seismic data. Classic seismic interpretation (horizon interpretation, slicing, and attribute analysis) technique and the neural-network's wavelets classification technique are used to identify reservoir bodies and their properties. Comparison of both techniques in terms of speed, reliability, and applicability to quantification is discussed in “Quantification” (Chapter 4).

Combining multiple attributes has proven to be a more effective way of defining complex architecture using automated processes (Taner et al., 1979), and Stratimagic^{TM} and Hampson-Russell^{TM} are commercially available software tools used to combine multiple seismic and log-derived attributes for classifying areas of common characteristics. These software packages have been used extensively within the industry to identify geological features, and for interpretation and integration (Russell et al., 1997; Addy, 1998; Stratimagic, 1999; Hampson et al., 2001; Linari et al., 2003).

5) A fifth objective is to overcome the limitations of seismic data by enhancing the resolution to interpret fourth-order flooding surfaces. To enhance the resolution of the seismic data, spectral balancing of the frequency was used. This process improves the seismic resolution by applying different gains to individual frequency bands (Landmark, 1996a). Another approach is to restrict the

analysis into the area with borehole coverage, along with knowing the stratigraphic position in great detail to maximize the accuracy of correlation.

THE PHILOSOPHY OF RESERVOIR MODELING

Creating a hydrocarbon reservoir model that incorporates all available physical information -- seismic, core, wireline log, and paleontological data -- in an accurate representation of the true nature of the system is the ultimate challenge for reservoir developers and resource managers. A reservoir model, in simplistic terms, has two major components: the architectural framework of the reservoir itself, and the rock-fluid properties of the reservoir. Each of these two parts has its own unique challenges, such as defining the architectural and depositional style of the reservoirs with data that is typically below the desired vertical and/or horizontal resolution, or trying to predict rock properties with spatially inhomogeneous measurements. A major challenge, which is usually underestimated, is to deal with so much data, and to incorporate all of the data into a model effectively.

Using existing computational technology, geophysical analysis currently produces more than 200 seismic attributes (Pennington, 2001). At the same time, petrophysical analysis of well logs brings another set of data with different depth resolutions and assumptions than seismically derived measurements. It is preferable that as much useful data as possible be arranged for an effective model. This often presents a nearly unfathomable challenge for the geoscientist in both collecting and conditioning the data, as well as for the modeler incorporating those data into a realistic model.

Various integrated approaches to reservoir characterization exist. The approach chosen usually depends on the available datasets, time, and budget. The most common solution is the geostatistical method. "Geostatistics" is defined by the *Glossary of Geology* (American Geological Institute) as "*statistics, applied to geology or the application of statistical methods in geology*". This definition has a very broad meaning, but it should also include the definition of "statistics driven by geology". Geostatistical approaches are preferred for integration of reservoir seismic and petrophysical attributes. Russell et al. (1997) grouped geostatistical methods used in reservoir attribute analysis into three categories as; "*the extension of* ***co-kriging*** *to include more than one secondary attribute to predict the primary parameter", "methods that use the* ***covariance matrix*** *to predict a parameter from a linearly weighted sum of the input attributes*" and "the *use of* ***artificial neural network*** *or nonlinear optimization techniques to combine attributes into an estimate of the desired parameter*".

The first method, *co-kriging*, has been used widely in geologic mapping as a technique to interpolate and extrapolate among given values. The only drawback is that for this method to be most effective requires dense and homogeneous seed-data coverage. In the second method, the *linearly weighted attribute matrix*, each independent (or semi-independent) attribute is multiplied by a factor to calculate wireline log parameters. Details of this method have been explained and applied by Russell et al. (1997). The third method, using *neural network analysis* to handle the weights and nonlinear relationship between the log data and seismic attributes, has recently become popular. The methodology is not particularly expensive and is easy to follow, and new data are easily added to the process (Ronen, 1994).

One question that should be at the forefront of any modeling attempt is one that asks "Is the model geologically meaningful?" While spurious sample correlations exist between many seismic amplitudes and rock and/or production parameters, geology is the discriminator for determining what is within the bounds of the natural system. Geological soundness must form the foundation in any reservoir study (Hart, 1999). **A reservoir model must place all the constituents of reservoir measurements, computations, predictions, and interpretations within a geologically realistic framework**. "Building an accurate stratigraphic framework is the most difficult and creative part of the 3-D modeling process" and "regardless of the method used for data distribution in 3-D model, it is important to determine if the model has geologic integrity" (Tinker, 1996).

A different approach to create a 3-D reservoir model is to transform seismic data into desired properties by finding a relationship between seismic attributes and petrophysical properties (e.g., effective porosity or volume of clay). The algorithm for quantification is not a mere interpolation and/or extrapolations, but the underlying principle is still the same and requires 1) an accurate sequence stratigraphic, rather than lithostratigraphic, interpretation (Tinker, 1996), 2) an improved data integration (petrophysical, paleontological, geological information and sequence stratigraphy), 3) instituting a reliable, verified transformation algorithm between attributes and petrophysical properties at the well-bore.

Pennington (1997) summarized the current state of reservoir characterization studies (in reference to quantification by seismic attributes) by saying "*…unfortunately, much of the application of seismic attributes falls into the category of metaphysics, in that relationships are assumed to be valid, rather than tested and either confirmed or rejected*."

On the other hand, Vinson et al. (1996) presented the effectiveness of attribute analysis and visualization techniques to map sequence boundaries for identifying and targeting reservoirs. In an inverted process from this, Raeuchle et al. (1997) demonstrated the methodology for integrating genetic stratigraphic analysis for improving attribute analysis. Even mapping average amplitude can yield insights into reserve growth opportunities in many architecturally complex environments. Lei (1999) showed that root-mean-square (RMS) amplitude corresponded to porosity, and interval velocity corresponded better to net pay in fluvial reservoirs. A similar study by DeAngelo and Wood (2001) used RMS amplitude to target undrilled prospects in a clastic fluvial/deltaic/shelf system in the study area. Likewise, Zeng and Kerans (2003) and Zeng et al. (2000) showed the use of properties of amplitude versus frequency to resolve reservoir architecture and lithology. Wood et al. (2000), in a study of fluvial deposits, showed a methodology for the integration of seismic attributes, coherency, and impedance, within a framework of sequence stratigraphic units derived from seismic facies and well log integration. Gastaldi et al. (1997) delineated delta mouth bars by integrating the well data with seismic amplitude. They recognized a high correlation between net sand values and seismic amplitudes, as well as correlation between hydrocarbon pore thickness and seismic amplitude. However, they indicated the need for more geological study for reservoir characterization. A reservoir study by Addy (1998) showed the utility of using seismic facies to identify fluvial channel fills, braided deposits, point bars, crevasse splays, fan deltas and deltas from the Upper Wilcox. Recently, Hampson et al. (2001) used neural-network analysis to perform full conversion of seismic data to log properties. They also discussed the advantages and disadvantages of the multilayer feed-forward network and the probabilistic neural network.

Previous research also suggests that the geologic setting is a key control on the amount of unrecovered mobile oil (UMO) in a reservoir system. The remaining movable oil, after primary and secondary recovery, is tied to complexity of the depositional system's architecture, and advanced recovery techniques are needed to further recovery rates (Tyler, 1988, 1991; **Figure 1-2**).

In fluvial systems and fluvial dominated deltas, as in this case, UMO could be around 50%. In the lower part of the Middle Miocene we start to see slope fan deposits and related turbiditic deposits. In this case, UMO is as high as 75%. There is a 50% probability that more than 1 Tcf of original gas in place is present in 54 opportunities that were identified in the area (Hentz et al., 2002). This is a significant potential resource, which needs to be addressed by this kind of detailed stratigraphic study, in order to reduce the uncertainty and increase the probability of finding gas in place.

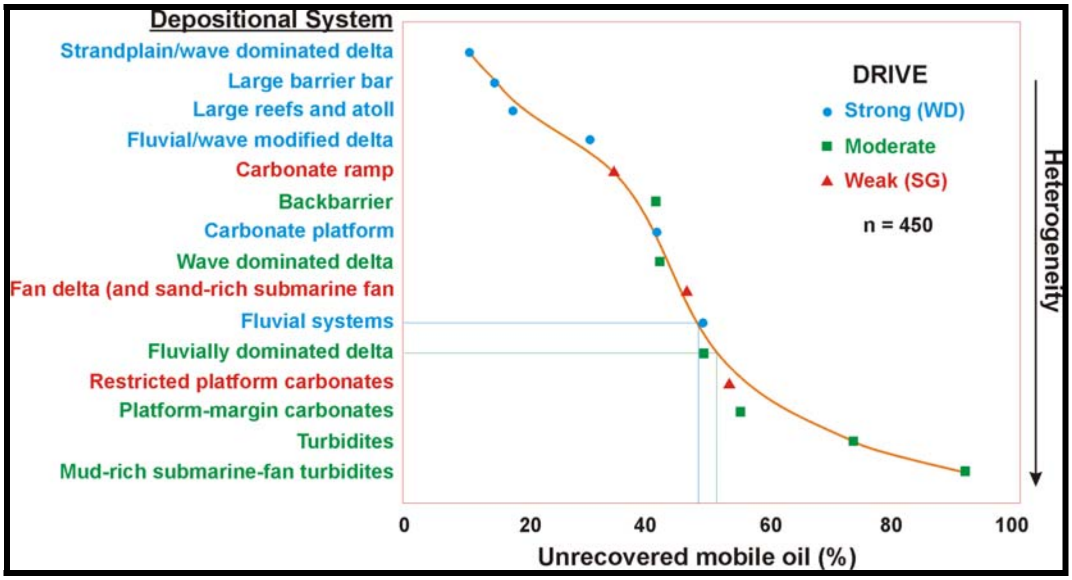

Figure 1-2 Unrecovered Mobile Oil (UMO) volumetrically increases as reservoir architecture gets more complex. (Modified from Tyler, 1988).

STUDY AREA

The focus area of this study comprises 300 mi^2 (Vermilion Blocks 30, 31, and 50 and South Marsh Island 210, 217, 218, and 219) and is located ~10 mi south of Vermilion Bay, Louisiana (**Figure 1-3**). Several major hydrocarbon fields dot the study area, but two primary fields, Tiger Shoal and Starfak, provide the bulk of log and core data. The structurally updip Tiger Shoal field has been producing hydrocarbons (gas and oil) from Middle and Upper Miocene reservoirs since the late 1950's, and Starfak field has been producing primarily gas, mostly from upper Lower and Middle Miocene reservoirs since the mid-1970's.

The structurally higher Tiger Shoal field has 103 wells, most of which are shallow and produce from the Upper and Middle Miocene. Starfak field has 53 wells, which are deep and produce from the Lower and Middle Miocene. Detailed sequence-stratigraphic analysis using these 156 wireline logs and paleontologic data from 15 wells indicates that there are 60 fourth-order and 10 third-order sequences present in the research area. Five productive depositional facies have been identified in both fields. Starfak field is producing mainly from lowstand-wedge, incised-valley, transgressive-bayhead-delta and late-highstand deltaic/strandplain sands. Tiger Shoal field produces from highstand deltaic and lowstand incised valley sands (Hentz et al., 1999, 2000, 2001; Hentz and Zeng, 2003).

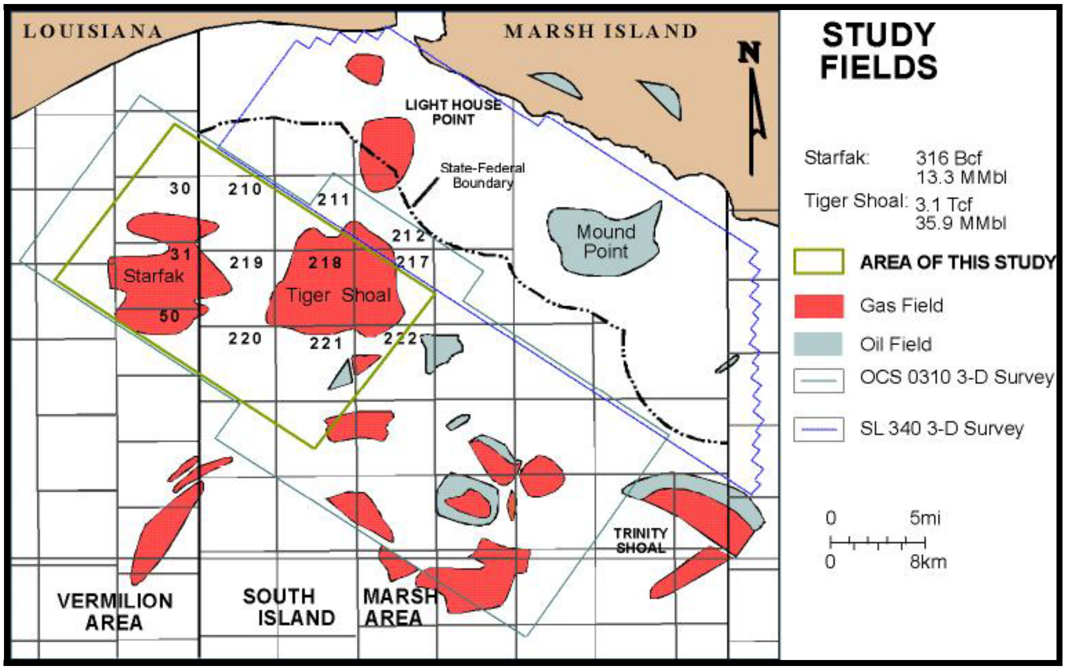

Figure 1-3 Map of study area, offshore Louisiana. Available 3D seismic surveys and interest area. Starfak, Tiger Shoal, and surrounding fields (modified from Hentz and Zeng, 2003).

Both fields are considered to be mature in their production life, but additional resource opportunities identified by recent workers may provide the “creaming curve” for the productive life of the reservoirs (DeAngelo and Wood, 2001; Hentz and Zeng, 2003). These opportunities exist in the stratigraphically deeper, Lower Miocene-age reservoirs, in numerous stratigraphic traps involving Lower and Middle Miocene reservoirs, and in additional stratigraphic and structural traps located in saddle areas between structural highs. Several of these traps have been successfully tested (DeAngelo et al., 2000 and 2001), and two wells discovered deep-gas (18,700 ft and 22,000 ft) resources in JB Mountain and Mound Point fields (MMS, 2003a).

GOM PRODUCTION HISTORY

The Gulf of Mexico Outer Continental Shelf (GOM-OCS) is one of the most prolific petroleum systems in the world. Currently, it provides 23% of the domestic natural gas production in the United States (Crawford et al., 2000), and is contains approximately 16% of the proven natural gas reserves nationwide (Lore et al., 1999). It has produced 10.9 billion barrels (MMb) of oil and 132 trillion cubic feet (Tcf) of gas. As of December 1998, the GOM shelf had produced 3.4 MMb of oil and 30 Tcf of remaining proved gas reserves, which are 31% and 23% of total shelf production, respectively (Crawford et al., 2000, **Figures 1-4 and 1-5**).

Natural gas consumption in the U.S. is expected to rise from 22 Tcf in 1999 to more than 30 Tcf in 2015, a 1.5 to 2.5% annual increase (MMS, 2001). According to this projection, yearly production in the GOM must rise to about 7 Tcf from the current 5.0 Tcf. But shallow-water gas production has declined from 4.76 Tcf/y in 1997 to 3.36 Tcf/y in 2002, or approximately 29% in 5 years (MMS, 2003b; **Figure 1-6**).

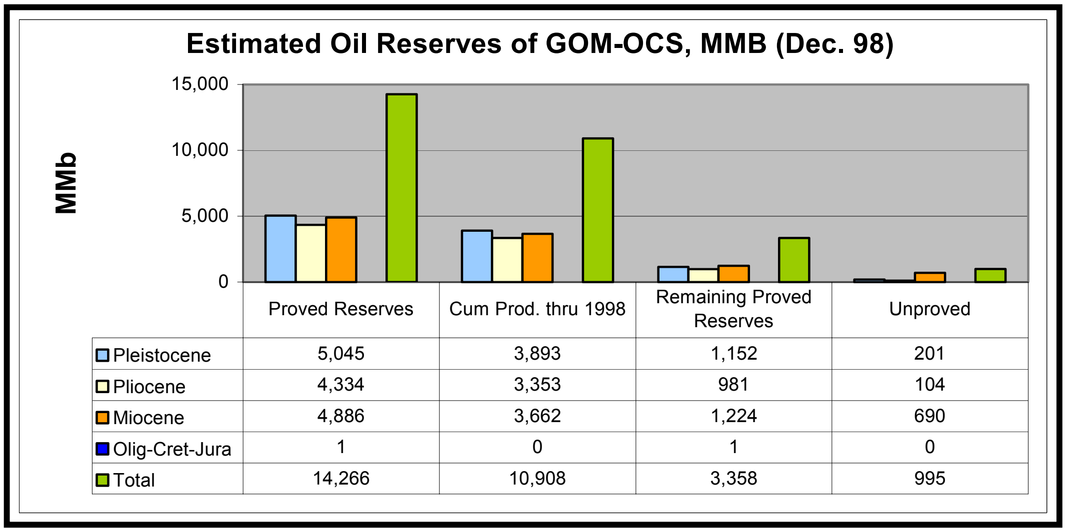

	Proved Reserves	Cum Prod. thru 1998	Remaining Proved Reserves	Unproved
🟦 Pleistocene	5,045	3,893	1,152	201
🟨 Pliocene	4,334	3,353	981	104
🟧 Miocene	4,886	3,662	1,224	690
🟦 Olig-Cret-Jura	1	0	1	0
🟩 Total	14,266	10,908	3,358	995

Figure 1-4 Estimated oil reserves of GOM-OCS. Miocene reserves and production comes second after Pleistocene, and has largest remaining proved oil reserves (modified from Crawford et al., 2000).

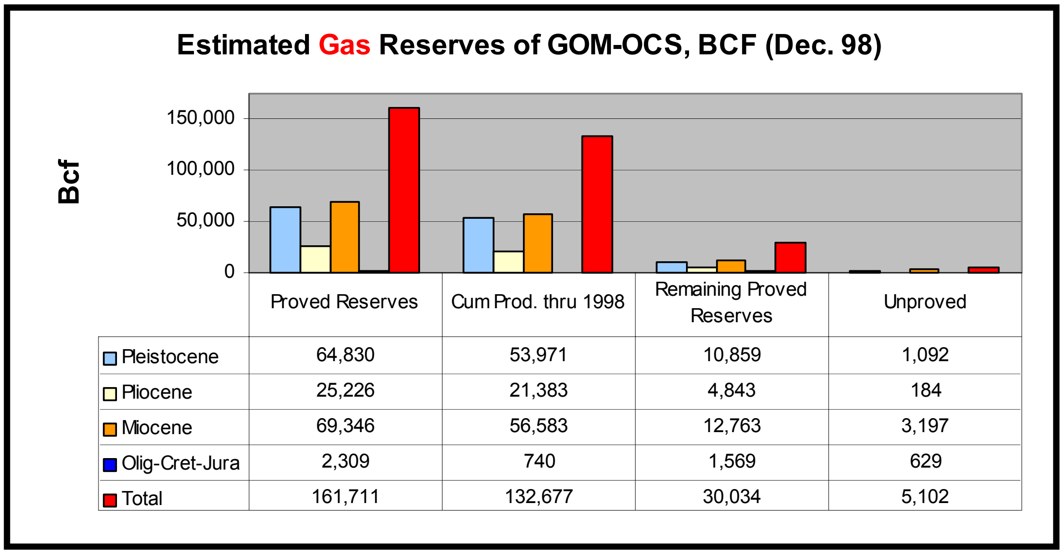

	Proved Reserves	Cum Prod. thru 1998	Remaining Proved Reserves	Unproved
🟦 Pleistocene	64,830	53,971	10,859	1,092
🟨 Pliocene	25,226	21,383	4,843	184
🟧 Miocene	69,346	56,583	12,763	3,197
🟦 Olig-Cret-Jura	2,309	740	1,569	629
🟥 Total	161,711	132,677	30,034	5,102

Figure 1-5 Estimated gas reserves of GOM-OCS. Miocene has largest reserves, production, and remaining proved gas reserves (modified from Crawford et al., 2000).

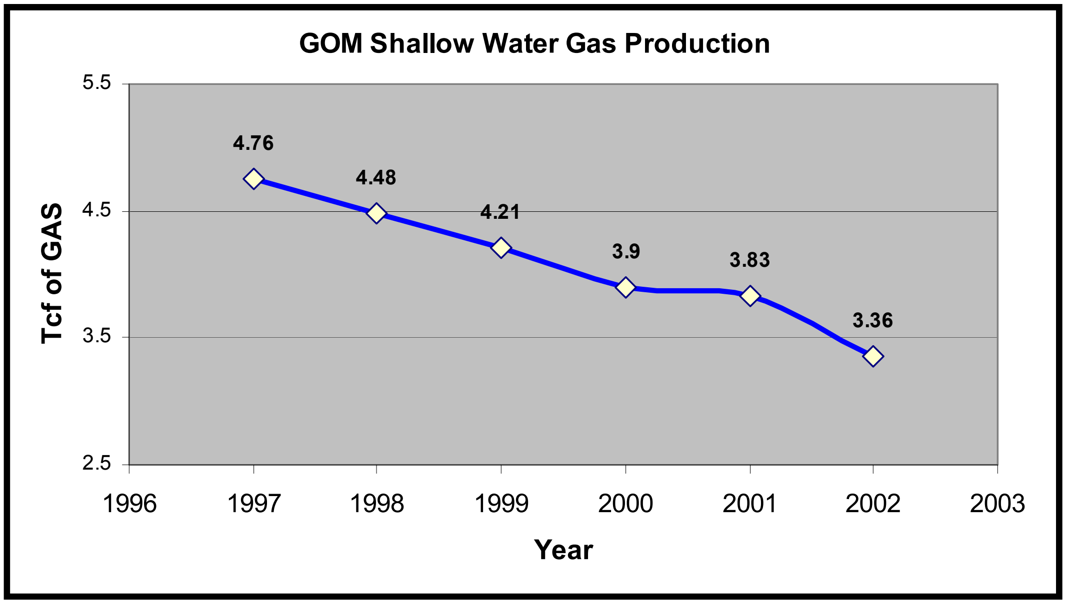

Although there is a strong impetus to find new fields, 7 years (1991-98) of exploration and production on the GOM OCS has added 4.8 billion barrels of oil equivalent (BBOE[1]) to old fields through reserve growth, which represents about 2.6 times more than newly discovered reserves during the same era (**Figure 1-7**). Reserve addition to old fields will continue to play a significant role in the future of GOM shelf development. In every size of reserve addition, more reserves were added to old fields than new reserves found between 1983 and 1998, especially during the second half (**Figures 1-8 and 1-9**).

---

[1] 1 BOE = 5,620 cf (standard cubic feet) of gas

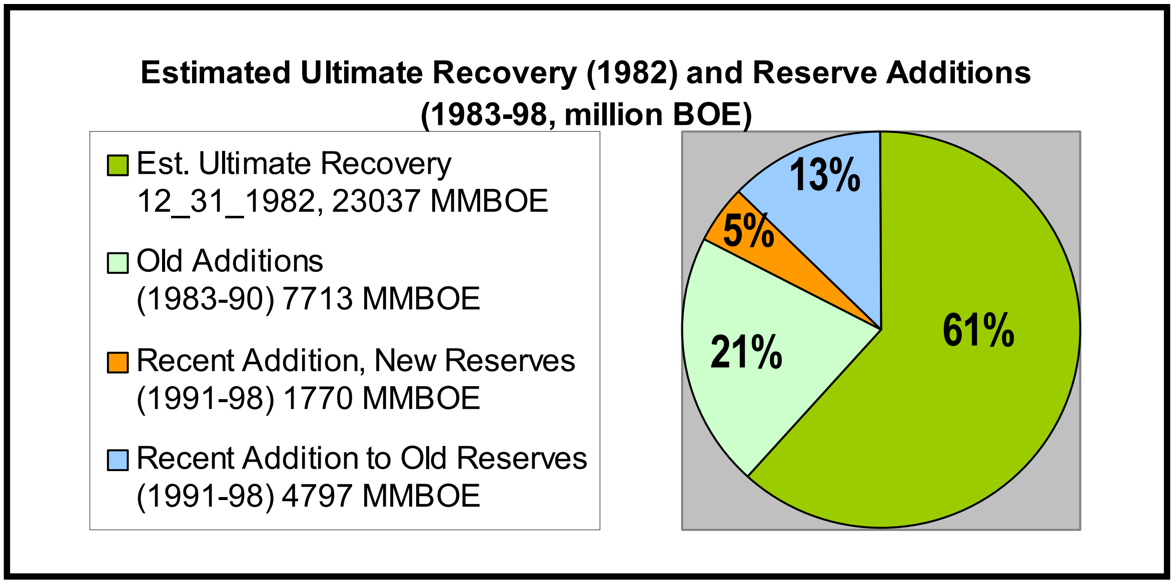

Figure 1-7 Estimated ultimate recovery (1982) and reserve additions after that (1983-98) in million barrels of oil equivalent. The largest addition of reserve is to old reserves (modified from Nehring, 2000).

Another promising solution to the shelf's decreasing proved gas reserve is to look for zones deeper than 15,000 ft subsea. There are only 1842 wells (out of 35,000) drilled deeper than 15,000 ft on the shelf. Since 1994, deep shelf reservoirs have produced 2.88 Tcf of gas. Although the number of deep wells drilled on the GOM OCS declined from 86 in 2000, to 75 in 2001, to 64 in 2002, production has increased from 284 billion cubic feet (Bcf) in 2000 to 421 Bcf in 2003 (MMS, 2003a; **Figure 1-10**). In 2003, after successful completions of large discoveries by McMoRan (JB Mountain and Mounds Point) in this study area and better production results from Anadarko (Hickory), El Paso (So. Timbalier 204) and Shell (Alex), the estimated deep shelf gas resource has increased by 175%, from 20 Tcf to 55 Tcf in 1 year (MMS, 2003a and b).

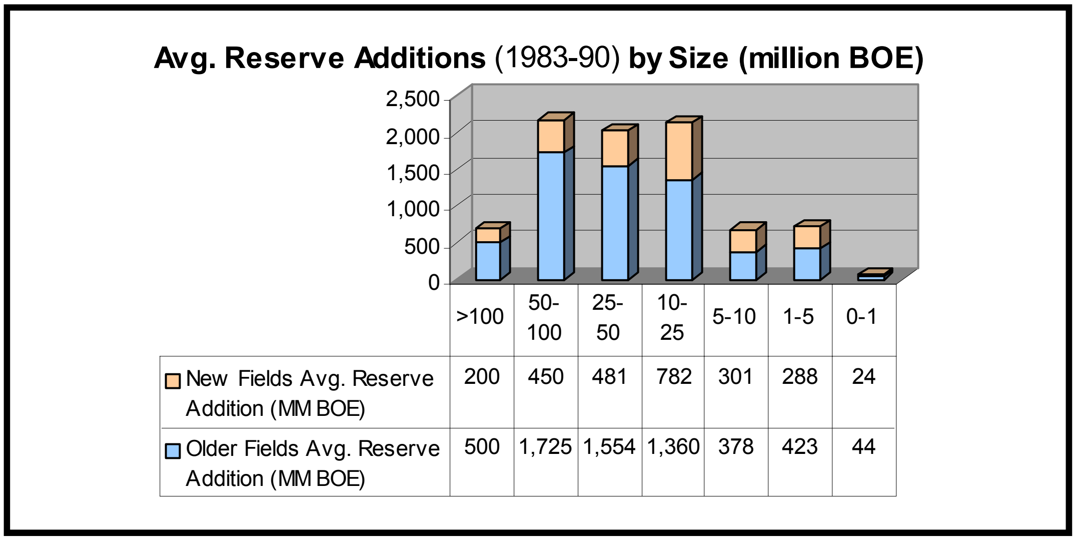

	>100	50-100	25-50	10-25	5-10	1-5	0-1
🟧 New Fields Avg. Reserve Addition (MM BOE)	200	450	481	782	301	288	24
🟦 Older Fields Avg. Reserve Addition (MM BOE)	500	1,725	1,554	1,360	378	423	44

Figure 1-8 Average reserve additions to old and new fields (1983-90). On average, more reserves were added to old fields than new fields. Compiled from Nehring, 2000.

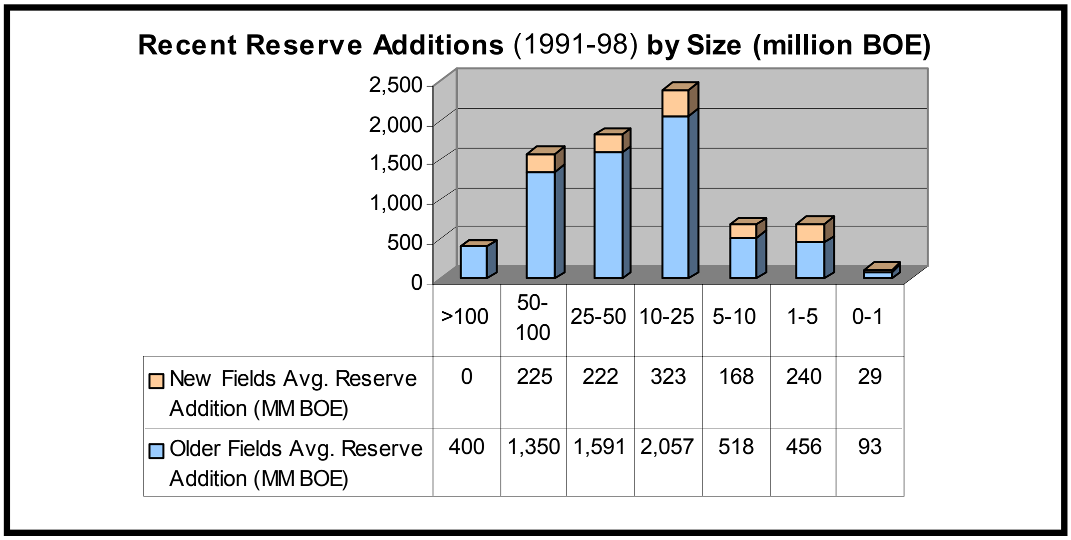

	>100	50-100	25-50	10-25	5-10	1-5	0-1
🟧 New Fields Avg. Reserve Addition (MM BOE)	0	225	222	323	168	240	29
🟦 Older Fields Avg. Reserve Addition (MM BOE)	400	1,350	1,591	2,057	518	456	93

Figure 1-9 Average reserve additions to old and new fields (1991-98). On average, size of additions to old fields has surpassed additions to new fields. Compiled from Nehring, 2000.

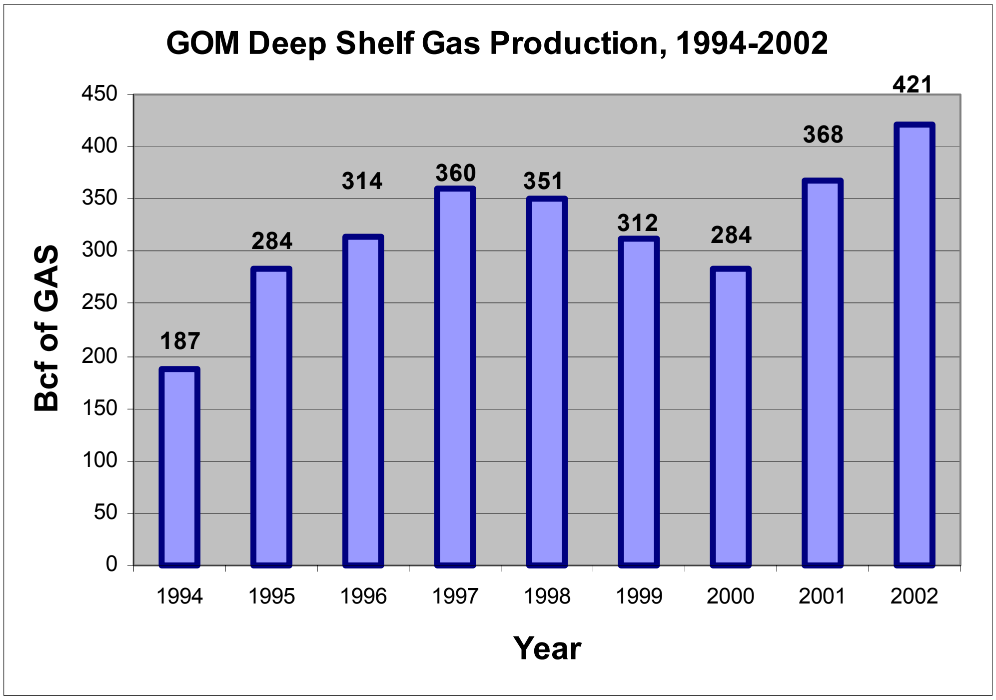

Figure 1-10 GOM deep shelf gas production (1994-2002). Overall production has increased, although drilling numbers decreased (MMS, 2003-release 3012).

Chapter 2. Available Data and Method of Investigation

DATA BASE

Texaco Exploration and Production Inc. provided 352 mi^2 of three-dimensional (3D) seismic data, wireline logs, production and paleontological data, core plugs, and laboratory analysis of porosity-permeability from 156 wells to The University of Texas at Austin for use in this research project. This research was part of a larger project, funded by the U.S. Department of Energy, whose aims were to develop new technologies and a better understanding of the geological framework of the Miocene section in the northern Gulf of Mexico (GOM) to increase gas reserves.

3D Seismic Data

Area

Approximately 352 mi^2 (23 x 14 mi) of merged 3D seismic data from two surveys (OCS 310, 250 mi^2, acquired by Halliburton Geophysical Services in 1990; and SL 340, 145.25 mi^2, acquired by Western Geophysical Corporation in 1994 and 1995) formed the primary seismic data set for this research (**Figure 2-1**). The seismic volumes were acquired in relatively shallow marine (0-40 ft) waters, and five separate hydrocarbon fields (Starfak, Tiger Shoal, North and South Lighthouse Point, Mound Point,) are included in the study area (Figure 2-1). The primary area of interest and the area in which the most detailed integration was done is in the OCS 310 seismic survey, between lines 1070 and 1500, traces 120 and 1200.

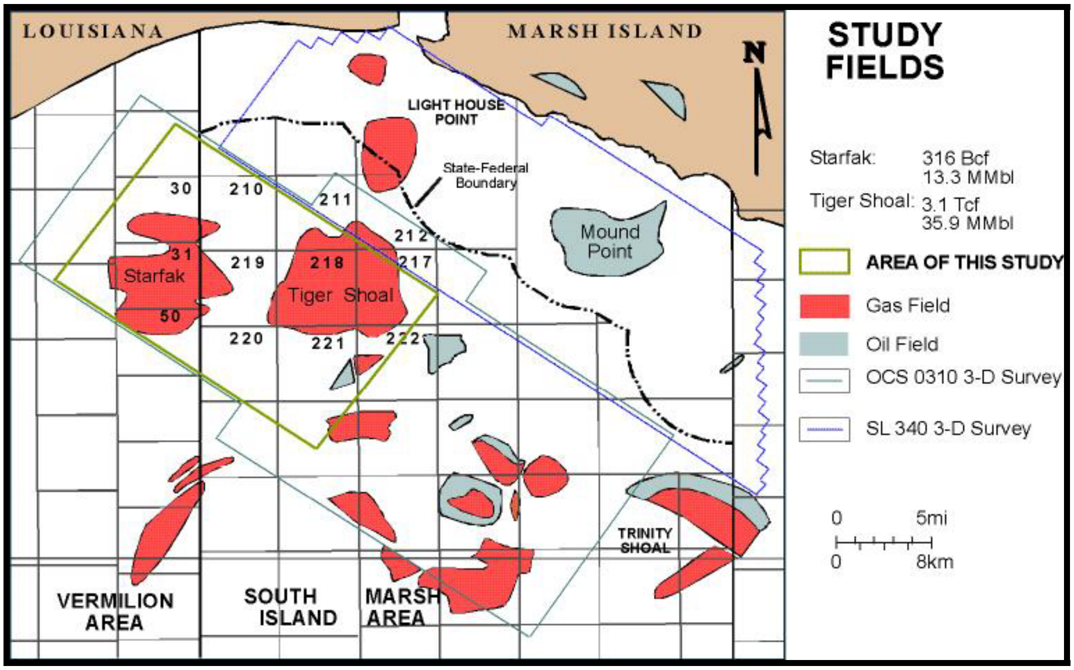

Figure 2-1. Map of study area, offshore Louisiana. Available 3D seismic surveys and interest area. Starfak, Tiger Shoal, and surrounding fields (modified from Hentz and Zeng, 2003).

Acquisition and Processing

The OCS-310 survey was processed in 1993 by Texaco Exploration and Production Technology Development in Houston using Prakla-Seismos, Texgraph Gridding (Texaco internal proprietary software), and Green Mountain Geophysics Refraction Static^{TM} software. The SL-340 survey was processed in 1993 by Western Geophysical Corporation. The two volumes were merged into one data set and processed by Texaco with the proprietary implementation of "3D-Phase-Shift-Plus-Interpolation-Migration-Algorithm (PSPI)" (Gazdag and Sguazzero, 1984). Available acquisition parameters are summarized in **Table 2-1**. The data quality is excellent, with high signal-to-noise ratio, with no blatant quality problem, no apparent multiples and no other coherent noises in the dataset (Hentz et al., 1999). This is excellent data to perform the type of seismic interpretations and neural-network analysis proposed here.

Table 2-1. Acquisition parameters of seismic data.

Field and Recording		
Parameter	**OCS 310**	**SL 340**
Sample rate	2 ms	4 ms
Record length	8 s	8 s
Low-cut filter, slope	8 Hz, 18 dB/octave slope	8 Hz, 18 dB/octave
High-cut filter. slope	90 Hz	177.6 Hz, 70 dB/octave
Channels	120X2 systems / shot	120X2 systems / shot
Airgun depth	8 ft	8 ft, or dynamite for shallow
Hydrophones depth	5-25 ft OCS-310,	5-25 ft OCS-310,
Acquisition system type	Swath type bay cable	Swath type bay cable
Spread type	Split spread	Split spread
Receiver lines per swath	2	2
Channels per line	120	120
Receiver group interval	220 ft	220 ft
Shot point interval	440 ft	440 ft
Original bin size	X = 220, Y = 110 ft	X = 220, Y = 110 ft
Final bin size	X = 110, Y = 110 ft	X = 110, Y = 110 ft
Final format	16 bit	32 bit
Inline fold	30	30
Cross-line fold	1	1
Maximum fold	30	30

In the two fields, the dominant seismic frequency ranges from a high of 40 Hz in the shallow zone to a low of 20 Hz in the deep zone. Most of the gas zones are recognizable as bright spots in the seismic data, and the quality is good enough to resolve the major gas reservoirs (Zeng et al., 2001). The initial seismic volume has approximately a 30^o phase shift, and it is brought to 90^o degree for easier interpretation (DeAngelo et al., 2000). A spectrally balanced seismic volume, ZMIX, has been created by amplifying the high-frequency seismic wavelet responses for better horizon picking. This volume allows more detailed and accurate horizon interpretation, which eventually leads to better reservoir delineation and characterization.

Well Data

There are 103 wells in Tiger Shoal field and 53 wells in Starfak field. A distribution list of spontaneous potential (SP), sonic (DT), neutron porosity (NPHI), bulk density (RHOB), deep resistivity (ILD), shallow resistivity (SN), and gamma ray (GR) data is given in **Table 2-2**. Starfak field is younger and has more complete and better quality log suites than does Tiger Shoal field.

Table 2-2. Distribution of curves in the Starfak and Tiger Shoal fields. See Table 2-3 for abbreviations.

Tiger Shoal	**SP**	**DT**	**NPHI**	**RHOB**	**ILD**	**SN**	**GR**
103	96	22	13	19	97	73	33
%	93%	21%	13%	18%	94%	71%	32%
Starfak	**SP**	**DT**	**NPHI**	**RHOB**	**ILD**	**SN**	**GR**
53	53	46	34	33	51	25	51
%	100%	87%	64%	62%	96%	47%	96%

Tiger Shoal field has been producing since 1958 from various stratigraphic depths (Hentz et al., 1999) and is divided by large normal faults that split the field roughly into two structural halves. On the eastern side, the footwall of the large normal fault, the structural closure is shallow and produces mostly oil. On the western side, the hanging wall, the structural closure is deeper than the footwall side and produces gas only.

Most of the 103 wells have a shallow total depth (about 9000 ft) and are relatively undeviated. Several wells at the edge of the field are the exception to this rule and show deviations of up to 35 degrees. Almost every well has SP and ILD, ILM/SN/SFL curves.

Table 2-3. Curve names and explanations.

GRCB	Gamma Ray in Cement Bond Log
GRPDK	Gamma Ray in PDK Log
GRTH	Gamma Ray in Thermal Neutron Log
GRPFC	Gamma Ray in Perforation
GR-EQ	Gamma Ray in GR Equivalent Log (0-5)
RHOG	Gamma Density
Gammaden	Gamma Density
ILD	Deep Induction
ILM	Medium Induction
SN	Short Normal
SFL	Spherically Focused Log
SFLU	Spherically Focused Log Unaveraged
MNOR	Micro Resistivity Normal
MINV	Micro Resistivity Reverse
LLD	Deep Laterolog
LLS	Shallow Laterolog
DT / AC	Sonic
NPHI / CN	Neutron Porosity
RHOB / DEN	Bulk Density
SP	Spontaneous Potential
SPBL	Baseline Shifted Spontaneous Potential
CALI	Caliper

About one-third of the Tiger Shoal wells have porosity logs (sonic, density and/or neutron), but many are missing caliper logs. GR logs are almost exclusively of the cased-hole variety and are limited in number. On the other hand, Starfak field, discovered in 1975, is a relatively new field. Wells in this field penetrate stratigraphically deeper, upper Lower Miocene reservoirs (about –

13,000 ft deep) and have more complete log suites. Eleven of 53 wells are deviated, and deviation surveys for these wells are contained in the database. Both gas and oil are produced from the Middle Miocene in this field.

Core Data

Sidewall core data

Texaco Inc. provided 99 sidewall core analyses from multiple stratigraphic zones. These cores are collected from 41 wells in Starfak field and from 58 wells in Tiger Shoal field. Laboratory measurements obtained from these sidewall core include porosity, permeability, oil and gas saturation, and in limited cases, descriptions of lithology. Although it is possible to incorporate these data into the qualitative reservoir property calculations, consistency of the information is a major concern. Nonetheless, these data are valuable for explaining tight streaks in sonic and resistivity logs, and they validate the log porosity calculations.

Continuous Cores

Unfortunately, there is no available continuous core over the Middle Miocene. Eighty-five feet of core has been recovered from well #6_31 (well #6 of block 31), over the *Robulus* L5 sand (Early Miocene). Texaco Inc. has conducted special laboratory analysis for pressure-volume-temperature (PVT) data. An extensive and detailed study by Hart et al. (1989) described the mineralogy, lithology, depositional systems, diagenesis, and lithofacies represented in the core. McBride et al. (1988) also presented a detailed analysis of two other cores from the #7_31 and #19_31 wells. They especially emphasized the cementation and diagenesis in the Lower Miocene reservoirs and their effects on porosity trends.

Paleontological Data

Texaco provided paleontological data collected from 14 wells (**Table 2-4**). Paleontological information gathered from foraminifers, nannofossils, and flora was incorporated in this study to age-date maximum flooding surfaces and unconformities as well as to assist in defining water depths at the time of deposition in certain intervals. These data allow analysis of the relationship between processes of sea-level change across this area compared to the global sea-level event (Haq et al., 1988).

Production-Perforation Data

Tiger Shoal (produced 3.3 Tcf) and Starfak (316 Bcf) fields, the main interest area of this study, have been producing for more than half a century, and both are located just beyond the state offshore line. In gas production, they are at the high end of the field reserve distribution in the central GOM (**Figure 2-2**). In oil production, the gap between Starfak and Tiger Shoal is smaller. Starfak has produced 13.3 MMbl and Tiger Shoal 35.9 MMbl (**Figure 2-3**).

Texaco Inc. has provided comprehensive perforation and monthly hydrocarbon production data from 103 wells to the research project (**Figure 2-4, and Table 2-5**). Middle Miocene production has surpassed the Upper and Lower Miocene and made the largest contribution, 78% of all production (in Boe).

Production has been allocated to the reservoirs in the two fields, which are named alphabetically A through Z, and roughly span -6000 ft to -11,500 ft (**Figure 2-5**).

Reservoirs have been perforated for the best production possible, and this creates some confusion regarding the allocation of production to specific system tracts as defined in this study. A perforation curve has been calculated and included with the useful well curves, and production amounts have been annotated in the logs at the production interval. Also available are PVT analyses from four wells in Tiger Shoal and water analyses from seven wells in both fields.

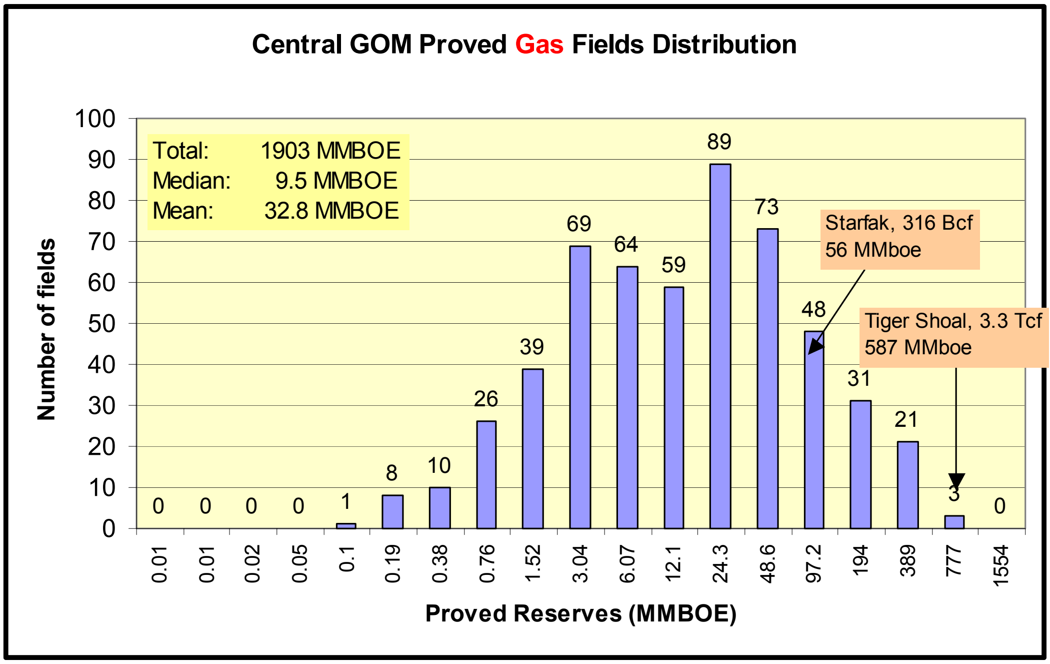

Figure 2-2. Proved gas field distribution in central GOM (Crawford et al., 2000). Both Tiger Shoal and Starfak fields are relatively large fields.

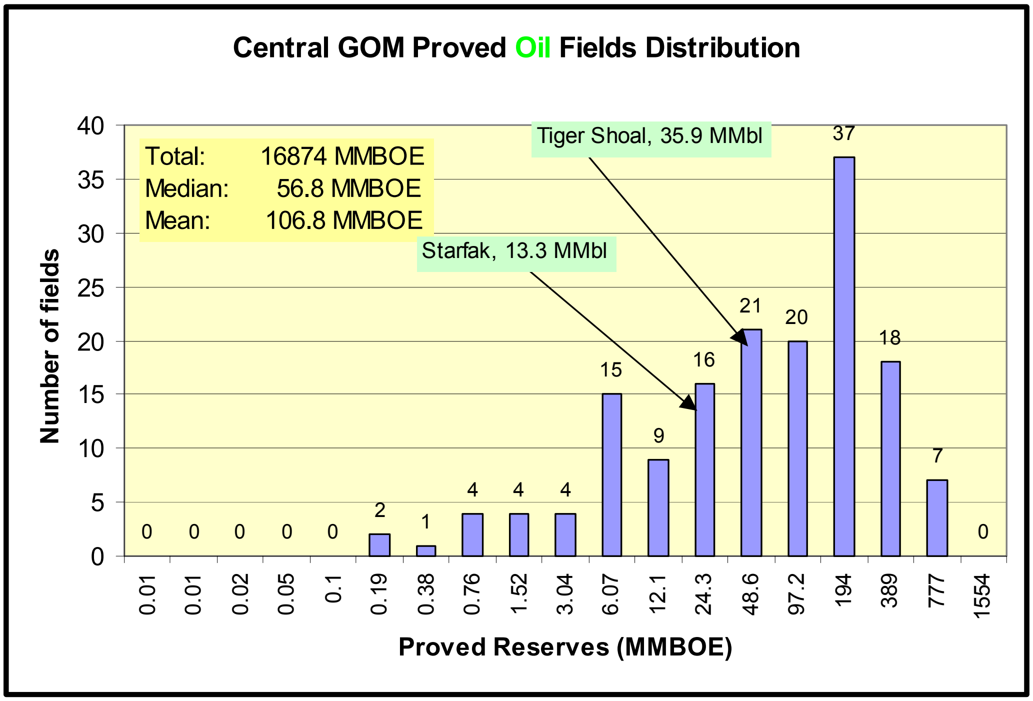

Figure 2-3. Proved oil field distribution in central GOM (Crawford et al., 2000). Both Tiger Shoal and Starfak fields are relatively mid-size fields.

Table 2-4. Paleontological data available from 14 wells in the study area. These index fossils provided high confidence in correlating fourth-order maximum flooding surfaces in seismic data and well logs.

	31_7ST	31_19	219_75	30_1	31_1	31_2	31_3	50_C3	210_93	218_83	217_86	218_65	222_45	218_19	221_146
Sampling begins at	*14000*	*10000*	*8900*		*8700*							*12000*	*9000*		
***Robulus* "E"**							5900								
***Bigenerina* "A"**				6110			6150								
***Bigenerina* "B"**				7175 prob. 7410 definite			7150 prob. 7590 definite		7190 prob. 7550 definite	7410					
***Textularia* "L"**				7960			8010	8100	8000	8100	7980				
Cibicides inflata				8550			8460		8580		8450				
***Cibicides carstensi* (zone 1, 2)**			8950 prob.	8640 prob. 8750 regi.	8840	9280 prob. z2	8710	8810 z1		8610 poss. z1 9080 poss. z2					8990 z1
***Textularia* "W"**			9690	9360	9610	9410	9575	9550	9380	9380	9000		9510		9750
Bigenerina humblei			10375	10010	10120	10350	10150	10300	10050	10000	9880		10300		10510
Christellaria "I"		10500	10540	10320	10500	10490	10410	10490	10350	10300			10610		10820
***Cibicides opima* - *Cristellaria* "49"**		10980 rare	11180 rare 11500 comm.	10980 prob. 11410 comm.	11100 rare 11480 regi.	11050	10950 rare 11420 prob.	11100 rare 11600 prob.	10830	10950	10700		11100	10970 rare 11260 comm.	12120
***Amphistegina* "B"**			12600 prob.		12610		12600	12700		12140				12110	13320
***Robulus* "C"**			13420				13290	13580		12850					
***Robulus* "L"**	14010		13860				13810	14020		13240		13320			
***Cibicides* "38"**			14175				13980	14120							
Undiffrentiated Fauna		<------ 10110	<------ 9650	<------ 9910		<------ 10200			<------ 7090	<- - - 7050	<------ 7350	<------ 12900	<------ 10100		<- - - 8350
			<- - - 10100			<------ 10590	<------ 9980		<------ 8250	<- - - 8500	<- - - 8230		<------ 10640		<------ 9380
			<------ 10380				<------ 11300		<------ 9300	<------ 9850	<------ 9600		<------ 11500		<------ 9650
			<------ 10650				<------ 13500		<------ 9950	<------ 10380	<------ 11100				<------ 10950
sb	Sampling begins						<------ 14550		<------ 11590						<------ 11500
comm.	common														<------ 13450
prob.	probable														
regi.	regional		<------	Faunal increase + change (faunal Flood)											
z1, z2	zone1, zone2		<- - -	Slight faunal Increase											

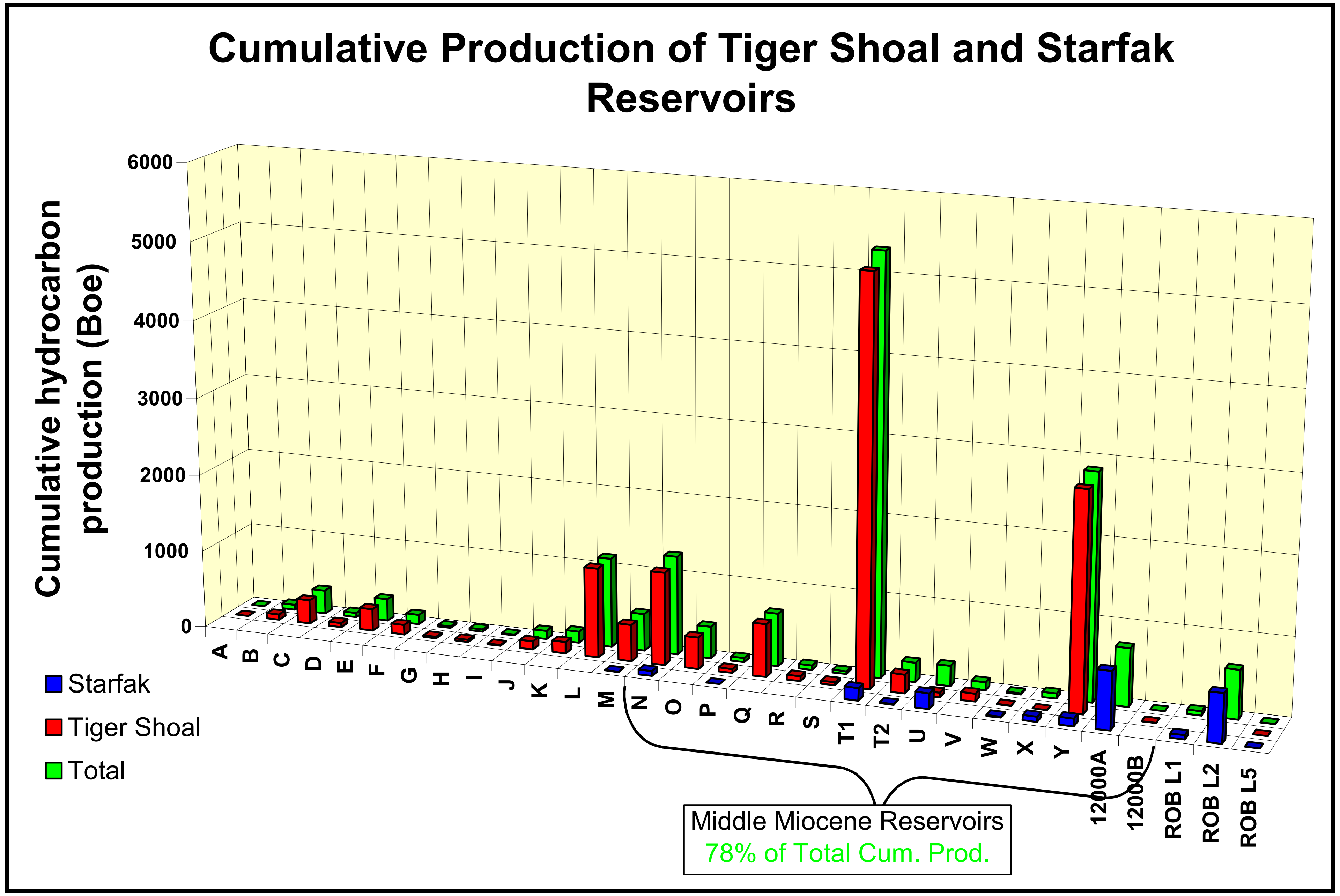

Figure 2-4. Production of hydrocarbon (Boe) information by reservoir and field. Middle Miocene reservoirs have produced 78% of total cumulative production from both fields. Reservoirs (A through RobL5) are named according to Texaco's established nomenclature.

Table 2-5. Cumulative hydrocarbon production (Boe) of Starfak and Tiger Shoal reservoirs. Middle Miocene reservoirs have produced 78% of all production in both fields.

Reservoirs	Starfak Cum Prod (Boe)	T. Shoal Cum Prod (Boe)	Cum Prod (Boe)
A		0.210	0.210
B		68.778	68.778
C		306.717	306.717
D		53.000	53.000
E		285.139	285.139
F		124.307	124.307
G		18.739	18.739
H		28.485	28.485
I		9.946	9.946
J		108.303	108.303
K		148.628	148.628
L		1149.948	1149.948
M	5.641	469.571	475.212
N	63.862	1190.393	1268.553
O		408.521	408.521
P	0.683	51.494	52.177
Q		677.642	677.642
R		60.566	60.566
S		35.794	35.794
T1	158.554	5165.392	5323.946
T2	10.211	238.024	248.235
U	197.824	60.982	258.806
V		102.635	102.635
W	11.986	3.605	15.591
X	65.114	0.329	65.442
Y	96.518	2770.923	2867.441
12000A	736.156		736.156
12000B		1.894	1.894
ROB L1	53.768		53.768
ROB L2	620.869		620.869
ROB L5	1.478	13539.966	1.478
TOTAL	2022.664	27079.933	15576.929
Middle Miocene	1340.908	10768.194	12123.401
Middle Miocene / Total (%)	66.294	39.764	77.829

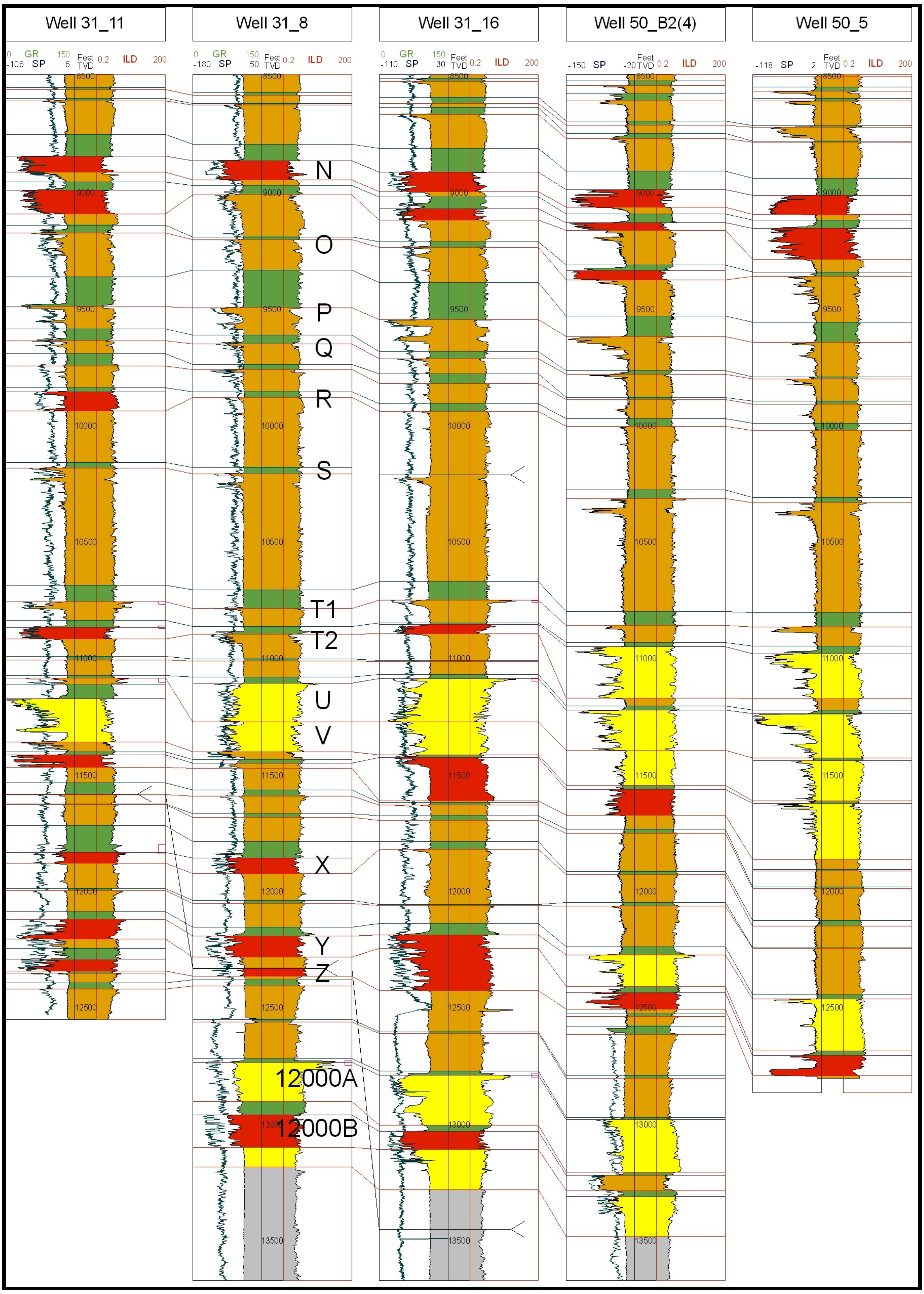

Figure 2-5. Sequence stratigraphic framework and interest zone, from N sand to 12000B sand (Hentz, 2000).

Sequence Stratigraphic Framework

This study is developed upon the sequence stratigraphic framework, which is established by the Bureau of Economic Geology, The University of Texas as a part of the U.S. Department of Energy funded OSGR (offshore secondary gas recovery) project (Hentz et al., 2002, 1999; Wood et al., 2001; and DeAngelo et al., 2000).

The project was a product of a successful collaboration between many scientists and students, each of whom has brought their individual talent and experience to the project. It is imperative to acknowledge the contributions of these scientists to the interpretation I have relied on and incorporated in my study.

I have used the sequence stratigraphic surfaces picked on the petrophysical well logs and mainly relied on MFS (maximum flooding surfaces) to divide the section into smaller units and segregate two of them for neural-network analysis. Petrophysical properties (average porosity, average reservoir thickness, porosity*thickness of reservoirs, and similar parameters) were computed for each fourth-order genetic sequence, which are defined between MFS surfaces.

On the seismic interpretation, the MFS picks and biostratigraphic tops from the well logs were used as a guide, but the fourth-order interpretation in this work expands from the OSGR project. In some cases, flooding surface interpretation was modified from the surfaces picked by the OSGR project.

METHOD OF INVESTIGATION

The primary intent of this study is to illustrate an ability to create a fourth-order earth-model of a Middle Miocene depositional system under conditions of limited sources of quantitative data, and in the absence of continuous core and detailed core analysis, using low-resolution seismic data, or in situations of moderate log quality. This study will introduce new techniques in integrated earth model building that incorporate (a) rock properties by petrophysical analysis and (b) geological facies modeling (reservoir definition, spatial distribution). To accomplish this geologically meaningful model we will use (1) sequence stratigraphic analysis with log and seismic interpretation, (2) classic seismic-attribute interpretation, (3) neural-network seismic-facies analysis, and (4) existing knowledge of Middle Miocene depositional systems.

The steps involved in this research process are shown on **Figure 2-6**. Each step is summarized below.

Step 1. Post-stack Seismic Data Edit

Phase Shift

Post-stack processing, involving a 90° phase shift, was applied to the approximately 30° phase seismic data (Figures 2-7 and 2-8) by the OSGR team (Hentz et al., 1999). Seismic impedance typically occurs at the physical property boundary of different geological units, typically sand and shale boundaries. This impedance contrast, which is defined in the reflection coefficient, is imaged by a maximum peak or trough of a seismic wavelet, in this case a Ricker wavelet.

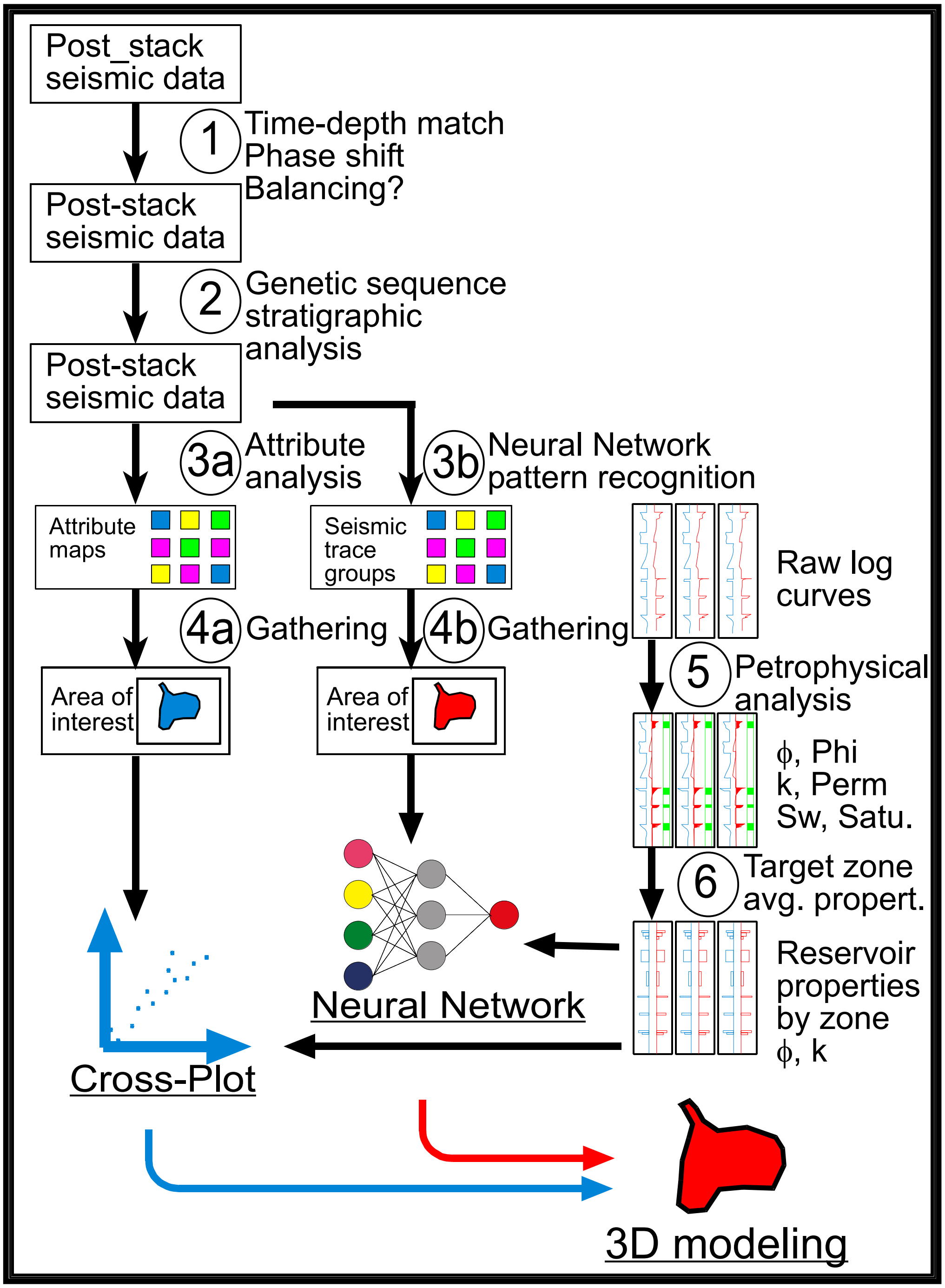

Figure 2-6. Flow chart of the method for reservoir quantification. Steps from 1 to 6 are discussed in this chapter. Neural networks and quantification are explained in chapter 4.

Phase shifting enables the maximum deflection point of a seismic wavelet to coincide with the actual lithology, not with the properties (lithologic) boundary. This shifting allows easier stratigraphic interpretation of the seismic data because the impedance curve, derived from the log data, as well as other curves then coincide with the seismic wavelet peak or trough. It also prevents confusion in the case of multiple close events, as in the case of thin-bedded units (DeAngelo et al., 2000).

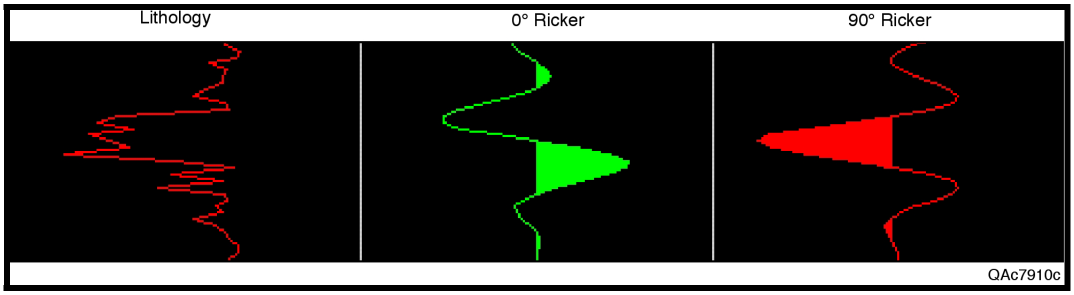

Figure 2-7. Seismic phase rotation and lithology matching. The red curve excursion to the left is a representation of the changing lithology from shale (to the right) to sand (to the left). The 0^0 Ricker wavelet reflects the boundaries of those lithologies (DeAngelo et al., 2000).

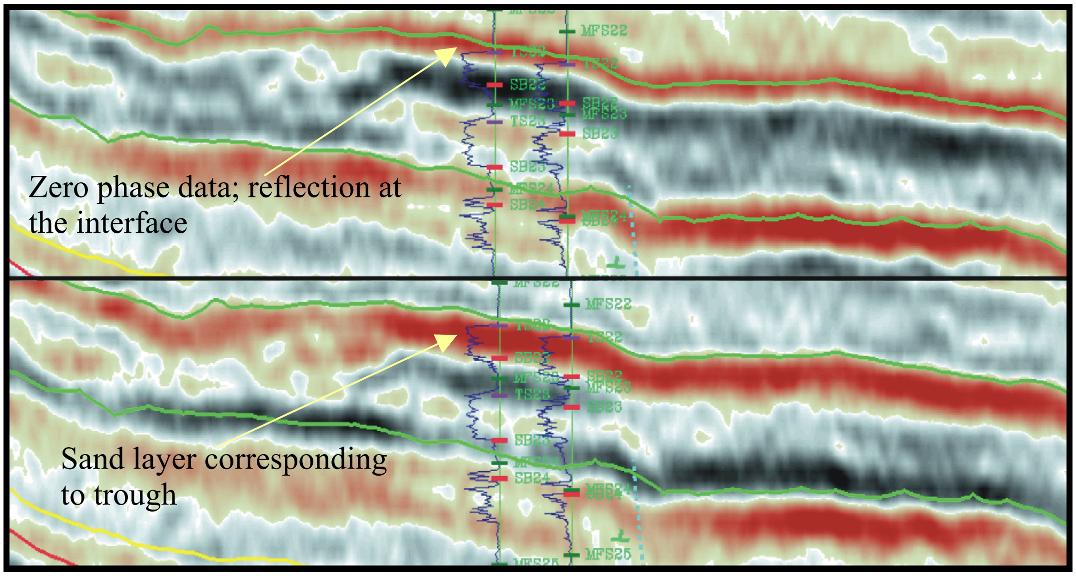

Zero phase data; reflection at the interface

Sand layer corresponding to trough

Figure 2-8. 90^0 phase rotation (bottom half of figure) aligns sands with trough for accurate interpretation.

Time-Depth Match

Five check-shot measurements are available from five wells (#5_30, #C1_50, #95_210, #176_210, and #122_219) in Starfak field. Synthetic seismograms were generated from two of these wells, which were deemed to have the best quality sonic curves. These synthetics were used to tie well depth with seismic time (DeAngelo et al., 2000). All other wells in both fields had their depths "shifted," either up or down to match the seismic time after using these check-shot surveys, with consideration of their distance to the five wells (**Figure 2-9**).

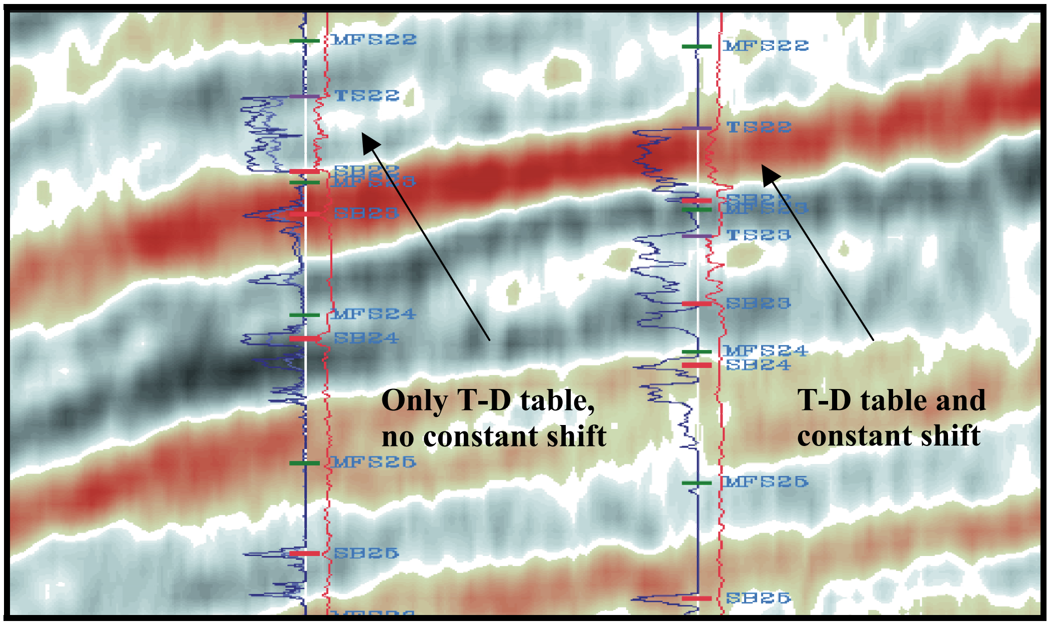

Figure 2-9. Constant depth-shift was applied to each well according to the Time-Depth (T-D) tables derived from 5 key wells in the study area. See text for well names.

Spectral Balance

Spectral balancing (Landmark, 1996) has been applied to improve seismic data resolution, especially for the Middle Miocene and Lower Miocene reservoirs (DeAngelo et al., 2000). This typically is the section 2 seconds and deeper in the seismic data. With this process, diminished high-frequency reflections that fell between the low-frequency reflections were amplified to achieve a more “complete” imaging of the stratigraphic section and allow additional interpretation (**Figure 2-10**). Two seismic-panel comparisons are shown in **Figure 2-11** that illustrates the addition that this change makes in the appearance of the data. Caution must be used with interpreting the resulting seismic data, since this approach does not discriminate true stratigraphic seismic signal from seismic noise.

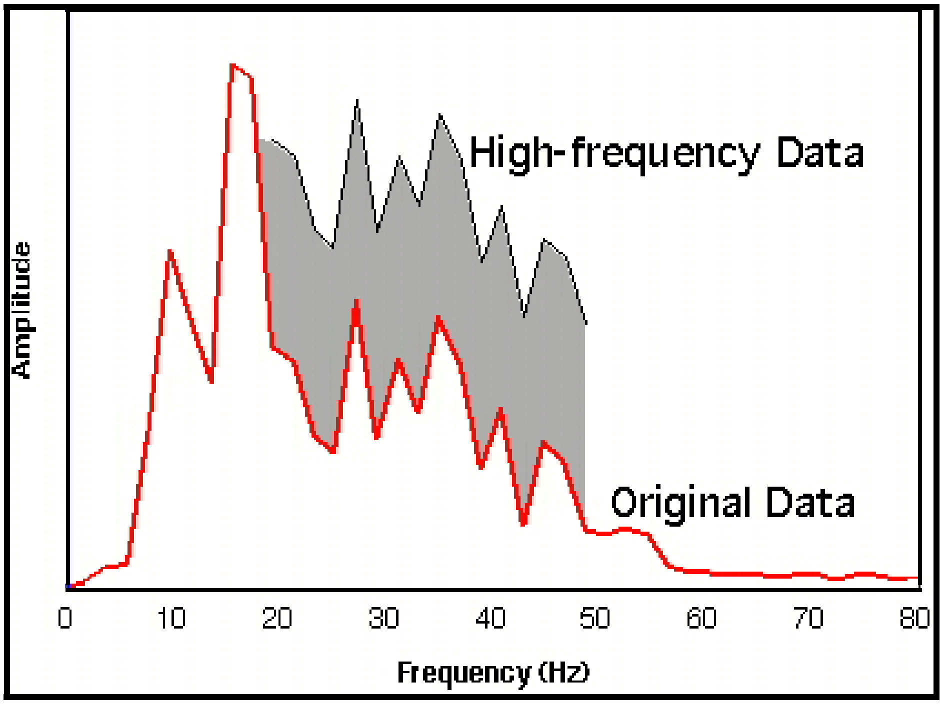

Figure 2-10. High-frequency boost for detailed interpretation (DeAngelo et al., 2000).

A similar approach by Countiss (2002) showed that convolving the seismic data with increasing high-frequency Ricker wavelets improved stratigraphic resolution and enabled additional geologic interpretation. Countiss (2002) first increased seismic frequency up to 120 Hz, which caused the generation of non-geologic artifacts. He then filtered frequency back to the level at which they would not get erroneous reflections, which eliminated the noise and enhanced the stratigraphic resolution. This process enabled him to identify additional resources in the thin reservoirs.

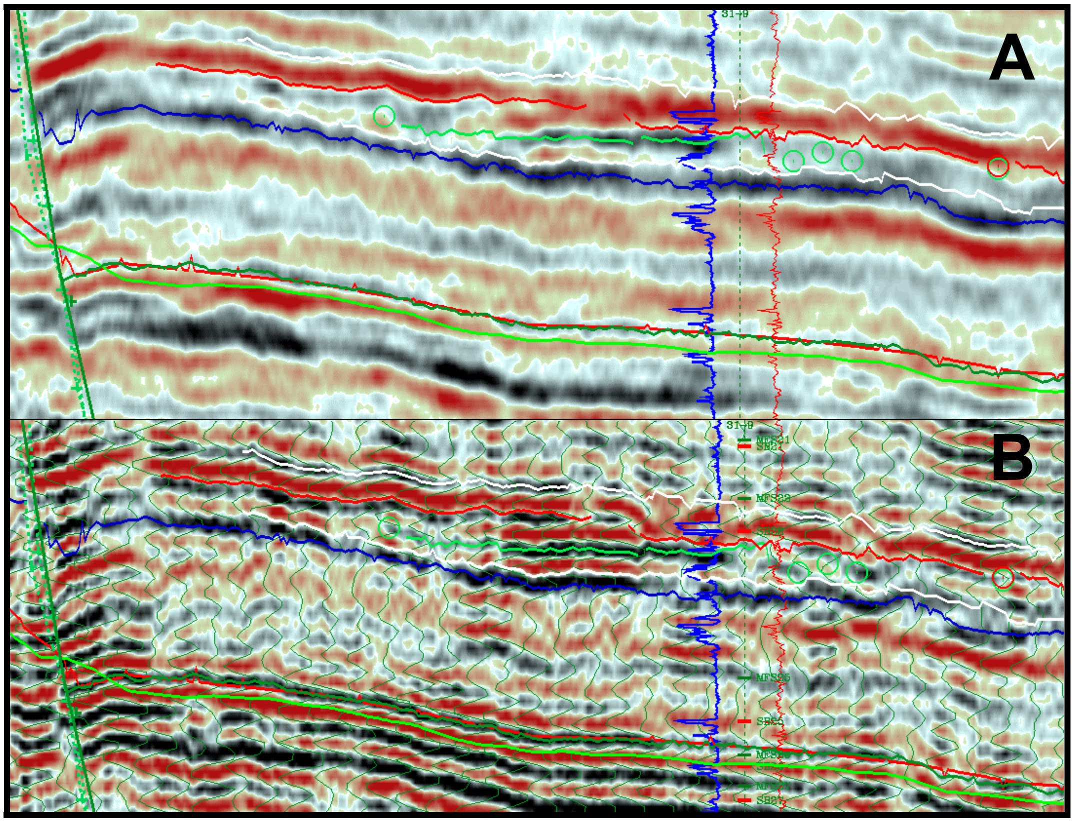

Figure 2-11. A comparison of (A) original seismic volume and (B) high-frequency seismic volume of the study.

Step 2. Stratigraphic Analysis

The Middle Miocene interval in the study area comprises roughly 4,300 ft of sediment and 15 reservoir groups (Figure 2-5). At least 24 fourth-order sequences (~0.25 my) have been defined in the interval (**Figure 2-12**). Reservoir nomenclature is according to Texaco E&P Inc., and reservoir ages are established through integrated paleontological analysis (Table 2-4).

The Middle Miocene basal boundary is marked by a *Robulus* "L" extinction horizon (~16.6 my), and its top boundary is marked by the *Cibicides* *carstensi* extinction horizon (~10.8 my). The upper two-thirds of the Middle Miocene section shows a regressive stacking pattern, and the bottom one-third of the section (below *Cristellaria* “I” (~13.5 my)) shows transgressive stacking patterns (Fillon et. al., 1997). Third-order sequence (~1.5 my) boundaries defined within the area coincide with third-order sea-level events on the Lawless et al. (1997) coastal-onlap curves (**Fig. 2-13**).

Detailed 3D seismic sequence stratigraphic analysis of the modified seismic volume (as previously discussed) allows interpretation of these 24 fourth-order sequences. The spectral analysis of the seismic data and high-frequency amplitude boosting significantly increased the ability to resolve the morphology and seismic expression of valleys, shoreline, shelves, and deep-water setting at the systems tract level.

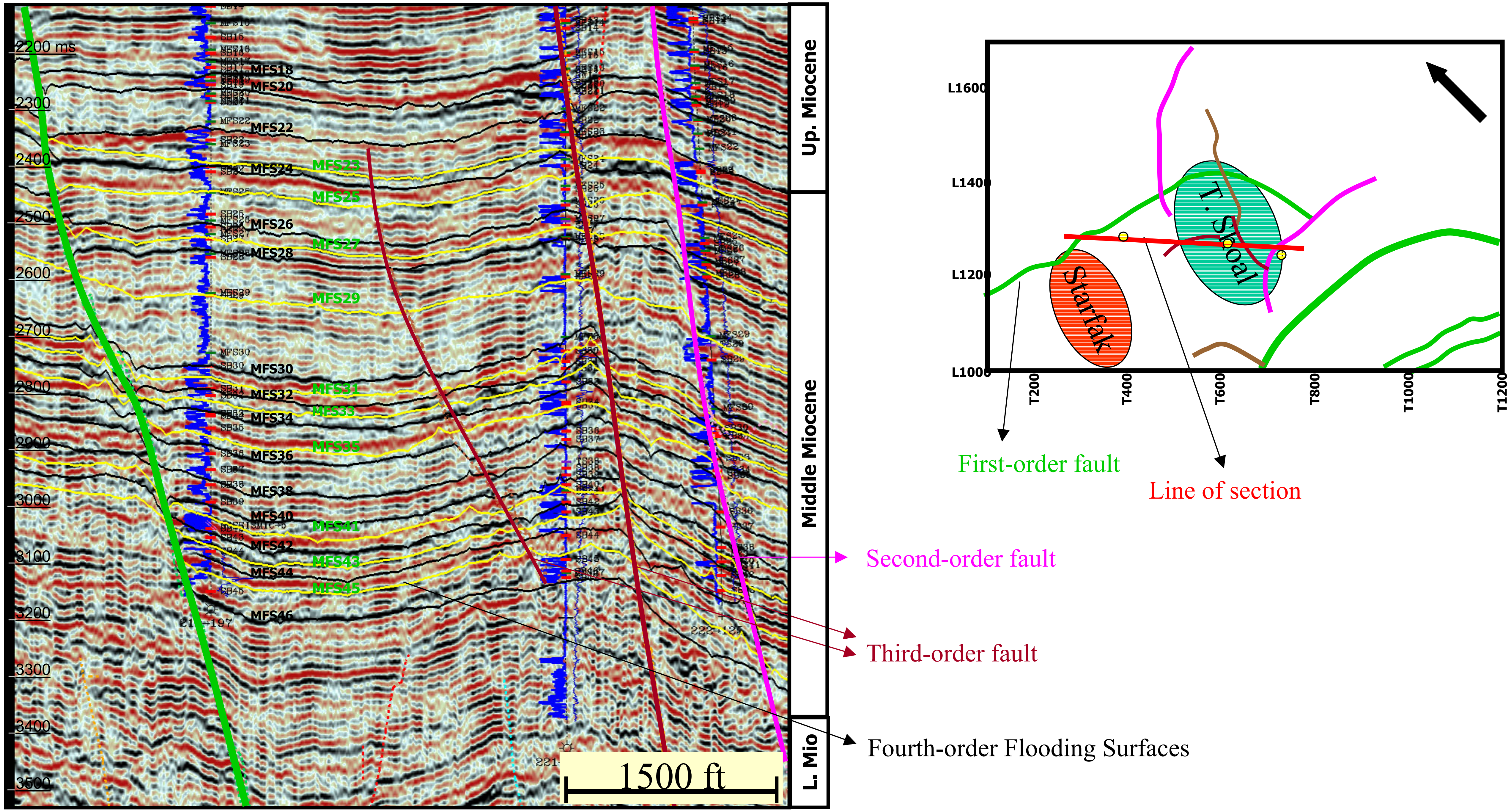

Figure 2-12. An arbitrary seismic section (NE-SW) and fourth-order flooding surfaces of the Middle Miocene.

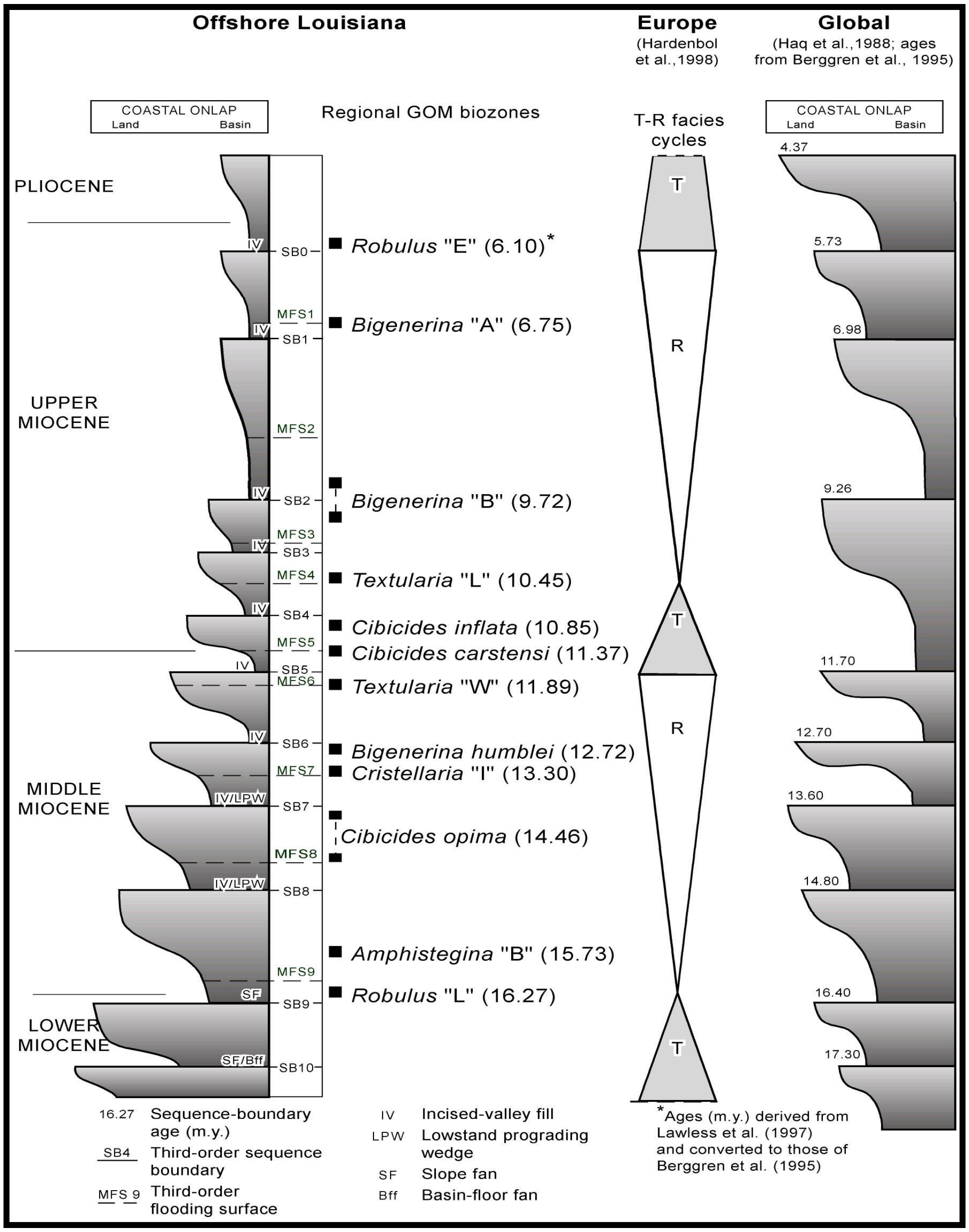

Figure 2-13.Comparison of the coastal-onlap curves; study area and the global, and transgressive-regressive cycles within European basins (Hentz and Zeng, 2003).

Step 3. Attribute Analysis

While it is possible to see the seismic architecture (onlap, offlap, toplap and downlap) associated with some of the major sequence boundaries in the 3D seismic volume without any additional processing, most of the sequence stratigraphic surfaces are not resolvable through simple analysis of vertical sections and require further detailed analysis of the volumes other attributes. Fourth-order maximum flooding surfaces over the two fields within the high-frequency seismic volume were interpreted, and genetic sequences between these flooding surfaces were established.

Two sets of attribute maps were created within each genetic sequence. The first set comes from classic seismic-attribute computations, by Landmark PAL^{TM} (**Figure 2-14**), and a general classification of seismic attributes, which are derived from or related to “time, amplitude, frequency, and attenuation”, is given by Brown (2001, **Figure 2-15**). The other set comes from neural-network analysis, by Stratimagic^{TM} (**Figures 2-16** and **2-17**). In addition to these two types of attribute/seismic facies maps, proportionally sliced amplitude maps were also utilized for detailed stratigraphic and internal architectural analysis of genetic sequences.

The maps that result from seismic attribute and interval analysis, including seismic facies maps, attribute maps, and proportionally sliced amplitude maps, are used in combination to identify geological elements of depositional system architectures and to assemble evidence for the nature of surfaces that bound intervals under analyses - sequence boundaries, flooding surfaces, and possibly ravinement surfaces. Details of how the maps were created, types of maps created, and their interpretation are explained in Chapter 4.

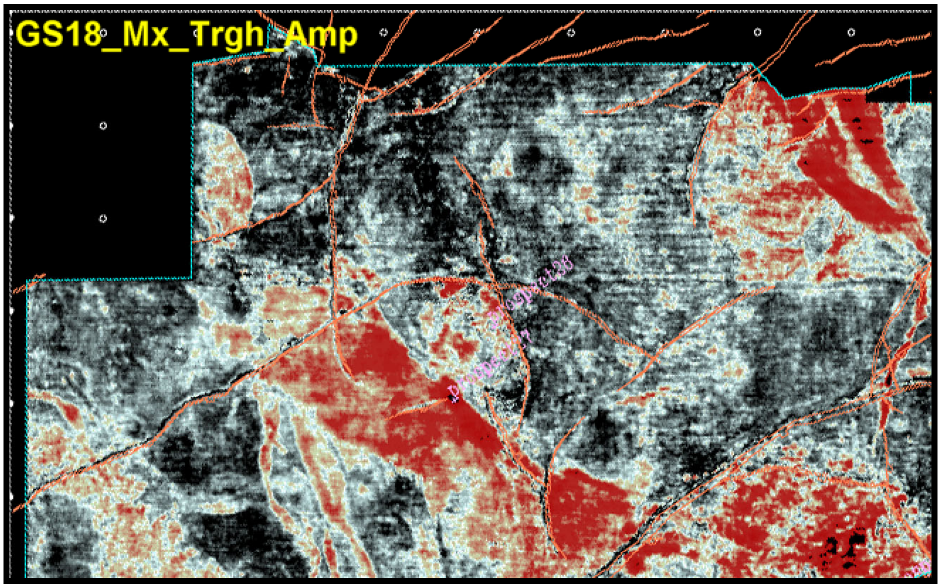

Figure 2-14. An example of a maximum trough amplitude extraction map, generated from the seismic amplitude data volume within the GS18 interval.

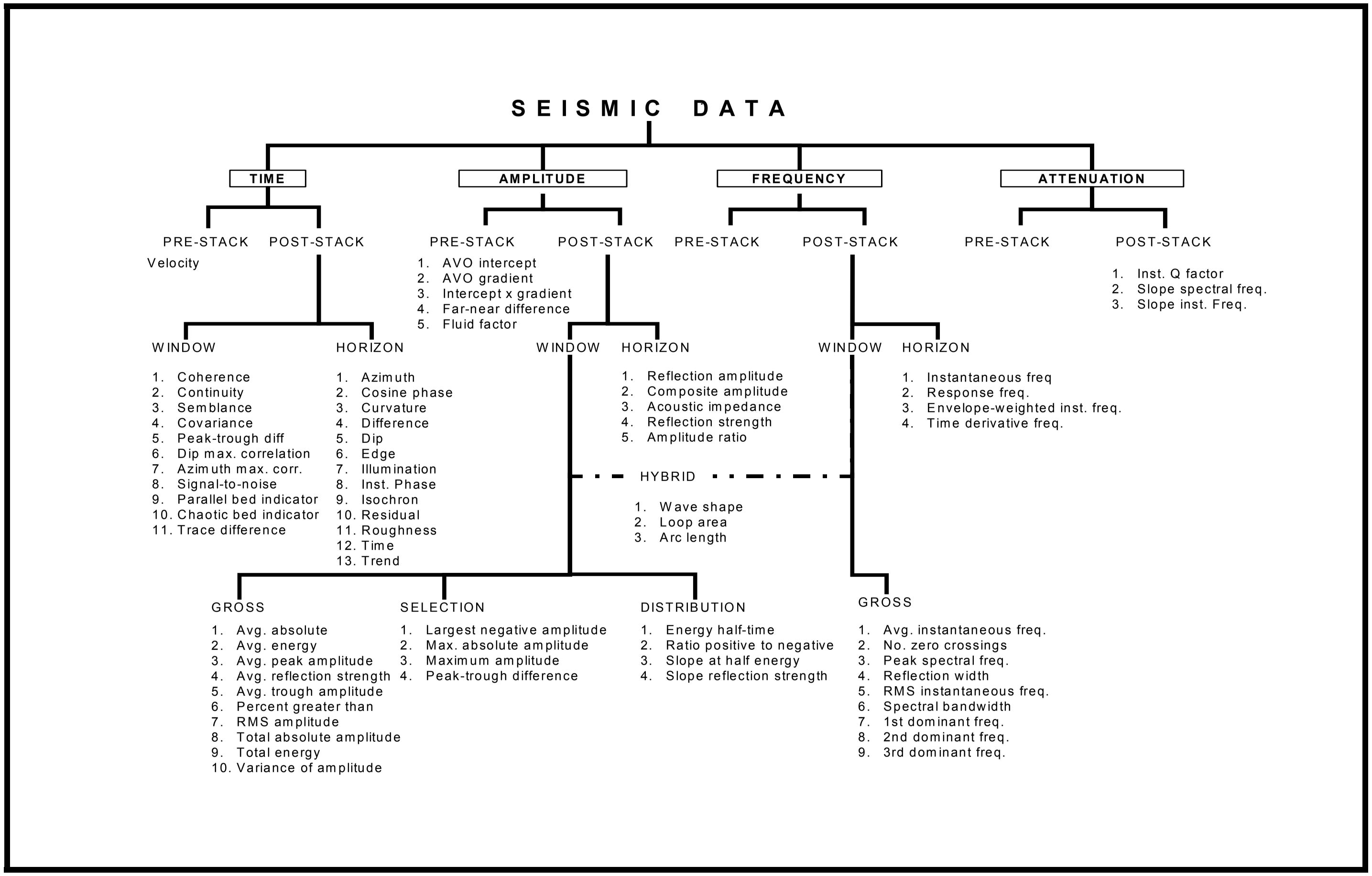

Figure 2-15. Classes of seismic attributes, which are derived from or related to time, amplitude, frequency, and attenuation (Brown, 2001).

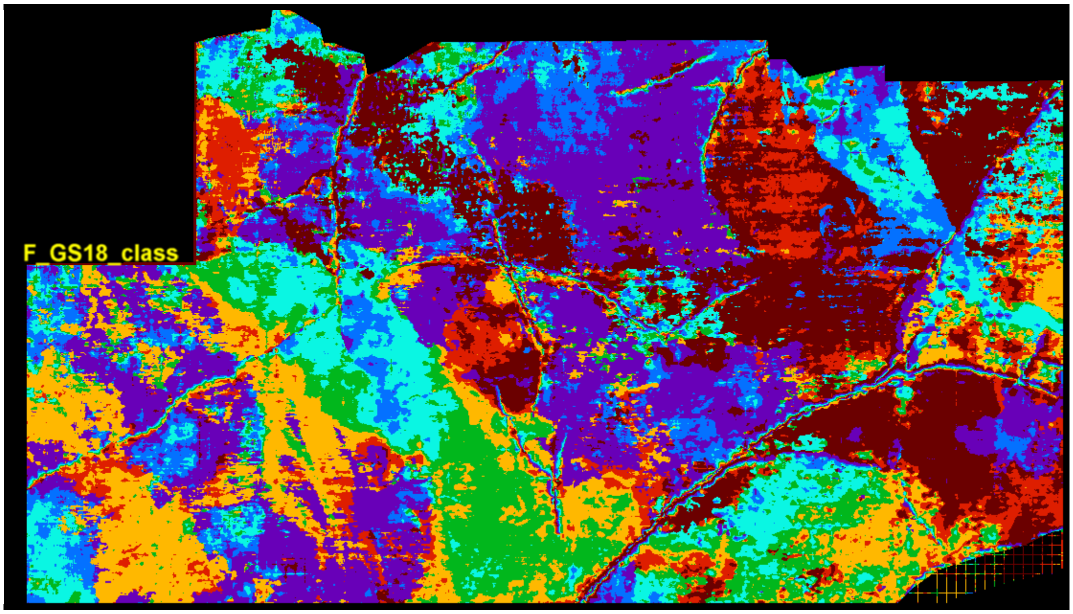

Figure 2-16. An example of a seismic facies classification map of GS18. Classified waveforms were extracted from the seismic data volume within the GS18 interval, and based on Stratimagic^{TM} software.

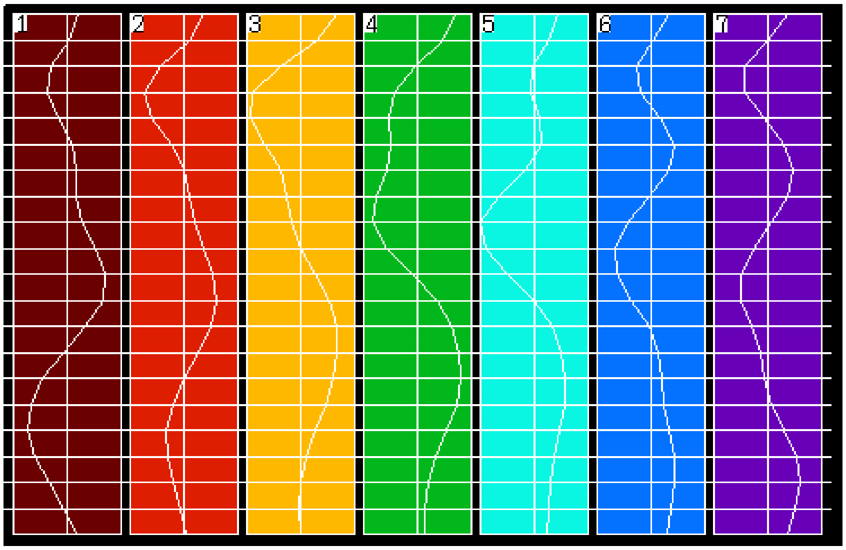

Figure 2-17. The seven color-coded representative wavelets of seismic volume. These wavelets used to create seismic-facies map of GS18 (above).

Step 4. Data Gathering

Classifying architectural elements using amplitude extraction form and seismic wavelet geometry is at best an uncertain proposition. Therefore, in interpreting environments of deposition it is critical that all available data -- well-log, core and fossil, and initial interpretations; well-log stacking patterns, log motif, seismic waveform motif and plan form amplitude geometries -- must be incorporated, if one is to generate as accurate an interpretation as possible. Likewise, log and seismic information can be used to control the quality of interpretation of fauna and flora occurrences and abundances, since problems can also exist in paleontologic data sets if they are examined in isolation. This quantitative data-gathering stage will involve the geological interpretations of seismic and log data, and descriptions of geological depositional facies. This step is very similar in definition to creating “Discrete Models” of reservoir modeling described by Haldorsen and Damsleth (1993). This step is intended to divide the Middle Miocene section into geologically/stratigraphically meaningful divisions and to define the elements of the depositional system - fluvial channels and incised valleys, deltaic wedges, and lobes. The second stage is the quantification/transformation of seismic into log. As outlined before, the main target is to visualize the geo-bodies and geological facies and then to assign quantitative rock properties.

Step 5. Petrophysical Analysis

Quality Check

Approximately 70 wells have been digitized from 1 inch=100 ft or 5 inches=100 ft scale paper log copies. Most of the paper copies of Tiger Shoal wells are in 1 inch=100 ft scale, and resulted in poor quality in the digitized curves. In a few cases, where curves were not suitable for digitizing, deep resistivity curves were computed from conductivity curves.

The remaining 81 wells had some missing curves, and most were sampled at different rates. Sampling rates for computations were standardized for all the logs to 2 samples/ft, and large data gaps up to 2 ft on the curves were filled by interpolation. A vigorous log quality check showed that there were many problems including (1) poorly digitized resistivity curves, which wrapped around the track over pay zone and (2) shift in SP curves. Digital curves were compared to paper copies for accuracy of digitization and completeness of log suite. Common errors, such as curves wrapped to the tracks with wrong scales, were corrected. In addition, curves of similar types but from different log runs (i.e., gamma ray curves coming from both resistivity and density tool runs) were digitized and named accordingly for more accurate log analysis (**Figure 2-18**). Finally, SP curves have been baseline-shifted, and gamma ray curves have been corrected for mud weight and hole size.

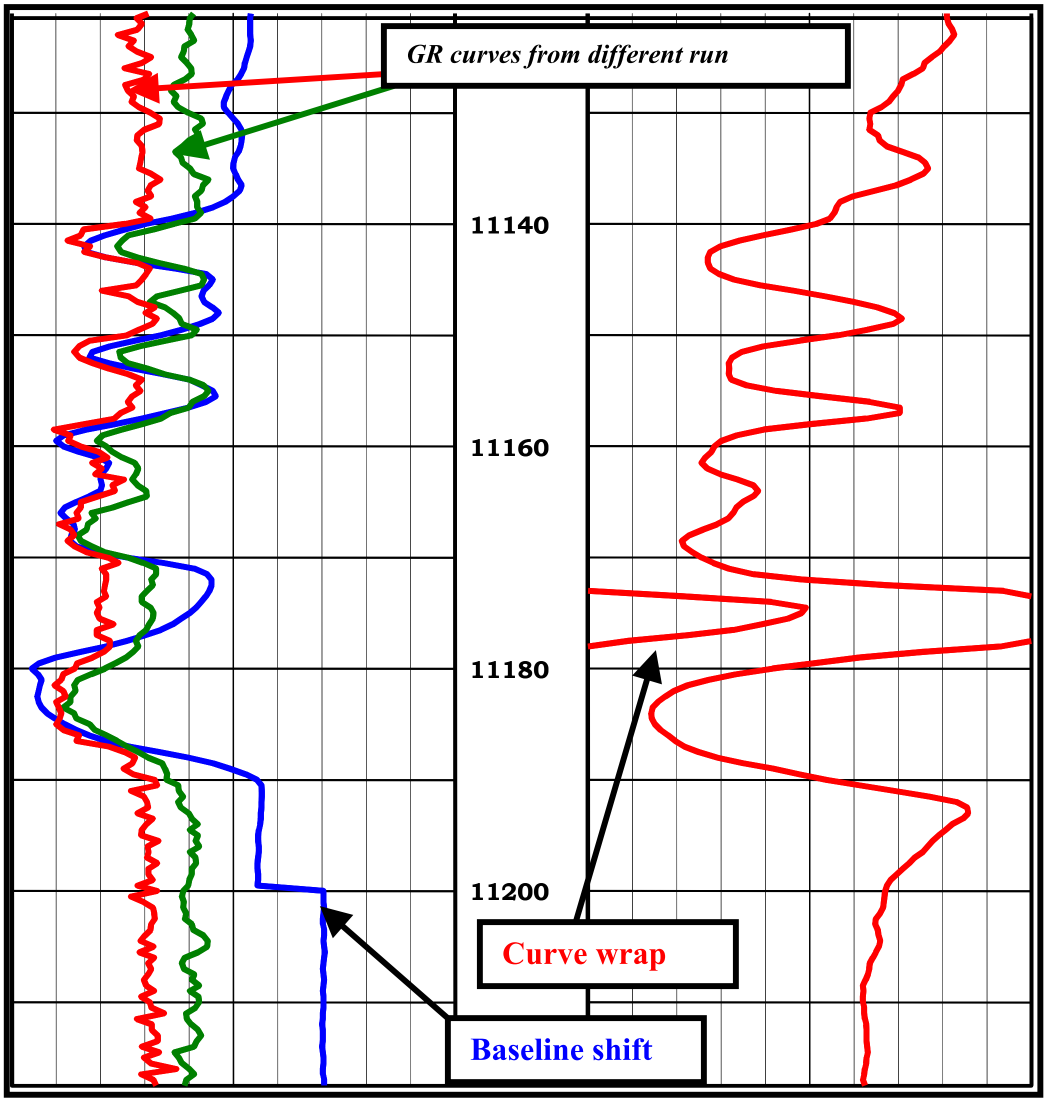

Figure 2-18. **Quality check for individual well log data. First, digital data were compared to paper logs. Second, problems with overlapping curves were fixed and GR curves from different run were depth shifted. All the SP curves were baseline shifted and used as input curve for VCL, along with GR.**

Shaly Sand Analysis

1. Porosity Analysis

Because of diverse and poor-quality log data, porosity was calculated by different approaches and results were crosschecked for accuracy. In the first step, both logs and core plugs were used to calculate porosity, and in the second step, the porosity curve was modified by the clay content.

There are 41 multiple-zone sidewall-core analysis data available in Starfak field and 58 in Tiger Shoal field. Core-plug porosities were used to estimate the porosity distribution in the field. Core plug porosities were plotted against the depth, and an approximate maximum line was drawn (**Figure 2-19**). The relationship obtained from the plot was applied to all the wells in the study area to give a maximum expected porosity (PHIAMAX) per depth, which is assumed shale-free porosity value. The relationship is:

PHIAMAX=0.42-0.00001*depth

This ϕMAX (PHIAMAX) value was converted to an effective porosity (ϕe) using the following equation:

$\phi e = \phi MAX * (1-VCLAY)$

Core-plug measurements were corrected for net overburden conditions using data from whole-core from well #31-6. The conversion equations used to obtain porosity and permeability to air at in-situ conditions are:

PHINOB = 1.208*(CPHI/100)-0.0659

KNOB = CPERM*(0.1097* ln (CPERM)+0.2663) where:

PHINOB = Overburden corrected core porosity

CPHI = Core plug porosity

KNOB = Overburden corrected core permeability

CPERM = Core plug permeability.

In the zones with neutron and density curves available, effective porosity was computed by

$\phi_e = (\phi_{dc} + \phi_{nc}) / 2$ for oil

$\phi_e = [(\phi_{dc}^2 + \phi_{nc}^2) / 2]^{1/2}$ for gas

where:

$\phi_{dc} = \phi_d - (VCL * \phi_{dsh})$

$\phi_{nc} = \phi_n - (VCL * \phi_{nsh})$

ϕ_d = density porosity

ϕ_n = neutron porosity

ϕ_{dc} = density porosity corrected for clay

ϕnc = neutron porosity corrected for clay

ϕ_e = effective porosity

VCL = volume of clay

ϕ_{dsh} = density porosity for shale

ϕ_{nsh} = neutron porosity for shale

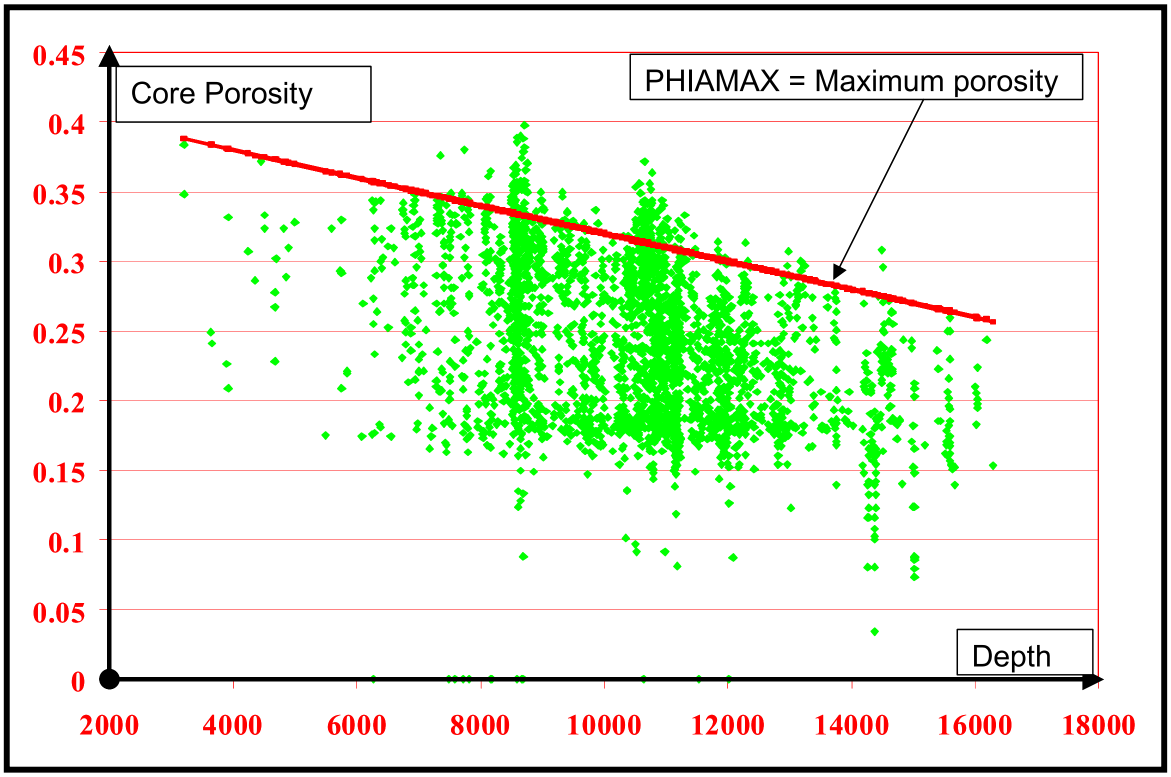

Figure 2-19. Core-plug porosity values vs. depth for maximum porosity estimation.

Because of bad wellbore conditions, porosity curves were of poor quality and, therefore, were adjusted to match the core porosities.

Clay in the rock causes porosity tools to read more or less than actual porosity. Because of this effect, neutron and density porosities were corrected for volume of clay in the rock. In the 100% clay (shale), effective porosity went to zero, and in 0% shale (clean sand), effective porosity reached its maximum value. In between the extremes, porosity was computed linearly.

2. Volume of Clay Analysis

Both effective porosity (ϕe) and effective water saturation (S_{we}) calculations require corrections for volume of clay in the rock.

Although gamma-ray curves are available for half of the wells in Starfak field, they are provided for only one-third of the wells in Tiger Shoal field. On the other hand, SP curves exist in almost every well in both fields (Table 2-2). VCL (volume of clay) computed from baseline-shifted SP curve, is provided for every well with an SP curve.

VCL = (BSSP - (1.051 * SPCL - 5))/(95 - (1.051 * SPCL - 5))

where

VCL = Volume of clay

BSSP = Baseline shifted SP curve

SPCL = SP value of clean sand

Five percent clay has been excluded from the maximum and minimum ends to keep the volume of clay within 5% to 95% range. This range was based on several X-ray diffraction datasets from Miocene-age reservoirs. In numerous instances, there are low-porosity, well-cemented zones that have low gamma ray, low SP deflection, and high resistivity values. These zones limit the effectiveness of any VCLAY-to-porosity transforms to estimate porosity in poor borehole conditions. In instances where the SP is affected by outside conditions or is not available, the GR curve was used to estimate volume of clay.

3. Water Saturation

Water saturation was computed according to the Simandoux (Asquith, 1995) method:

$$Swe = \left[(C*Rw)/\phi e^{m}\right] * \left[\left[\left[(5*\phi e^{m})/(Rw*Rt)\right] + (VCL/Rsh)^{2}\right]^{1/2} - (VCL / Rsh)\right]$$

where

C = 0.40 for sandstones
= 0.45 for carbonates
ϕe = effective porosity corrected for shale
Rsh = resistivity of adjacent shale
Rw = formation water resistivity = 0.094 @ 77° Fahrenheit
Rt = deep formation resistivity
VCL = volume of clay
m = 2
temp = temperature = 77°+0.01*depth

This method assumes that clays are not dispersed (i.e., authigenic) and that the resistivity of clays in sandstone is equal to the resistivity of nearby shale. McBride et al. (1988) described the start of chlorite cementation below 9,000 ft and kaolinite below 11,000 ft, but the modified Simandoux model was used for water-saturation estimation, in the absence of detailed core analysis in the Middle Miocene section, between approximately 8,000 and 13,000 ft in the area.

An example of an integrated well log is given in **Figure 2-20**. Logs include all the available curves, core porosity and permeability, volume of shale, water and oil saturations, and effective porosity. Sequence stratigraphic interpretations are also included.

Net sand values were computed for each genetic sequence. Net sand is defined as less than 50% of VCL curve. This means, if the clay content is less than half (volumetrically), the rock is considered to be sand (**Figure 2-21**).

Net-sand maps are compared with attribute maps to confirm general sand distribution and depositional trends. Comparison between net-sand map of lowstand (LST) or highstand (HST) to RMS (root-mean-square) maps usually yields a reasonable match, but it is very sensitive to well coverage (**Figure 2-22**).

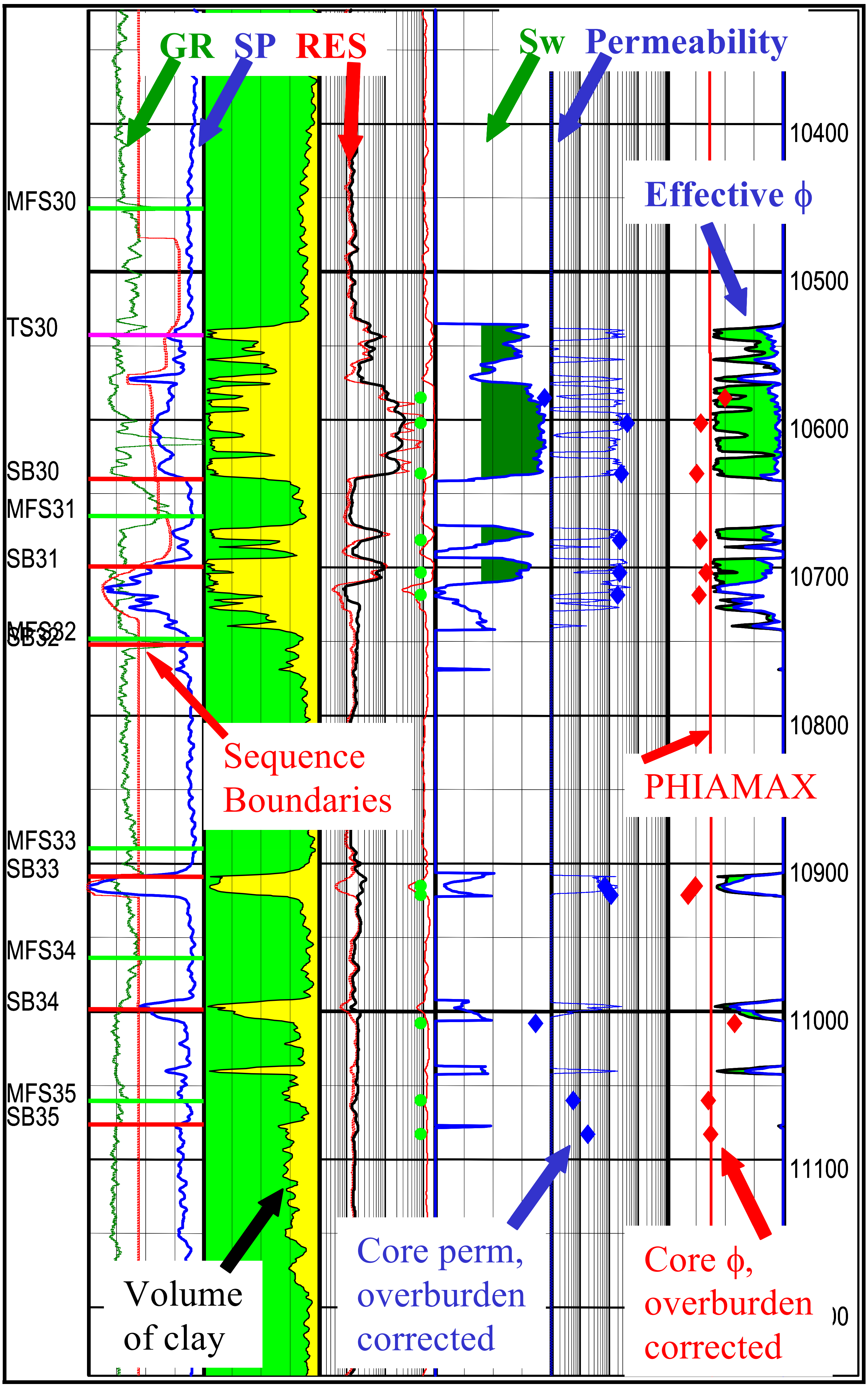

Figure 2-20. Typical well with log curves, sidewall core analysis, sequence stratigraphic interpretation picks, and petrophysical analysis.

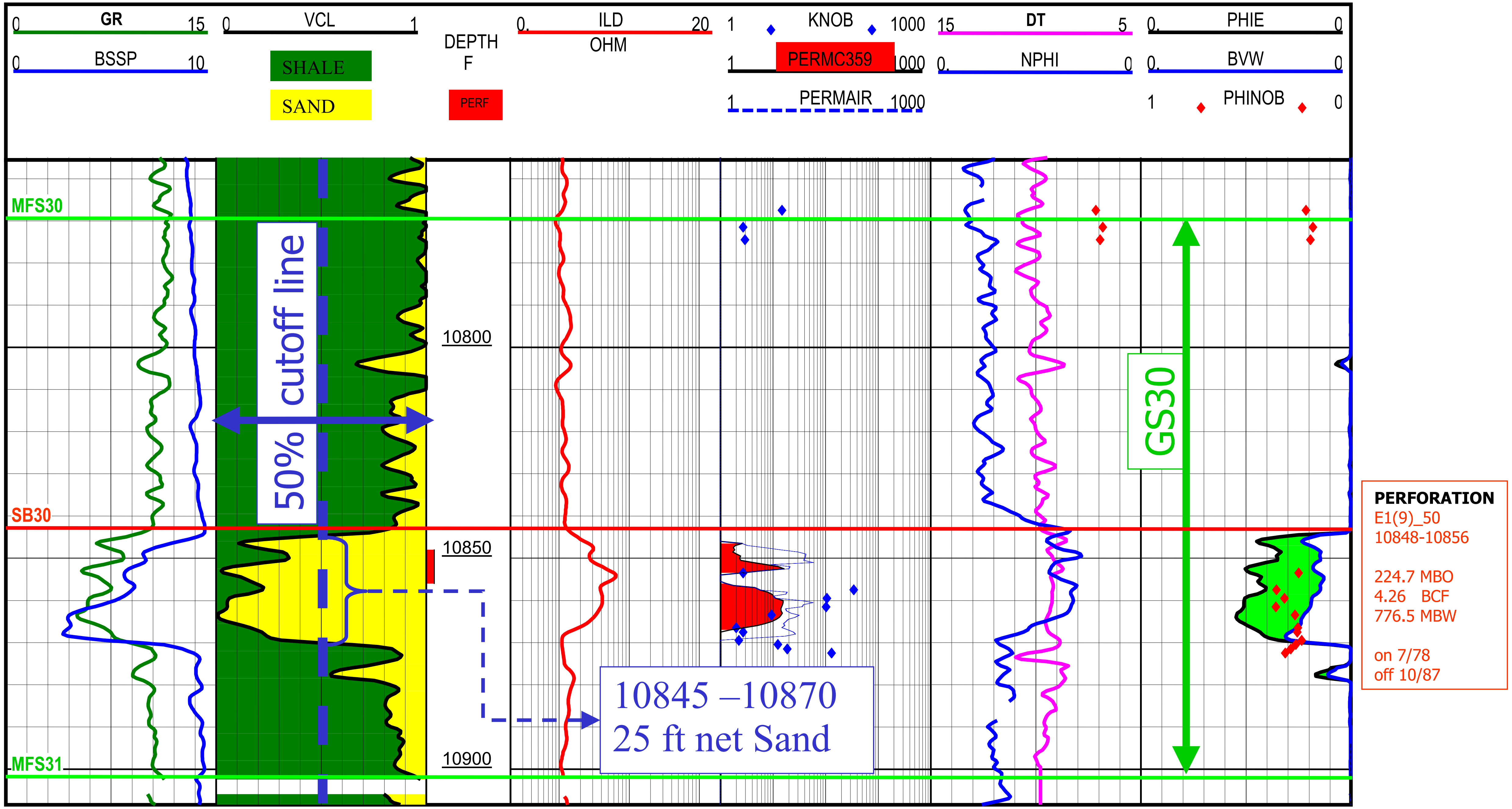

Figure 2-21 Net sand calculation from VCL with %50 cutoff. Well (50_E1(9), GS30 (MFS30-MFS31) has 25 ft of net sand and has produced oil and gas. GR-Gamma ray, BSSP-baseline shifted SP, VCLQ-volume of clay, ILD-deep resistivity, KNOB-corrected core permeability, DT-sonic, NPHI-neutron porosity, PHIE-effective porosity, BVW-bulk volume of water, PHINOB-corrected core porosity.

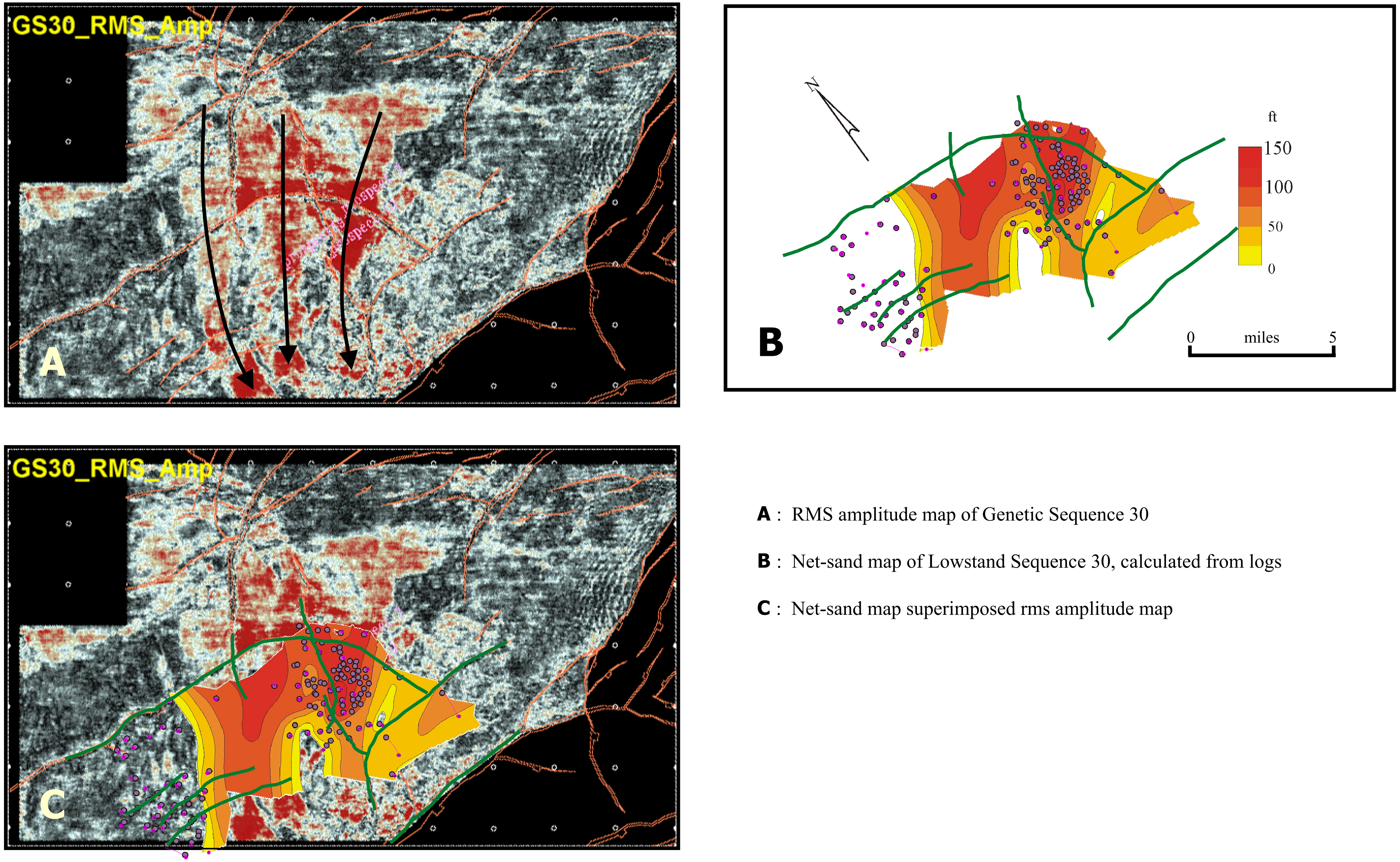

A : RMS amplitude map of Genetic Sequence 30

B : Net-sand map of Lowstand Sequence 30, calculated from logs

C : Net-sand map superimposed rms amplitude map

Figure 2-22. Comparison between RMS30 map and LST30 net-sand map. A: RMS amplitude map of GS30 with major incisions. B: Net-sand map of LST30. C: Net-sand map superimposed over RMS map. Major incision and sand deposition trends match very well.

Chapter 3. Geology

REGIONAL SETTING AND FRAMEWORK

The study area is located 10 mi south of the Louisiana coast, in the axis of the Central Mississippi sediment-dispersal system (Galloway et al., 2000; **Figure 3-1**). The Miocene in the study area is more than 11,000 ft thick and is divided into Upper, Middle, and Lower Miocene successions based on foraminiferal data. Ages of each succession were determined by faunal floods and extinction horizons identified in 14 wells using available faunal data (Wood et al., 2001, **Figures 3-2 and 3-3**).

The Miocene of northern Gulf of Mexico (GOM) is alternatively divided into four depositional episodes: Lower Miocene 1 (LM1), Lower Miocene 2 (LM2), Middle Miocene (MM), and Upper Miocene (UM) (Galloway et al., 2000). Fillon and Lawless (2000) combined LM2 and LM1 episodes and lower "Cristellaria I" (a fourth-order sequence from Middle Miocene) into one second-order supersequence of Lower Miocene. This second-order sequence starts with a major sea-level fall at the beginning of the Miocene, corresponds to LM1, and continued with sea-level rise, corresponds to LM2, from "Marginulina A" (Marg A) through "Amphistegina B".

The oldest and deepest sequence penetrated in the study area is the upper part of the Lower Miocene (LM2). This unit is bounded at its top by a strong faunal flood containing the "Robulus L/Cibicides 38" (Rob L/Cib 38) fauna and on the bottom by another strong faunal flood containing the "Marg A" fauna.

This basal event is described by Galloway et al. (2000) as a "short break in deposition between basin-floor fan, slope fan, and shelf-edge deltas of LM1 and widely spread shelf and shelf edge deltas of LM2". This section between "Marg A" and "Rob L", mostly corresponds to the Late Early Miocene (LM2) depositional episode of Galloway et al. (2000), but the upper boundary of LM2, the "Amphistegina B" (Amph B) marker, is slightly higher than Rob L/Cib 38 (Figure 3-3).

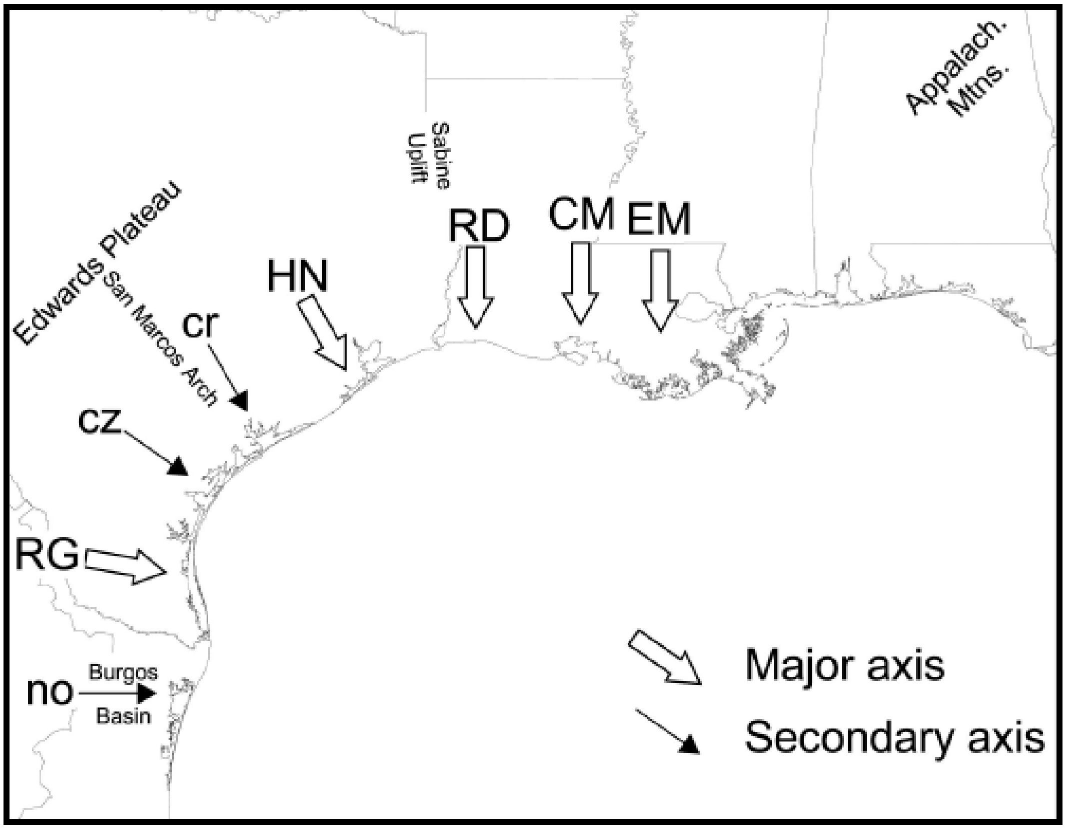

Figure 3-1. Cenozoic sediment dispersal axes. no=Norias, RG=Rio Grande, cz=Carrizo, cr=Corsair, HN=Houston, RD=Red River, CM=Central Mississippi, EM=East Mississippi (Galloway et al., 2000).

During the Early Miocene, "shifting fluvial axes created a widespread sediment dispersal system, and rejuvenated the Mississippi delta, which advanced the shelf edge 40 to 50 mi. seaward by apron offlap. The Texas sediment dispersal axis shifted from the Houston embayment to the Red River and created the fluvial-dominated Calcasieu delta on a collapsing margin and resulted in a sandy delta-fed apron, which was the main early Lower Miocene depocenter. This period of sediment influx was punctuated by marine flooding, which deposited the shale tongue containing "Marg A" fauna" (Galloway et al., 2000). After a short break in deposition, the central Gulf system progressed again and deposited basin-floor fan, slope fan, and shelf-edge deltas (DeAngelo et al., 2000). The "Rob L" sequence in particular exhibits the highest bulk deposition in the Lower Miocene but less sand content than previous sequences, indicating possible bypass into those basin-floor fans and slope-fans (Fillon and Lawless, 2000).

The Middle Miocene is the most densely logged section in the study area, and is bounded by flood events containing "*Robulus* L / *Cibicides* 38" and "*Cibicides carstensi*" faunas (Figure 3-3). This zone is defined slightly thicker than the Middle Miocene (MM) depositional episodes of Galloway et al. (2000), between two flooding events containing "*Amphistegina* B" and *Textularia* "W" / "*Textularia stapperi*" faunas (Figure 3-3). Central and East Mississippi deltas dominated the northern Gulf Margin and the Central Mississippi delta progressed rapidly and advanced the shelf margin more than 20 mi (Galloway et al., 2000). "*Cristellaria* I" sequence (Cris I), lowest member of the Middle Miocene, deposited mainly in South Texas initially as a part of Corsair Delta, and in southwestern Louisiana depocenters, afterward as Central and Eastern Mississippi deltas (**Figures 3-4, 3-5**). This shift is interpreted as the result of the capture of Red, Arkansas, and Canadian river drainage systems by the Mississippi River. “Cris I” sequence was deposited during high-stand of the second-order supersequence and covers the larger area than the following three Middle Miocene sequences. During falling sea level, *Bigenerina humblei* (Big hum) and “*Textularia stapperi* / *Textularia* W” (Tex W) sequences prograde and offlap underlying “Cris I”. “*Cibicides carstensi*” (Cib carst), the last sequence of the Middle Miocene, onlaps “Tex W” and indicates the end of falling sea level (Fillon and Lawless, 2000, Figure 3-5). In the study area, the Middle Miocene is composed of cyclic prograding and retrograding deltaic successions, shelf-edge deltas, and incised valleys. Based on work using faunal assemblages it is interpreted that the sediments in this interval were accumulated in upper slope/outer shelf to fluvial environments in marine water depths that ranged from upper bathyal to marginal marine (**Figure 3-6**).

The upper boundary of the Miocene is hard to define in the GOM. In this study, it is marked at the first downhole appearance of “*Robulus* E” zone, which coincides with Galloway et al.’s (2000) Upper Miocene Pliocene *Buliminella* 1 (UMPB1) boundary. In the study area, the Upper Miocene is primarily composed of cyclic proximal deltaic and shelf successions and incised-valley fills. Based on work using faunal assemblages it is interpreted that the majority of the sediments in this interval were accumulated in inner-shelf to fluvial environments in marine water depths that ranged from middle neritic to marginal marine. Regionally, the composite Mississippi Delta System dominated deposition along the central Gulf margin and thick shelf-margin delta and slope apron accumulations advanced the shelf edge some 20-25 miles basinward.

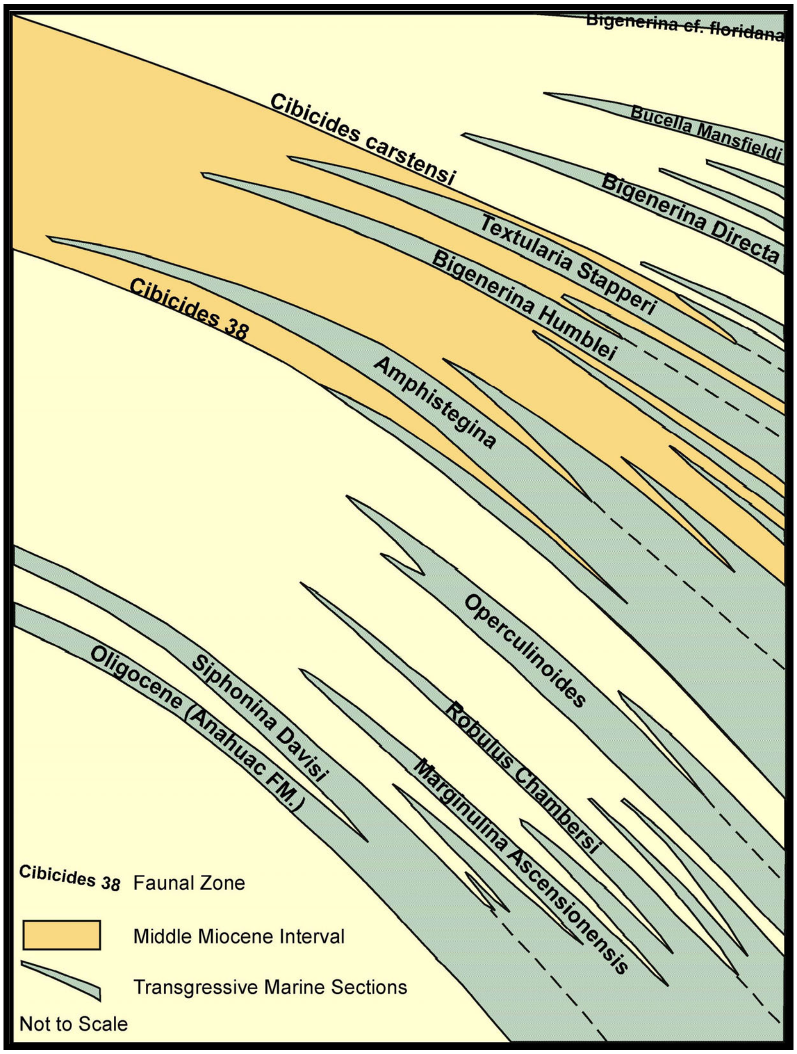

Figure 3-2. Schematic section of marine transgressive tongues in the Gulf of Mexico (modified from Rainwater, 1964).

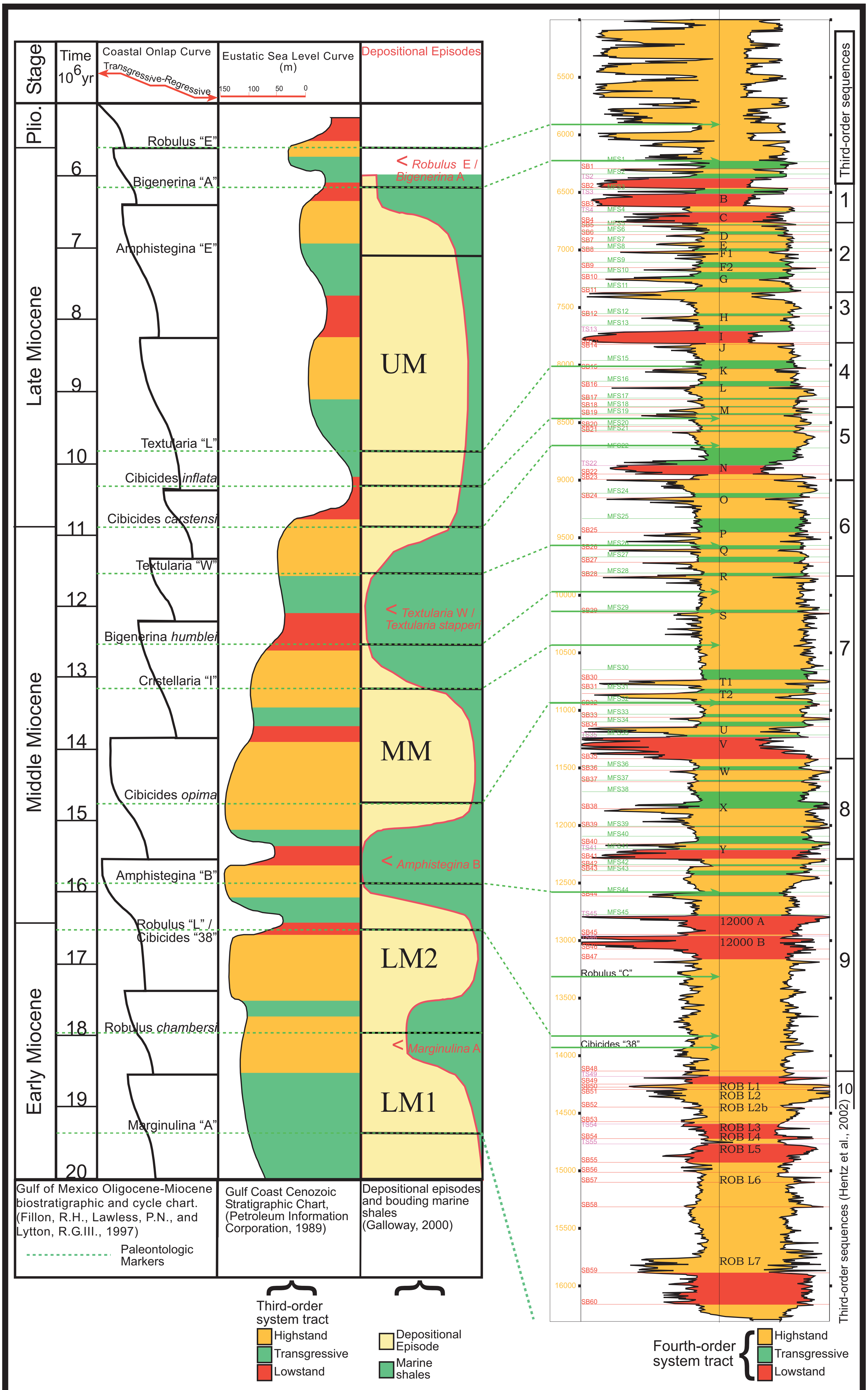

Figure 3-3- Comparison of GOM coastal onlaps, eustatic sea-level changes, depositional episodes, biostratigraphic extinction horizons with sequence stratigraphic interpretation and paleontological data from well_3_31. Although similar depositional trends can be observed in all charts in third-order scale, there are many fourth-order cycles that are not identified in those charts. Especially, salient low-stand deposits between 11,000 ft and 13,500 ft (U, V, Y, 12,000A and B sands) indicate higher frequency sea-level fluctuations.

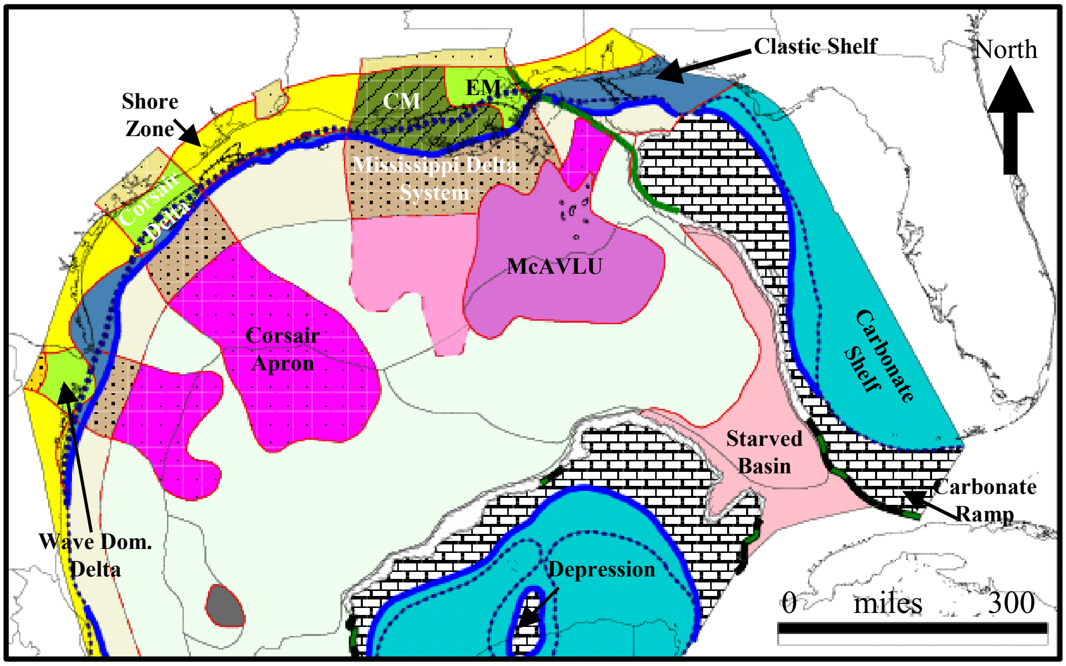

Figure 3-4. **Paleogeography of the Middle Miocene. Central and Eastern Mississippi (CM and EM) dominated the northern GOM (modified from Galloway, 2000).**

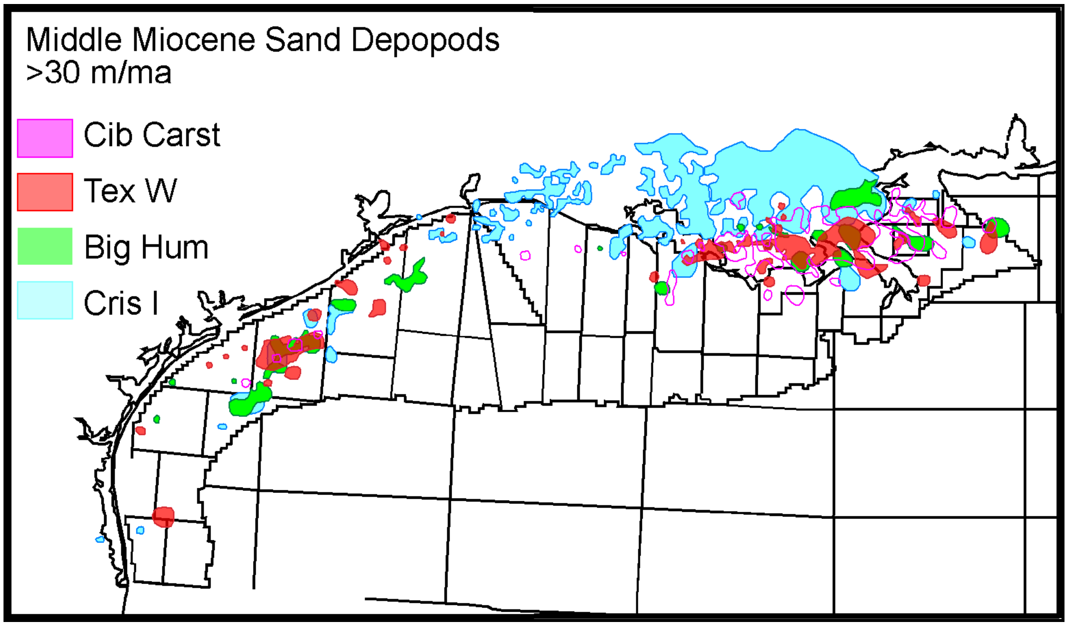

Figure 3-5. **Middle Miocene sand depocenters. Most of the sand was deposited in eastern Mississippi (modified from Fillon and Lawless, 2000).**

STRATIGRAPHIC FRAMEWORK

The data used to establish a stratigraphic framework for this study included log curves from 157 wells, detailed paleontological information available at 15 wells and 300 mi^2 of 3-D seismic data. SP (Spontaneous Potential) and ILD (Deep Resistivity) are the most common curves in all of the wells. These were the curves most commonly used in making correlations across the study area. Where no SP curves were available or they were affected by gas presence, the GR was substituted for correlation purposes. Ages of flooding surfaces and sequence boundaries were established on fossil content. Samples were recorded every 30 ft, and fossil assemblages, presence of individual species, and abundances in each well were accounted for.

Biostratigraphy

Although the International Union of Geological Sciences (IUGS) Committee on Mediterranean Neogene Stratigraphy recommends that key stratigraphic boundaries be identified by the first appearance upward in the section of certain species, other studies have also shown the utility of carefully used first downward appearances (Galloway et al., 1991; Pocknall et al., 1998; Wood et al., 2000). Our data support this observation regarding the utility of the first downward appearance of certain fauna as their “extinction” horizon. All first upper and first downward appearances, as well as abundances of any fauna, must be observed in consideration of potential horizons of reworking or casing point filtering of caved microfauna.

Texaco's paleontological reports have been examined for prominent fossil extinction horizons and paleobathymetric environments. There are 14 foraminifera-based biozone reported in the study area, ranging from the "*Cibicides* 38 / *Robulus* L" (~16.5 my) zone at the bottom of section to the "*Robulus* E" (~6.1 my) zone at the top of the Miocene section (Figures 3-3 and 3-6). Indicator benthic fossils, which lived in narrow ranges of water depth, were used to reconstruct the paleobathymetric conditions under which the sediments were deposited (**Table 3-1**). Environments across the section range from subaerial to bathyal. Overall the section shallows upward with the deepest water depths conditions (>600 ft, upper bathyal) recorded at the bottom of the sections. The basal sections are typically characterized by slope fan and basin-floor fan deposits. In addition several deepening events occur in shales associated with specific fauna flooding events such as "*Cristellaria* I", and "*Bigenerina humblei*" (~15 my, Wood et al., 2001; Figure 3-6).

Table 3-1. Characteristic paleobathymetric indicator fossils (foraminifera) in the Miocene section of Starfak and Tiger Shoal fields (Picou et al., 1999).

Marginal Marine	***Ammonia beccarii*** ***Elphidium spp.***
Inner Neritic (0-60 ft)	***Bifarina vicksburgensis*** ***Bucella mansfieldi*** ***Cibicides concentricus*** ***Eponides spp.*** ***Noniella spp.*** ***Reusella spp.***
Middle Neritic (60-300 ft)	***Bolivina floridana*** **(rare)** ***Cancris sagra*** ***Cibicides carstensi*** ***Cibicides floridanus*** ***Gyroidina hannai*** ***Uvigerina peregrina*** **(rare)**
Outer Neritic (300-600 ft)	***Ammobaculites nummus*** ***Bolivina floridana*** **(common to abundant)** ***Chilostomella spp.*** ***Cibicides opima*** ***Gaudryina atlantica*** ***Gyroidina scalata*** ***Liebusella spp.*** ***Pullenia salisburyi*** ***Textularia baretti*** ***Uvigerina altacostata*** **(rare)** ***Uvigerina carapitana*** ***Uvigerina howei*** ***Uvigerina lirettensis*** ***Uvigerina peregrina*** **(common to abundant)** ***Valvulinaria spp.***
Upper Bathyal (600-1500 ft)	***Anomalina alazanensis*** ***Cibicides matanzanensis*** ***Cyclammina cancellata*** ***Liebusella pozonensis*** ***Planulina harangensis*** ***Uvigerina altacostata*** **(common to abundant)**

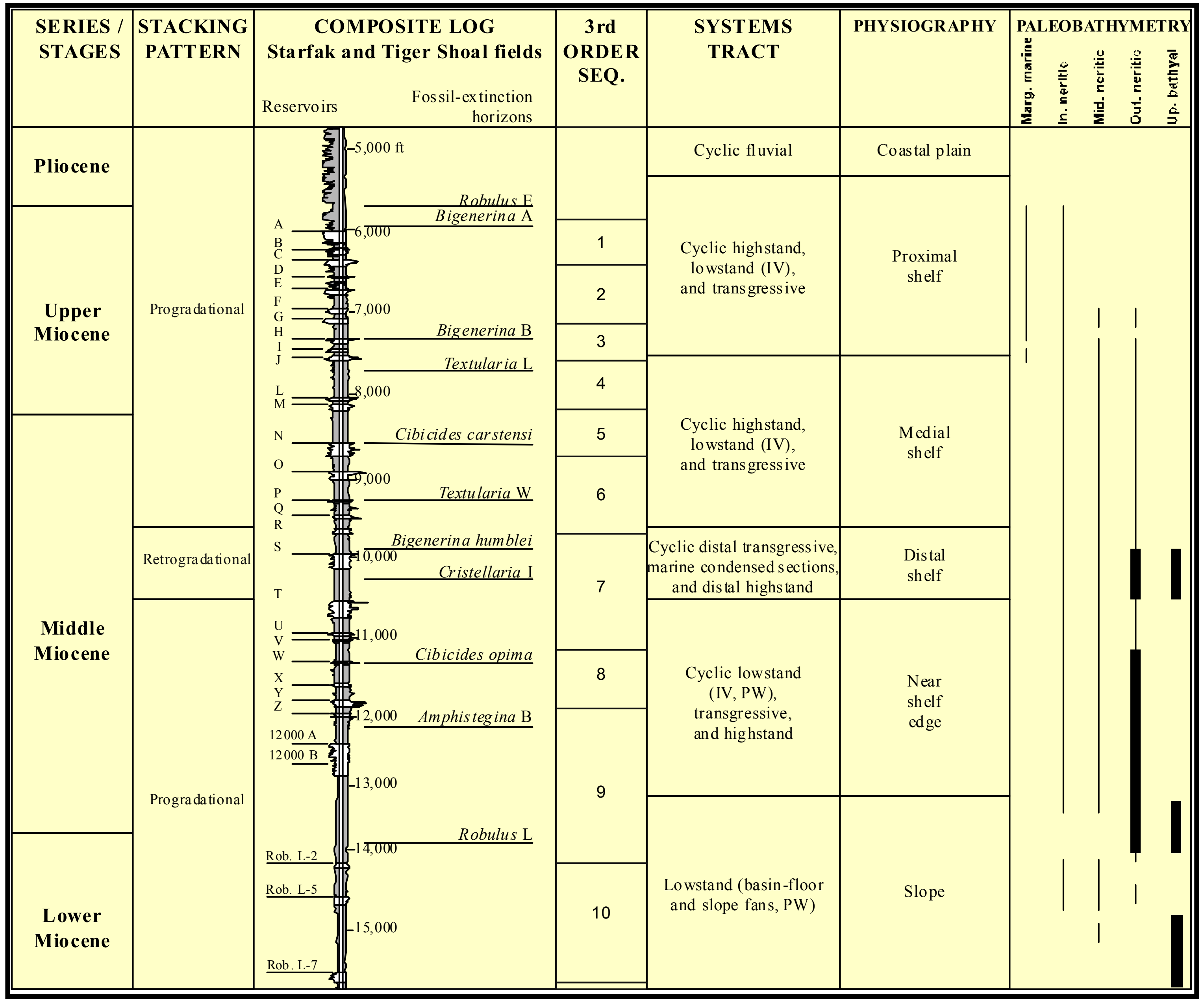

Figure 3-6. Type log of Starfak and Tiger Shoal fields that displays gross stacking patterns, reservoir nomenclature, fossil extinction horizons, sequence system tracts, basin physiography, and bathymetry (Modified from Wood, 2001).

Sequence Stratigraphy

The Miocene succession across the study area is more than 10,000 ft thick, and comprises 10 third-order and more than 60 fourth-order sequences. Each fourth-order sequence averages ~0.19 my in duration. Sequences are numbered from 1 (*Robulus* E, top of the Miocene) to 60 (base of *Robulus* L faunal zone) (Figure 3-3). Major flooding surfaces, which are characterized by major increases in faunal count and diversity, were used efficiently to divide the section. Depositional episodes, LM2, MM, and UM, were identified in both well-log and seismic sections, except the "*Marginulina* A / *Operculinoides*" flooding surface. This surface defines the boundary between two depositional episodes, LM2 and LM1, and is deeper than available log data.

The Middle Miocene interval includes 25 fourth-order sequences and extends from MFS48 (Maximum Flooding Surface 48), which coincides with the "*Robulus* L/*Cibicides* 38" regional biozone horizon (~16.5 my) to MFS22, which coincides with the "*Cibicides carstensi*" regional biozone horizon (~10.9 my). These 25 fourth-order sequences have been grouped into five third-order sequences, (sequence 9^{3rd}[1] through 4^{3rd} of Figure 3-6; Hentz and Zeng, 2003). Third-order system tracts and their stacking patterns vary relative to their position in the shelf-to-basin depositional profile (Mitchum and Van Wagoner; 1991; Mitchum et al., 1993); and in the study area Middle Miocene sequences are divided into two parts; upper slope (medial section), and shelf (proximal section) (**Figure 3-7**).

---

[1] 9^{3rd} indicates 9th third-order sequence

Middle Miocene Upper Slope; (MFS48 to MFS42)

The distal part of the Middle Miocene section is as thick as 2000 ft (Figures 3-7, and **3-8**), and extends from MFS48 to MFS42. This portion of the succession mostly corresponds to the 9th third-order sequence of Hentz and Zeng (2003), with the exception of the sequence boundaries at the top and bottom, SB48 and SB41, since they used the erosional surfaces as boundary of the sequences (Figure 3-6).

The bottom third of the sequence is dominated by a thick (~800 ft) shale section, periodic, upward-coarsening and upward-fining zones of interbedded thin (10') shaly sandstones (Figure 3-8, at ~14,200-13,500 ft). This thick shale contains "*Robulus* L and *Cibicides* 38" faunal biozones, marks the boundary between the Lower and Middle Miocene stages, and indicates outer neritic to upper bathyal paleobathymetric position of the depositional system (Figure 3-6 at ~13,800 ft). Shale-dominated lithology, fan-shaped sandstone distribution, and middle neritic fossil content suggest dominantly slope-fan complexes.

The middle third of the sequence is about 600 ft thick and is composed of interstratified, shale and upward-coarsening, blocky, blocky-serrate sand units. Each unit is about 200 ft thick. Sandstones have sharp erosional base, and were interpreted to incise into older beds (Figure 3-8, at ~13,000 ft). Individual sandy units are as much as 120 ft thick, and contain blocky, blocky-serrate sandstone units, which are characterized as basin floor fan, and prograding wedge deposits. These sandy units are interpreted to be deposited following the incision of shelf during lowstand (LST), and 'total absolute amplitude' of GS45 shows the extent of fourth-order wedges (**Figure 3-9**).

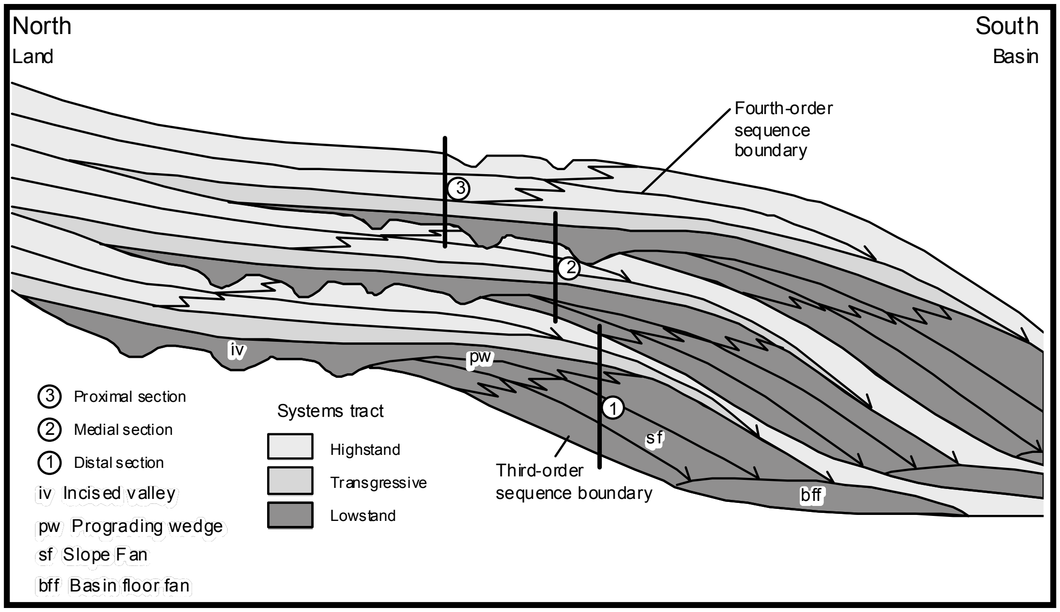

Figure 3-7. Stacking pattern of third-order sequences, and systems tracts. The Middle Miocene study interval comprises the second and third sections (Hentz et al., 2002).

The upper third of the sequences is dominated by ~ 400-ft-thick marine shales, with locally developed thin, upward-coarsening sandstone units. This section is interpreted as a third-order Highstand System Tract (HST), comprising fourth-order poorly developed sandy HST units and thin shaly Transgressive System Tracts (TST) units. A fourth-order flooding surface caps the "*Amphistegina* B" faunal biozones (Figure 3-8, at MFS44, ~ 12,600 ft), separates Galloway's (et al., 2000) LM2 from the MM depositional episode, and should have been identified as the third-order MFS, in place of MFS45.

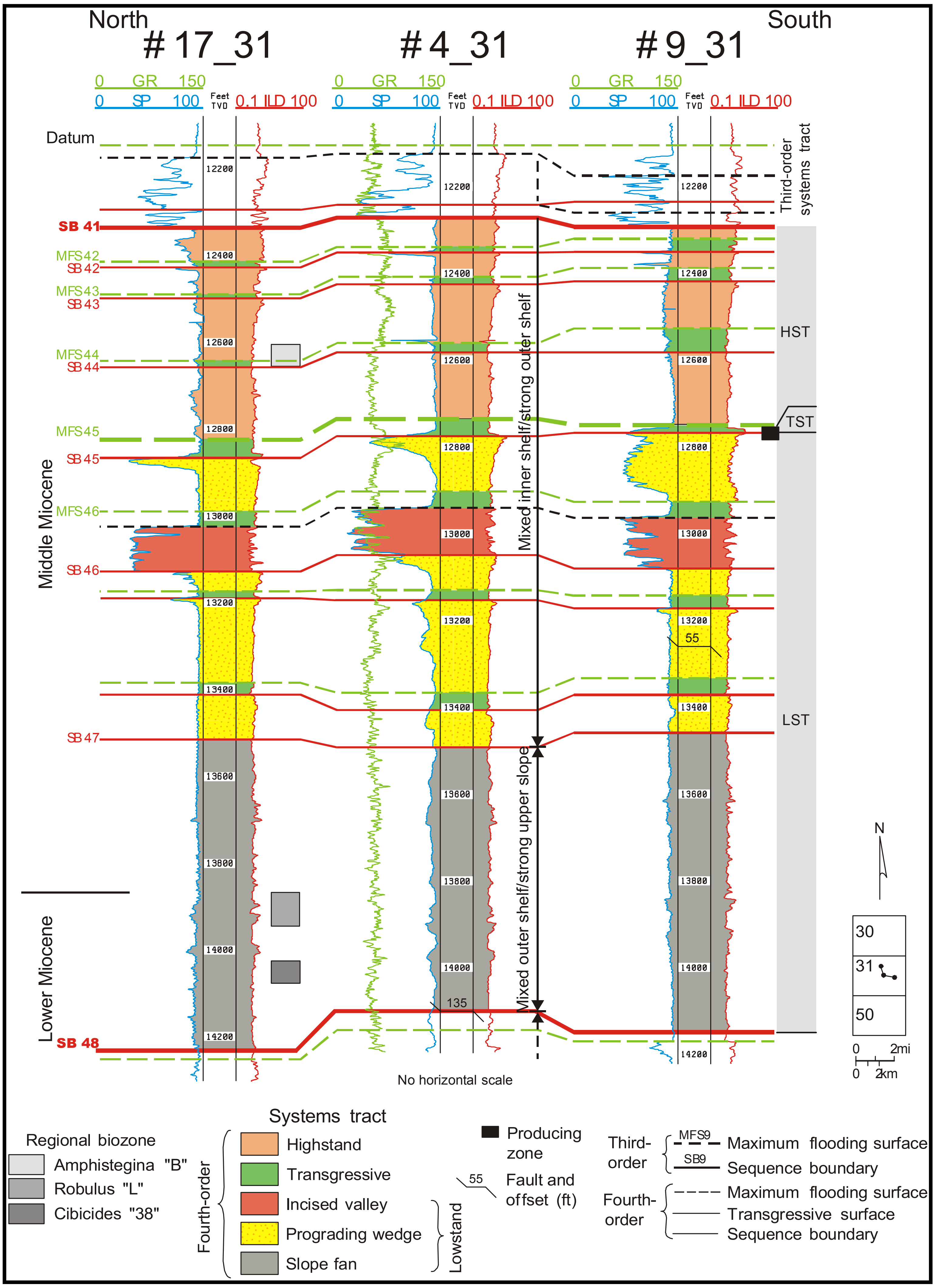

Figure 3-8. Middle Miocene Slope Sequences. Fourth-order prograding wedges (well 9-31 at 12,800 ft) and incised valley-fill sandstones of 3rd order lowstand system tracts are productive (Wood et al., 2001).

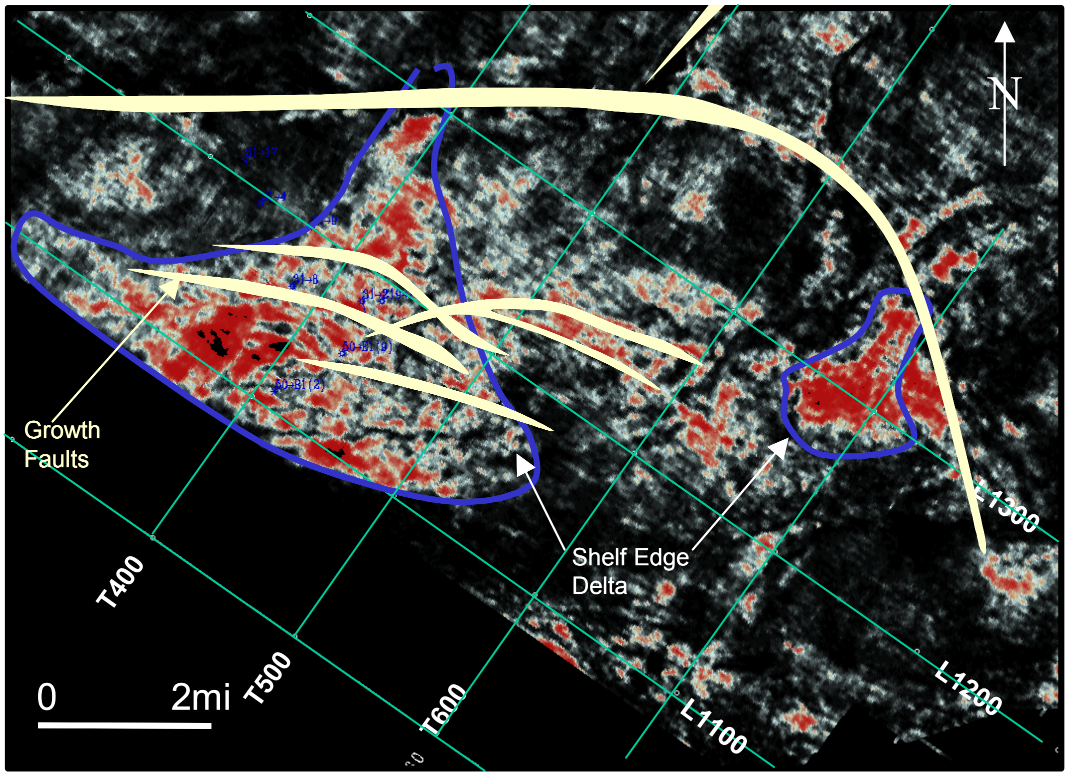

Figure 3-9. Total absolute amplitude map of GS45. Delta is located basinward of a large growth fault, which defines the shelf-edge. Delta front is dissected by growth faults.

Middle Miocene Shelf; (MFS42 to MFS22)

The middle part of the Middle Miocene section is about 3500 ft thick and extends from MFS42 to MFS22 (Figures 3-3 and **3-10**, reservoir Y to N). Its deposition was initiated by a sea-level drop shortly after the "*Amphistegina* B" flood and lasted until another large flood, containing "*Cibicides carstensi*" biozones (Figures 3-3, 3-6, and **3-11 through 3-14**). Sequences on the shelf are thicker, sandier, and have more fluvial components than slope predecessors. Initially they start as alternating incised valley and prograding wedge (shelf edge) and after a flood containing "*Cristellaria* I" continue as cyclic marine and fluvio-deltaic systems (distal to medial shelf, Figures 3-5, 3-6, 3-11 and **3-12**).

The lower part of the section is dominated by sharp-based, blocky, blocky-serrate, and upward-fining to aggradational (50-250 ft thick) sandstone units, which are bounded below with locally pronounced erosional surfaces (**Figure 3-11**, about 12200 ft). Sea-level drop following the "*Amphistegina* B" flood caused shelf exposure, fluvial incision of previous shelf mud and delta-front deposits. Fluvial entrenchment surfaces and overlaying sharp-based alluvial valley fills and amalgamated channel fills directly overlie open marine shales, indicating a significant basinward shift in facies, and the development of Type I and II sequence boundaries (*sensu* Wan Wagoner et al., 1990).

These prominent sequence boundaries can be correlated landward to the top of an upward-coarsening succession of relatively thinner deltaic sandstones (**Figure 3-11**, SB40 from well 11_31 to 5_31 at 12200), and basinward to the bottom of an upward-coarsening progradational (~ 300 ft) thick sandy units (**Figure 3-12;** SB35 from well 11_31 at 11420 to well 16_31 at 11500).

Progradational units are restricted to the south portion of the Starfak and Tiger Shoal fields, and they generally lack the upper-bathyal to outer-neritic basal shale of shelf sequences (Hentz and Zeng, 2003). Incised valley systems bypass sediment into the deeper basin and create lowstand wedges. Fourth-order sandstone units are the thickest at the crest of the lowstand wedge, which typically corresponds to the deposition of the coarsest sediment (Galloway, 1998).

Landward, sequence boundaries continue as exposure surfaces and fluvial system erode into older underlying prograding highstand shelf and coastal zone deposits (**Figure 3-12**, SB31 from well 11_31 to 4_31).

The upper part of the section, which begins with "*Cristellaria* I" flood (MFS30), is dominated by mostly upward-coarsening sandstone/shale units and local upward-fining incised valley deposits (Figures 3-12 and **3-13**). These sand/shale units stack to form a progradational third-order highstand sequence set. Both grain sizes and bed thickness increase upward in this sequence set. Fourth and third-order sequence boundaries represent periods of sediment bypass along incised valleys into slope, developed during the Upper Middle Miocene in the south of the study area. The N sand is one of the most prominent incised-valley deposits in the area developed during fourth-order lowstand in this third-order highstand, along with the M sand from genetic sequence 18 (GS18) of the Upper Miocene (Figures 3-10 and **3-14**).

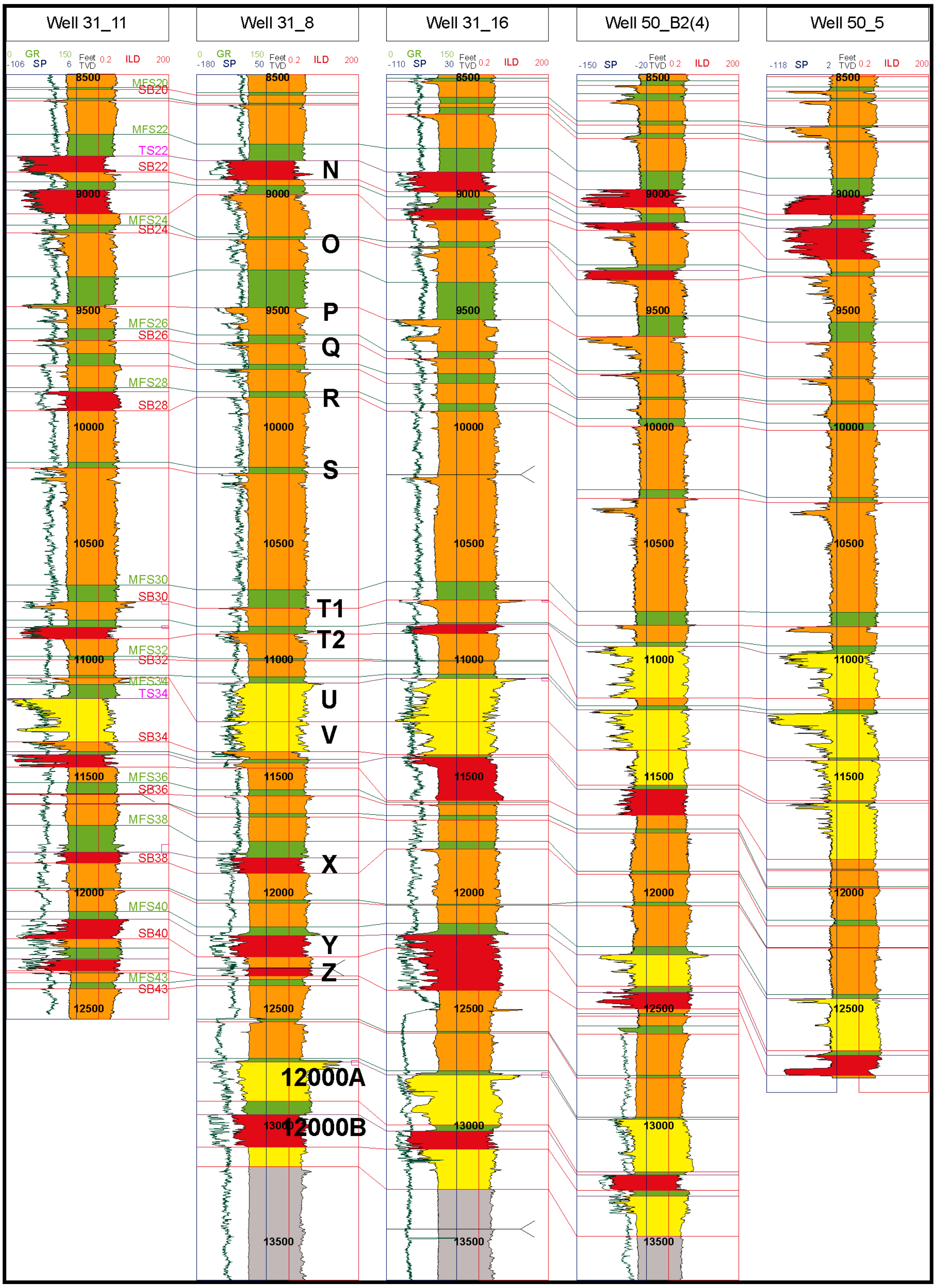

Figure 3-10. Middle Miocene sequence stratigraphic correlation and named reservoirs. Red=incised valley, yellow=lowstand wedge, green=transgressive and orange=highstand deposits.

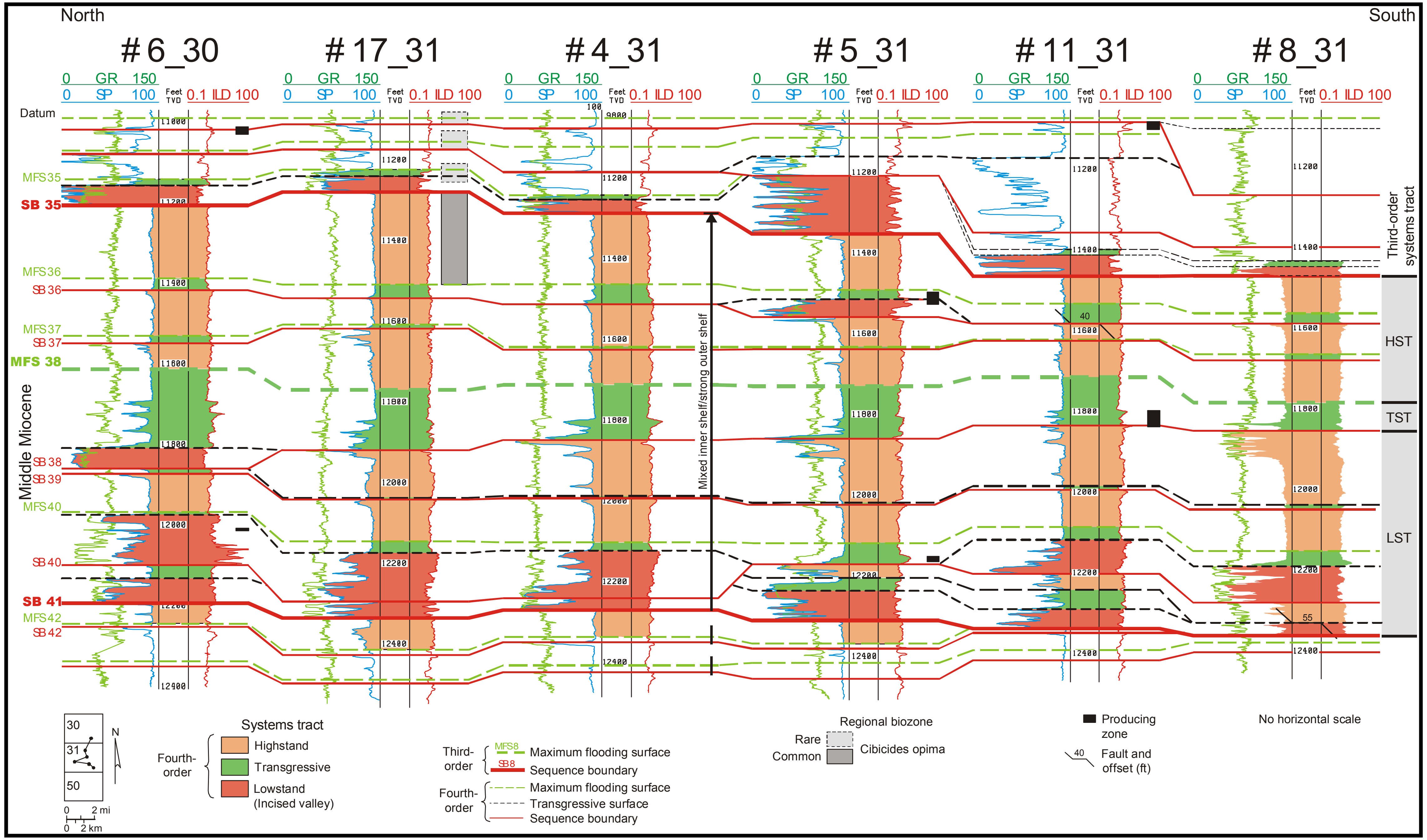

Figure 3-11. Dip cross section of Starfak field Middle Miocene shelf sequences, lower part. Fourth-order incised valley fill, transgressive and highstand deltaic strandplain sandstones, mostly in the lower third-order system tract produce hydrocarbon (Wood et al., 2001).

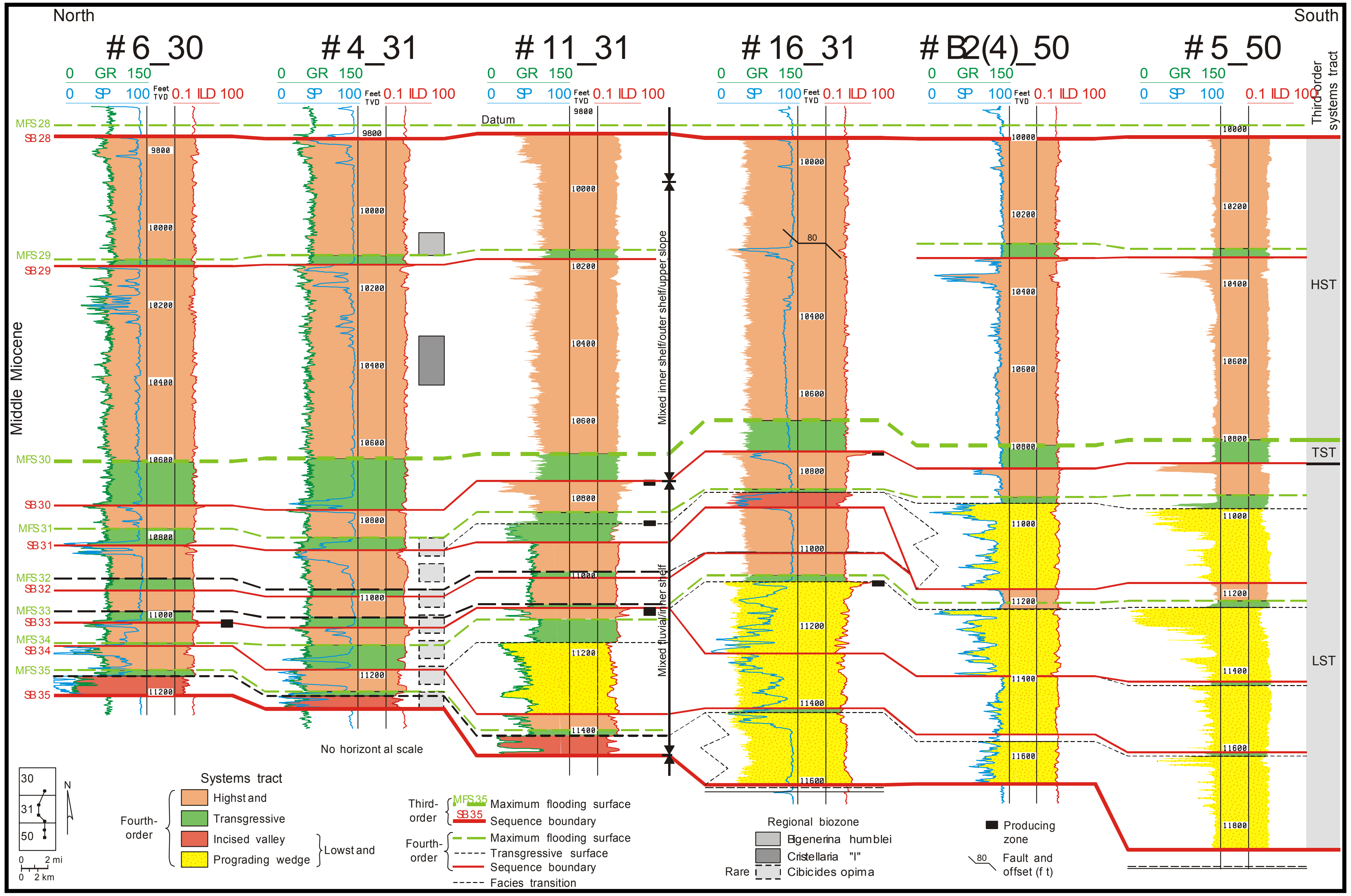

Figure 3-12. Dip cross section of Starfak field Middle Miocene shelf sequences, upper part. Fourth-order prograding wedge, transgressive and highstand deltaic strandplain sandstones, mostly in the lower third-order system tract produce hydrocarbon (Wood et al., 2001).

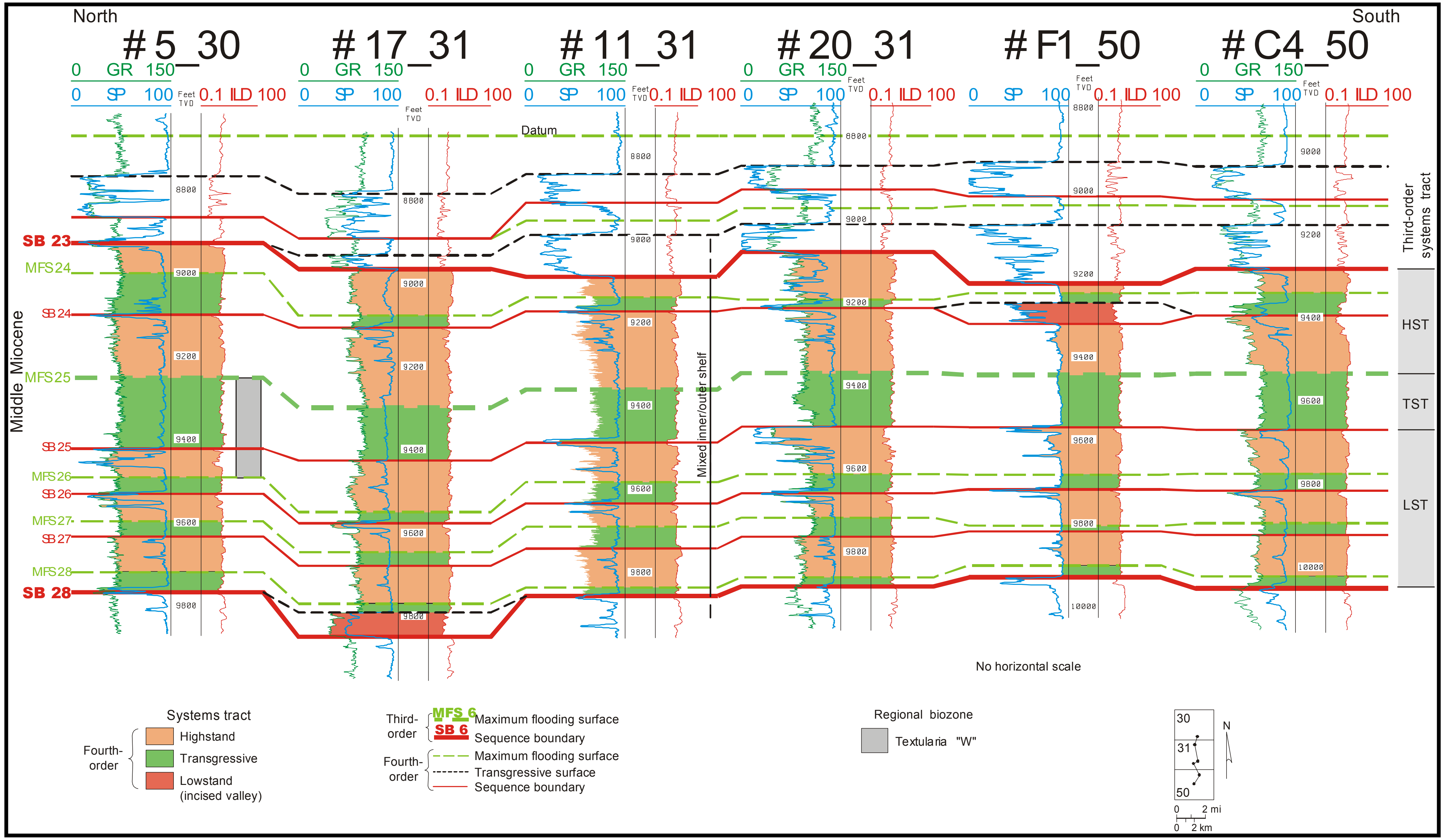

Figure 3-13. Dip cross-section of Starfak field Middle Miocene shelf sequences, upper part, continued. Structurally down dip Starfak field has less production than updip Tiger Shoal field (Wood et al., 2001).

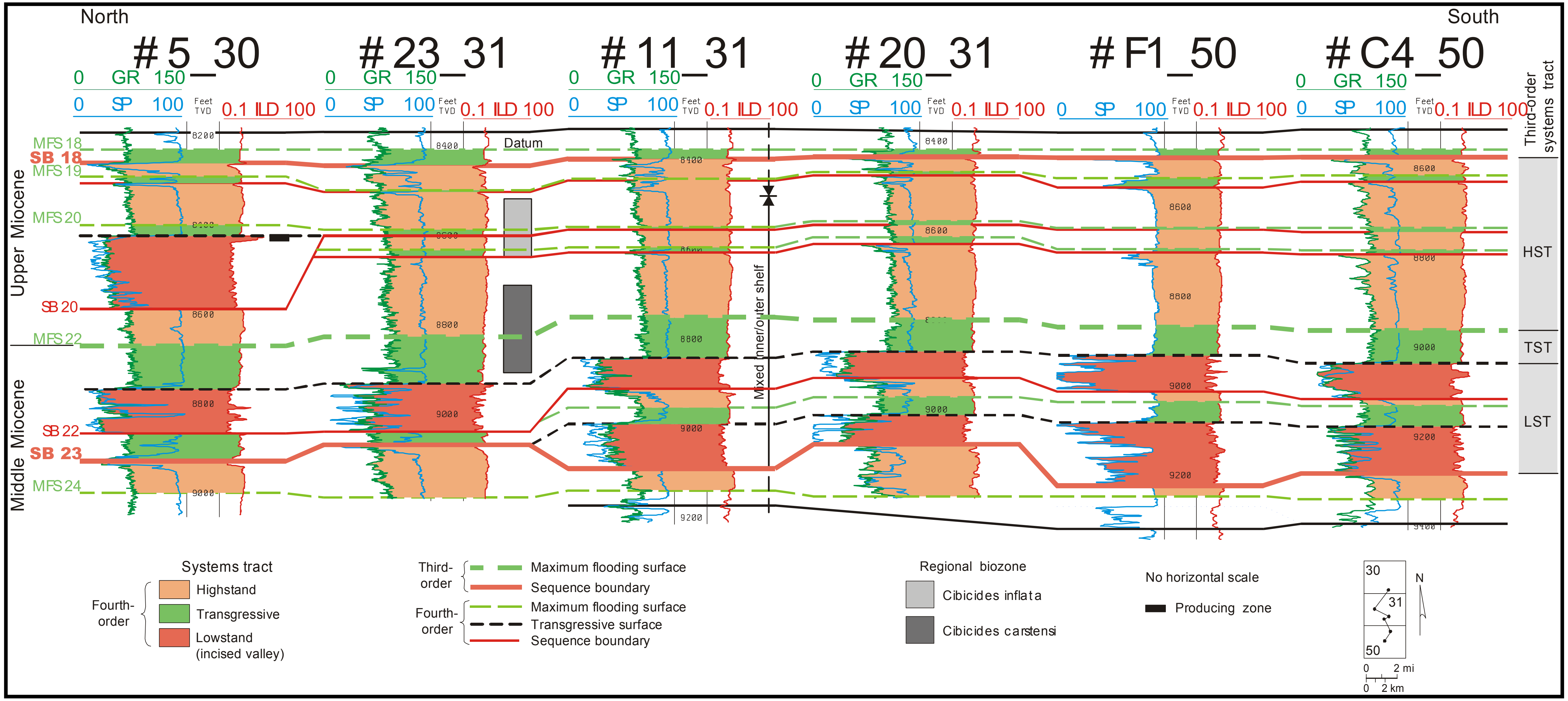

Figure 3-14. Dip cross-section of Starfak field. ***Cibicides carstensi*** **marks the transition from Middle Miocene to Upper Miocene during third-order transgression. Fourth-order incised valleys concentrated at third-order lowstand system tract (Wood et al., 2001).**

Ages and correlation with eustasy

While third-order sequence boundaries dictate the position and range of depositional systems, fourth-order sequences become more important for individual reservoir distribution in the third-order successions, reservoir quality and production predictions, and as well as for fault-seal analysis. Therefore, recognizing fourth-order sequence boundaries and flooding surfaces in 3-D seismic data and well logs is of utmost importance.

Depositional history of the study area and a detailed framework of reservoir distribution have been established by chronostratigraphic and sequence stratigraphic analyses. Study indicates 10 third-order and more than 60 fourth-order sequences in the first 10,000 ft of Miocene section, as well as second-order sequence boundary (SB23), slightly below the flood separating Middle and Upper Miocene units (Hentz et al., 2002). Ages of regional GOM biozones encountered in the study were derived from Lawless et al. (1997) and converted to those of Berggren et al. (1995; Figure 2-13).

In the study area, the overall succession indicates a prevalence of third-order, regressive depositional systems, an observation that deviates from Haq et al. (1988)'s global coastal-onlap curve (Hentz and Zeng, 2003). This can be explained by the location of study area to be in the "CM" (Central Mississippi) major sediment axis (Galloway et al., 2000). It is likely that within this area high volumes of sediment and overall strong regressive shorelines masked the global transgressive processes.

Chapter 4: Reservoir Characterization and Quantification

FREQUENCY ENHANCEMENT

Twenty-five fourth-order genetic sequences have been interpreted in the Middle Miocene section, using well logs and paleontological data. Although these sequences can be defined from well logs, it is not possible to identify every individual fourth-order flooding surface on standard 3-D seismic data. Unless they are third-order surfaces, many of the sequence boundaries cannot be resolved on the shelf.

Boosting amplitude of high-frequency reflections allows more accurate interpretation of fourth-order flooding surfaces. To identify and amplify the high-frequency reflections, an algorithm, “Spectral Balance”, was applied to seismic data, and the procedure is defined as:

“From each input trace, a series of component traces is derived. Each trace series represents various frequency ranges and individual traces are called “frequency-limited traces[1]”. Each frequency-limited trace is applied a gain (scaled) to normalize the contribution from different frequency ranges surrounding itself in the time window. The “scaled-frequency-limited traces” are then recombined into a single trace, and the average scalar factor is removed from the data*”* (Landmark PostStack/PAL User Guide, 1996).

Frequency content of the seismic data is identified and a spectrum of reflection amplitudes created (Figure 2-10). Frequency spectrum of the interest

---

[1] Trace transformed into time by an inverse FFT (Fast Fourier Transform)

zone is divided into a certain number of groups, and amplitudes of frequency-limited traces are gained by a factor. This scaling factor is determined for each sample based on statistical averaging of the amplitudes in a time window surrounding that sample (Landmark PostStack/PAL User Guide, 1996).

A seismic volume, ZMIX, was created with this technique, and fourth-order maximum flooding surfaces were interpreted in this volume. The same surfaces were carried into the main volume, MIG90, and fourth-order genetic sequences were created between flooding surfaces. After this point, two different techniques were used to identify depositional systems and system tracts.

The first technique is to create similarity maps of individual fourth-order genetic sequences with neural-network analysis. The second technique is to create attribute maps and a series of proportional amplitude slices of genetic sequences.

NEURAL-NETWORK ANALYSIS

An unsupervised neural network method was chosen to identify major seismic facies by classifying seismic wavelets according to similarity. In order to achieve geologically meaningful facies maps, fourth-order genetic sequences were taken as base intervals.

Each fourth-order interval was classified into seven distinct representative wavelets, and a distribution map of these seven classes was plotted (**Figures 4-1 and 4-2**).

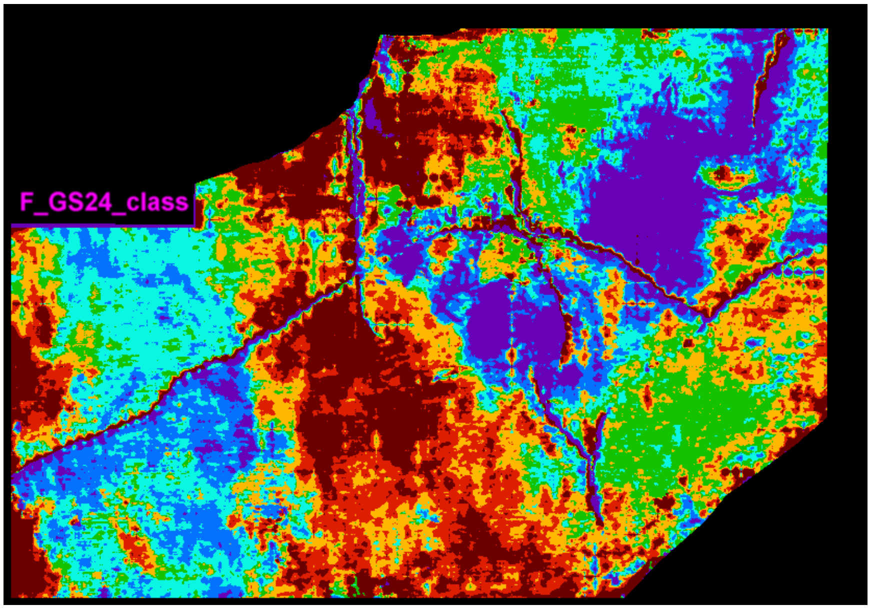

Figure 4-1. An example of seismic facies (a classification of waveforms) within the GS24 interval extracted from the seismic data volume. Classes are based on Stratimagic™ software.

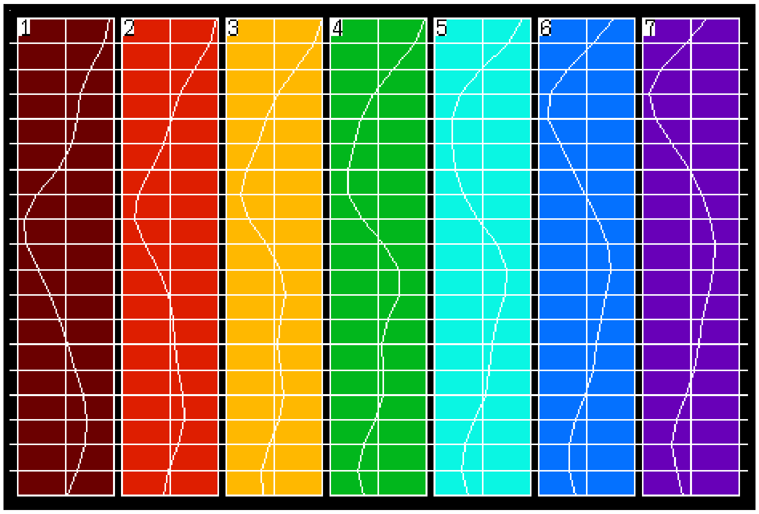

Figure 4-2. Seven representative color-coded wavelets of seismic volume used to create the "seismic facies" map.

These seismic wavelet classification maps yield major seismic events in a genetic sequence, and each seismic event is interpreted to define a depositional facies of the sequence. Since the wavelet distribution map is seismically defined, it is named a 'seismic facies map'. These maps project the summary of all the facies in the entire genetic sequence. Although they detect the edges of different facies classes, stratigraphic position of individual facies can be resolved confidently by a series of proportional amplitude slices, which is discussed in the next section.

PROPORTIONAL SLICE ANALYSIS

In order to achieve geologically meaningful facies maps with correct stratigraphic positions, nine proportionally spaced amplitude slices were taken through each fourth-order genetic sequences, defined between flooding surfaces (**Figure 4-3**). These amplitude slices, representing a parasequence time scale, were interpreted to identify individual system tracts and depositional systems.

Proportional slices were created for every fourth-order genetic sequence of Middle Miocene intervals. Two of the sequences with significant, well-identified depositional systems were interpreted in detail, and these sequences are discussed in the next section.

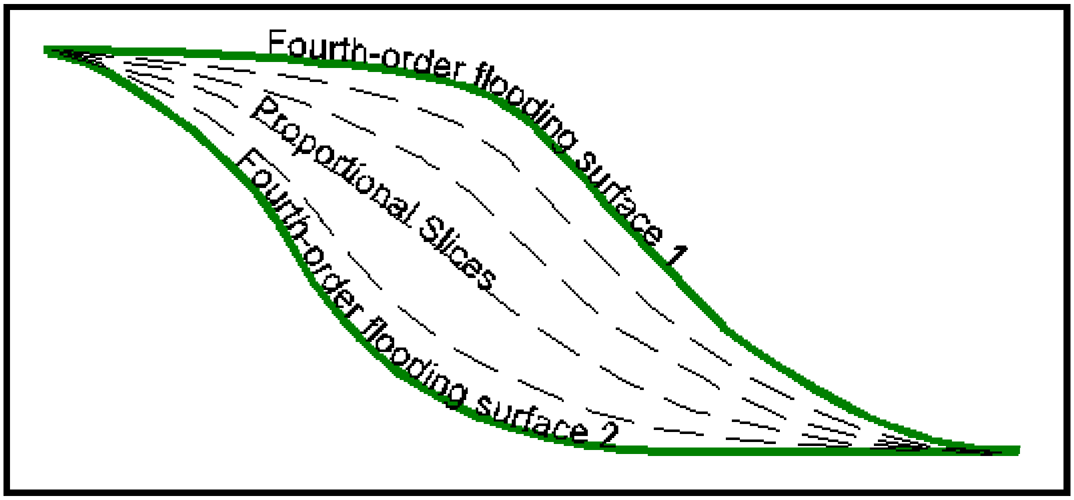

Figure 4-3. Definition of genetic sequence and application of proportional slices.

FOURTH-ORDER DEPOSITIONAL SYSTEM ANALYSIS

With confining flooding surfaces and nine proportional slices, 11 amplitude maps were produced for each sequence. In order to simplify the presentation of the maps, even-numbered slices were skipped. Depositional features were outlined on the odd-numbered slices, and their progress was tracked over time along with the interpretation of system tracts.

In some of the cases, it is possible to interpret the depositional history of the area differently than was done by Hentz et al. (2002). For those intervals, an alternative interpretation is presented.

Genetic Sequence 22 (GS22; MFS22 – MFS23, N SAND interval)

GS22 is defined between MFS22 and MFS23. With the initiation of MFS23, little sand deposition is observed in the north, and no deposition in the center and south of the area (map 11), as expected during the initial flood (**Figure 4-4a,b**).

Sediment is introduced to the area by long, relatively straight channels (map 9). These shifting semi-confined channels and lobes are interpreted as delta-front at distal shelf and/or upper slope. It is possible to see meandering channels on the west side, to the north of a large growth fault. Main sediment input is from the north.

Starting with map 7, the sand sediment system reaches the south edge of the area. Sediment load slightly shifts to the west, and deposition continues in two flanks. Although the frequency differences between the two seismic data cause a problem in the north half of the map, elongate distributary channels and delta lobes become more prominent.

By map 5, the system becomes E-W oriented and shows arcuate features in the west side of Starfak field, interpreted as wave reworking of a delta lobe. However, this lobe is more prominent than previous ones. It develops to the south of a first-order growth fault, and shows the signs of rapid development to the east of a crevasse splay. The apex of the lobe can be tied to the channel feeding itself in the north of the growth fault.

According to Hentz et al. (2002), these are the incised valley and lowstand prograding wedge. However, there is an alternative explanation, which can be brought in the light of these slices. That is, sediment load shifts from east to west, and finally the delta develops at the growth fault.

As shown in map 3, the delta reaches a mature shape. The north half of the seismic data tunes in and displays other well-developed channels.

By map 1, the system reaches another flooding stage (MAF22), and sand deposition has ceased. Alternatively, this can be interpreted as deposition that has shifted beyond our survey, and with subsidence the delta was flooded quickly (**Figure 4-5**).

Overall sandy facies can also be resolved from seismic attribute maps of the genetic sequence. The "Maximum Trough Amplitude" map shows the sandy depocenters clearly (**Figure 4-6a,b**).

However, the seismic facies map, which is also created from GS22, reveals better composition of facies (**Figure 4-7a,b, and 4-8**). It brings the sandier channels, delta (red, yellow, and green) and muddier channels (light blue) together and displays a more complete picture.

All three methods are heavily affected by the problem of merging the two seismic data sets with different frequency content, but different facies can still be imaged, and their relationships resolved.

GS22 Proportionally Sliced Amplitude Maps

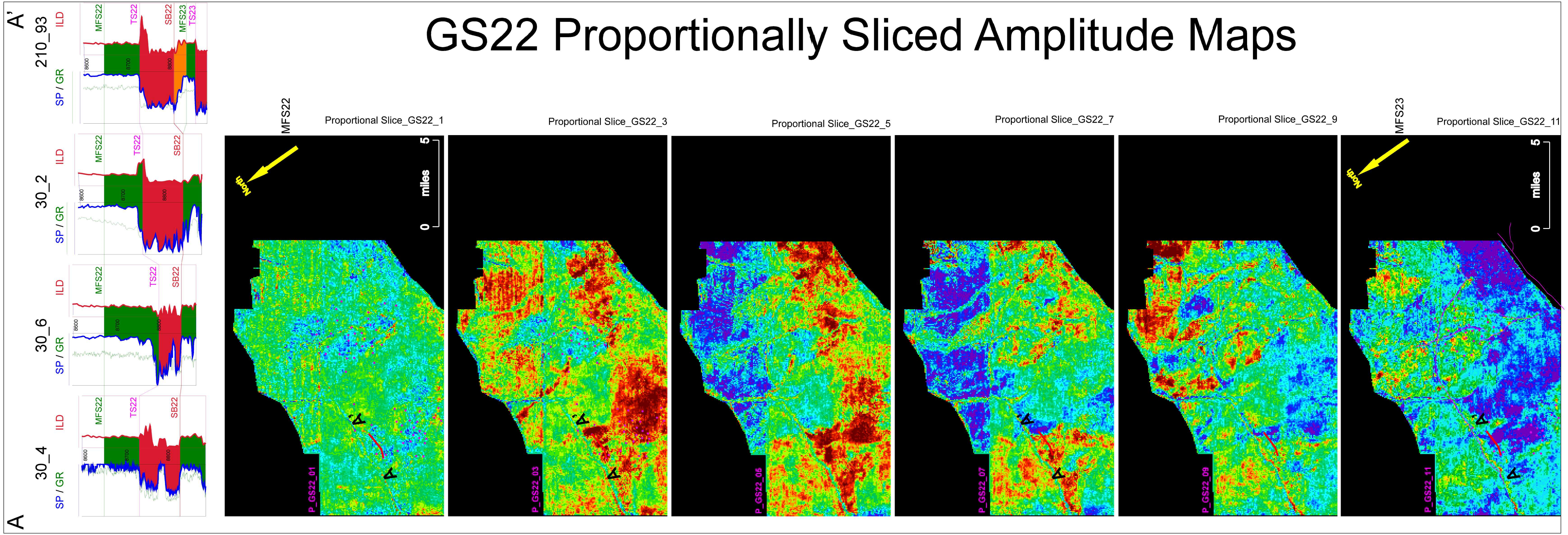

Figure 4-4a. Nine intermediate proportional slices of GS22 (defined between MFS22 and MFS23) and log cross-section showing valley incision. Proportional slices allow visualizing the progress of individual geobodies, their vertical and lateral changes, and overall life of genetic sequence.

GS22 Proportionally Sliced Amplitude Maps

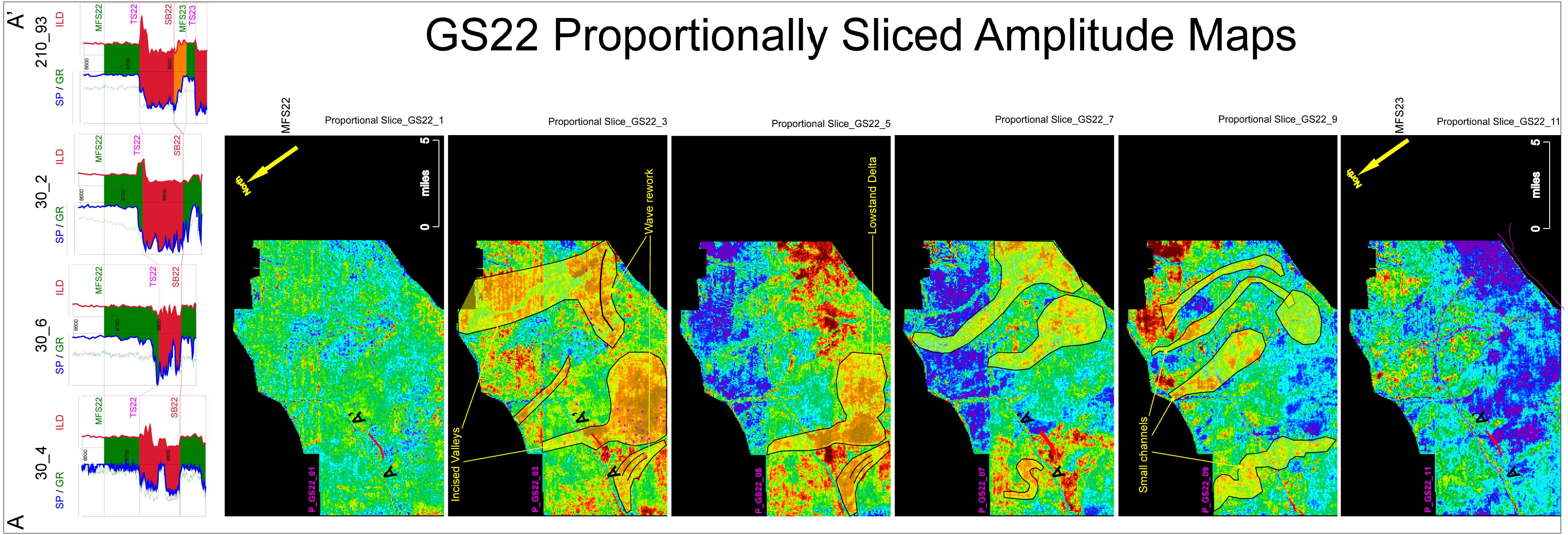

Figure 4-4b. Sand deposition begins following the flood-22 (map-11). It is brought by many N-S oriented small channels in to the area (map-9).
By map 5, small channels coalesce into two main channels in the north and northeast part of the area and a delta develops at Starfak field, interpreted as dropping sea-level. The system becomes E-W oriented in the south and reworking of a delta lobe(s) starts, indicating rising sea level (map-3).

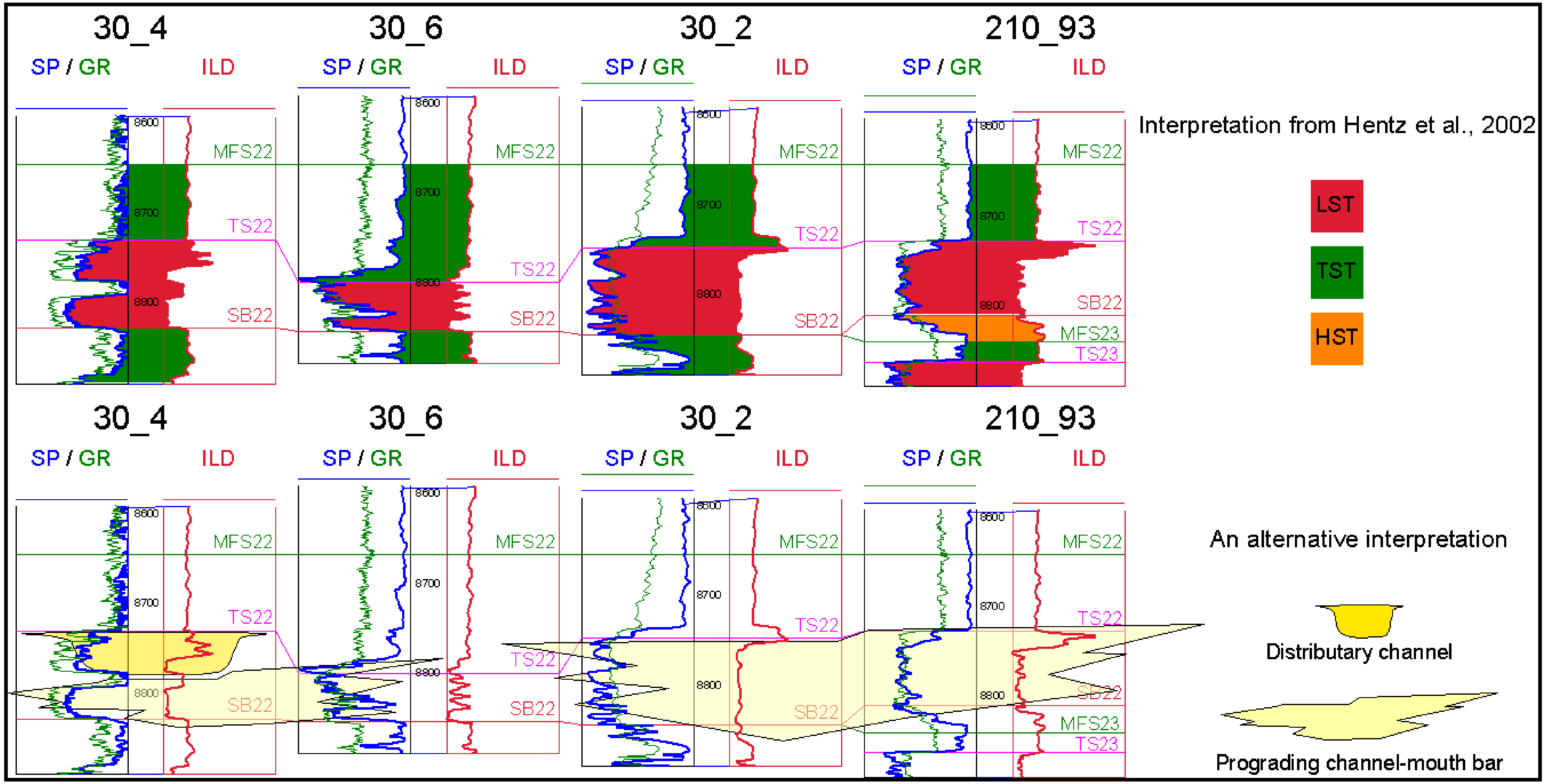

Figure 4-5. An alternative interpretation to Hentz et al. (2002). Sharp based sandstones in wells 30_6, 30_2 and 210_93 (top section) can be interpreted as upward-coarsening, prograding channel-mouth bar sands (bottom).

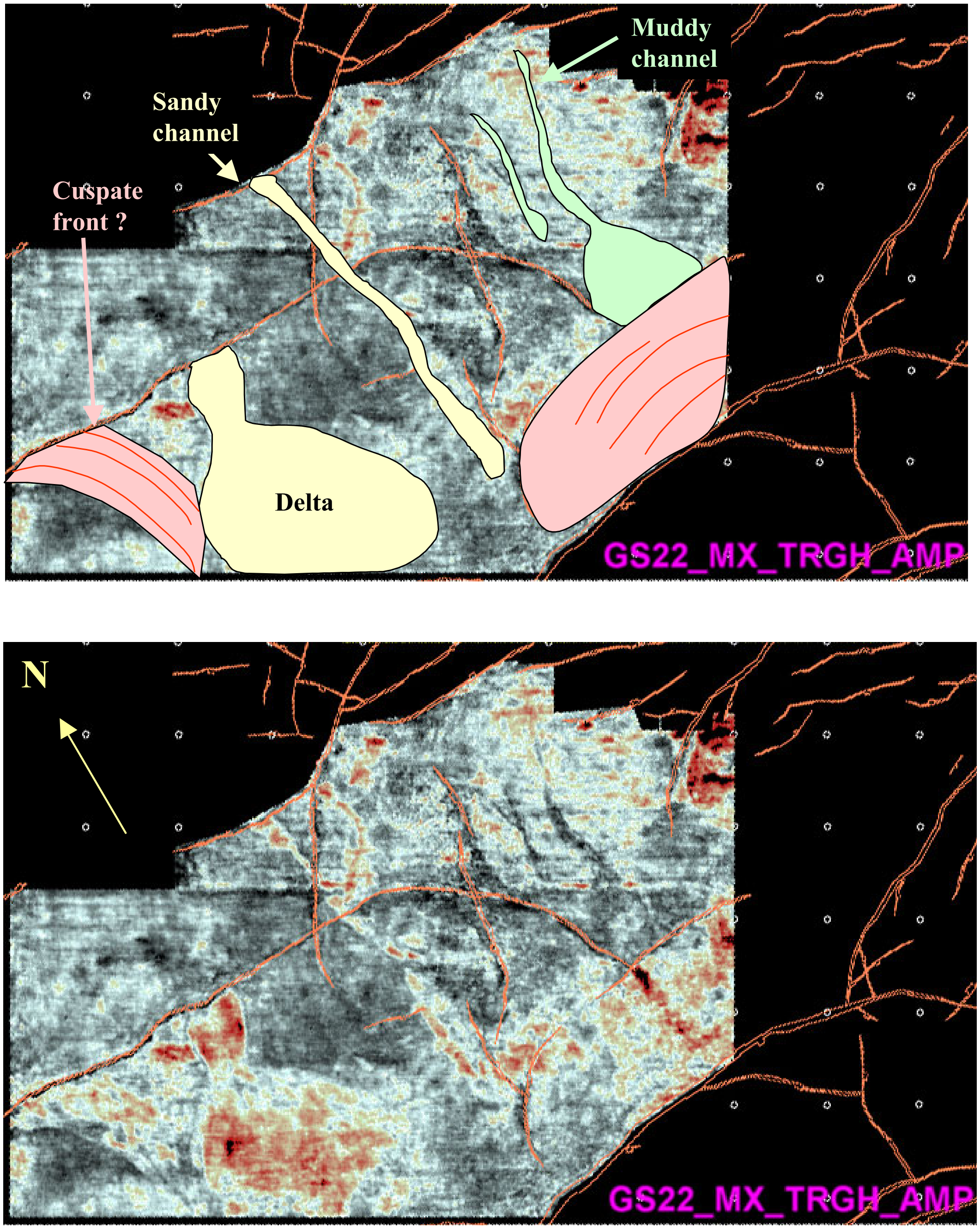

Figure 4-6. a) The maximum trough amplitude of GS22. Hot colors correspond to sand, dark colors shale. First-order growth faults act as a depositional brake, and the delta develops to the south of it. b) Uninterpreted map of GS22.

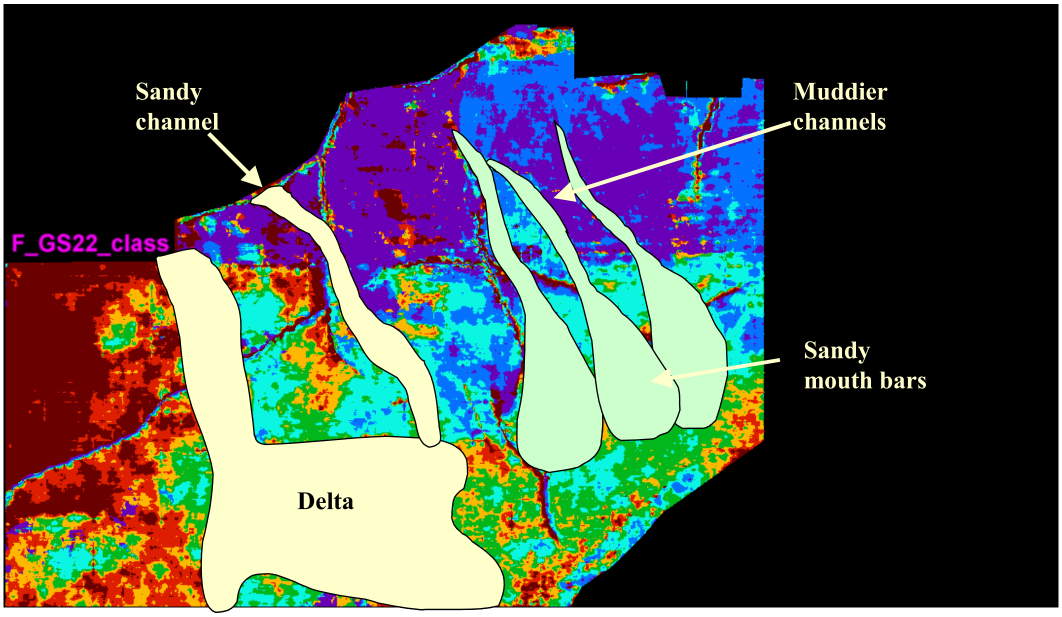

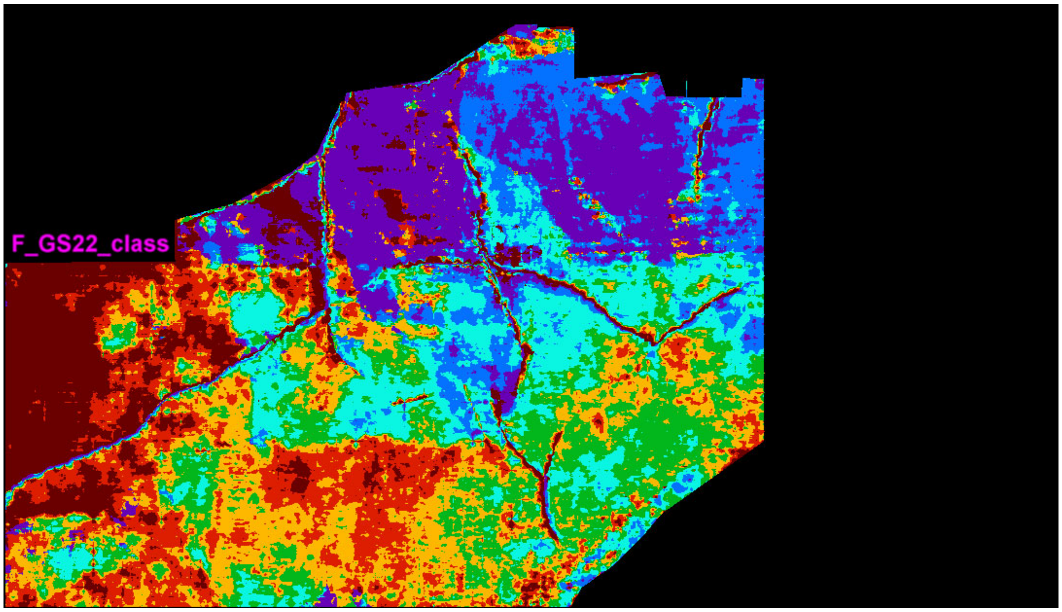

Figure 4-7. a) Seismic facies map of GS22. Hot colors correspond to sand, cold colors shale. Seismic facies map shows the connection between delta and feeding river to the west, and similarly prograding channel-mouth bars and muddy channels. B) Uninterpreted map.

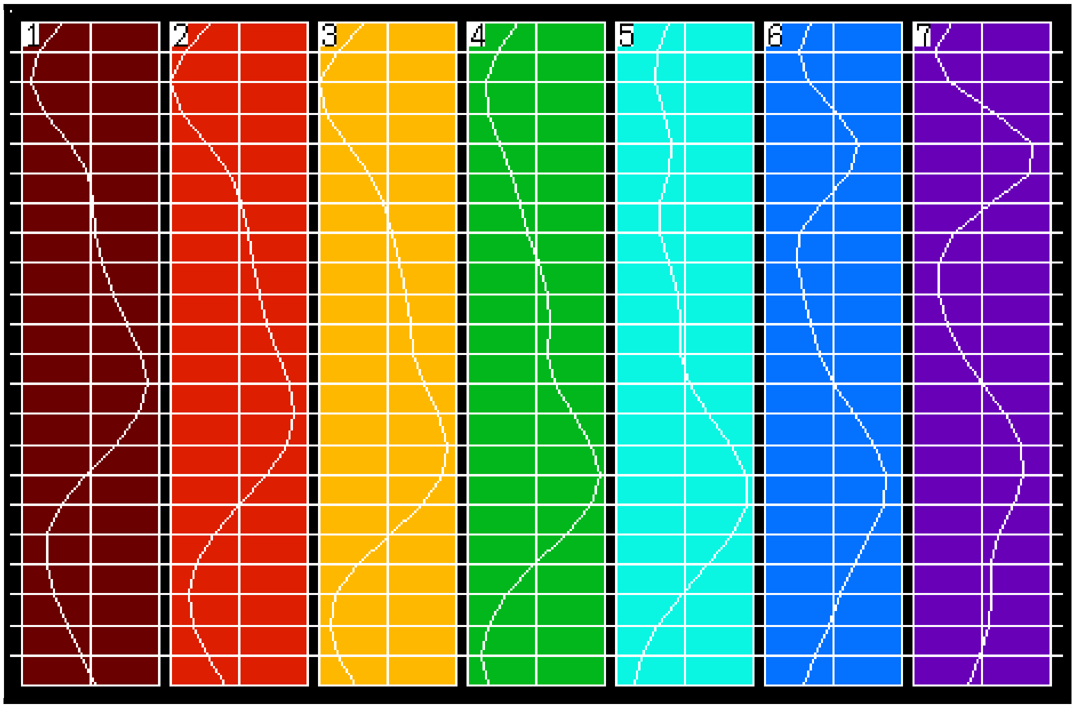

Figure 4-8. Seven representative color-coded wavelets of seismic volume used to create the “seismic facies” map.

Seismic Attributes

A seismic attribute presents a map of anomalies within the section it is created. These anomalies are mostly driven by the changes in elastic and acoustic impedance, which reflects on the lithology, fluid and gas content. Attribute maps are easy to create, and lateral changes can be detected in map view; however, they cannot distinguish individual stratigraphic order of finer depositional elements, which make up or contribute to overall picture.

A series of seismic attributes were created for each genetic sequence. These are:

Average Peak Amplitude
Average Reflection Strength
Average Trough Amplitude
Maximum Absolute Amplitude
Maximum Peak Amplitude
Maximum Trough Amplitude
RMS (Root-mean-square) Amplitude
Total Absolute Amplitude

Attribute maps created for GS22 (between MFS22 and MFS23) have clearly displayed the delta in Starfak Field, but failed to image thinner channels in Tiger Shoal (**Figure 4-9a and b**). When it is compared to individual proportional slices, the net-sand map shows a good match with amplitudes for both fields, but in separate slices. The amplitude anomaly in Starfak matches the net-sand trend at the 4th slice, and the anomaly in Tiger Shoal matches at the 9th (Figure 4-9 c1 and c2). This separation is interpreted as the sand in Tiger Shoal belonging to the previous highstand.

Attributes are also used to isolate gas effect in reservoirs and to identify the trapping mechanism. GS22 has produced only in one well (2_30) in Starfak field, and a nearby well (93_210) has shown gas (**Figure 4-10a and b**). Maximum Peak Amplitude was able to isolate the gas effect in Starfak, and also confirm the gas accumulation in well 93_210 (Figure 4-10c and d).

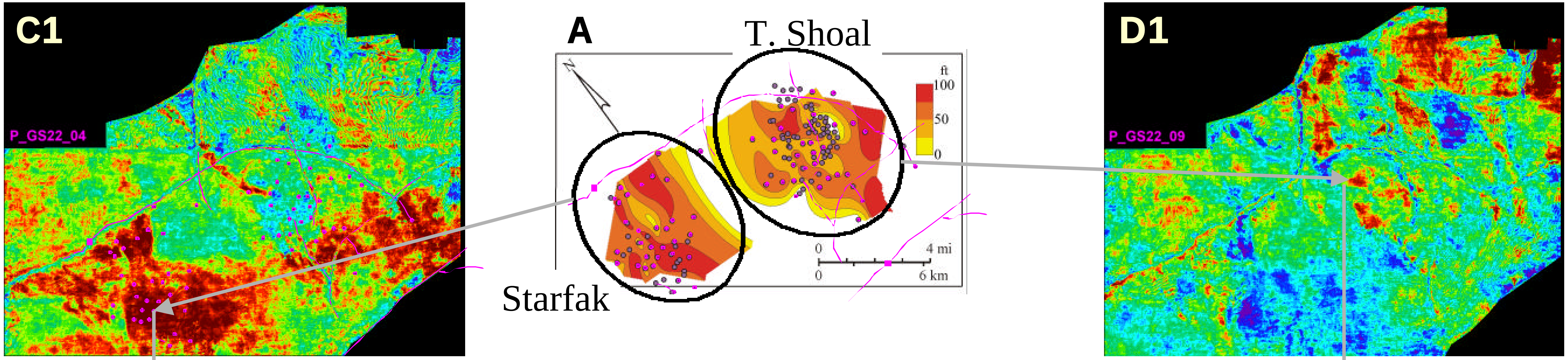

C1- 4th proportional amplitude slice of GS22

A- Net sand map of LST22

D1- 9th proportional amplitude slice of GS22

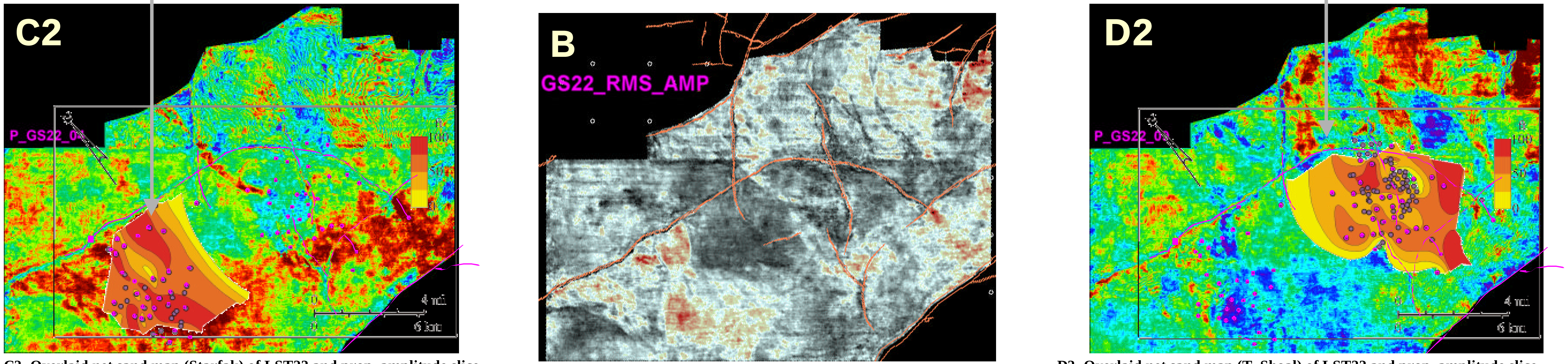

C2- Overlaid net sand map (Starfak) of LST22 and prop. amplitude slice.

B- RMS amplitude map of GS22

D2- Overlaid net sand map (T. Shoal) of LST22 and prop. amplitude slice.

Figure 4-9. Net sand map of LST22 (picture A) shows two main sand deposits over Starfak and T. Shoal fields. Attribute maps, including rms amplitude map (picture B), were able to image only the delta in Starfak field but failed to image thinner channels in the Tiger Shoal. Proportional amplitude slices, C1&C2, show a very good match with net-sand map for Starfak field, and D1&D2 for T. Shoal field. This separation is interpreted as thin sandy channels in T.Shoal are belong to previous highstand (slice-9) and thick sandy delta is belong to following lowstand delta (slice-4).

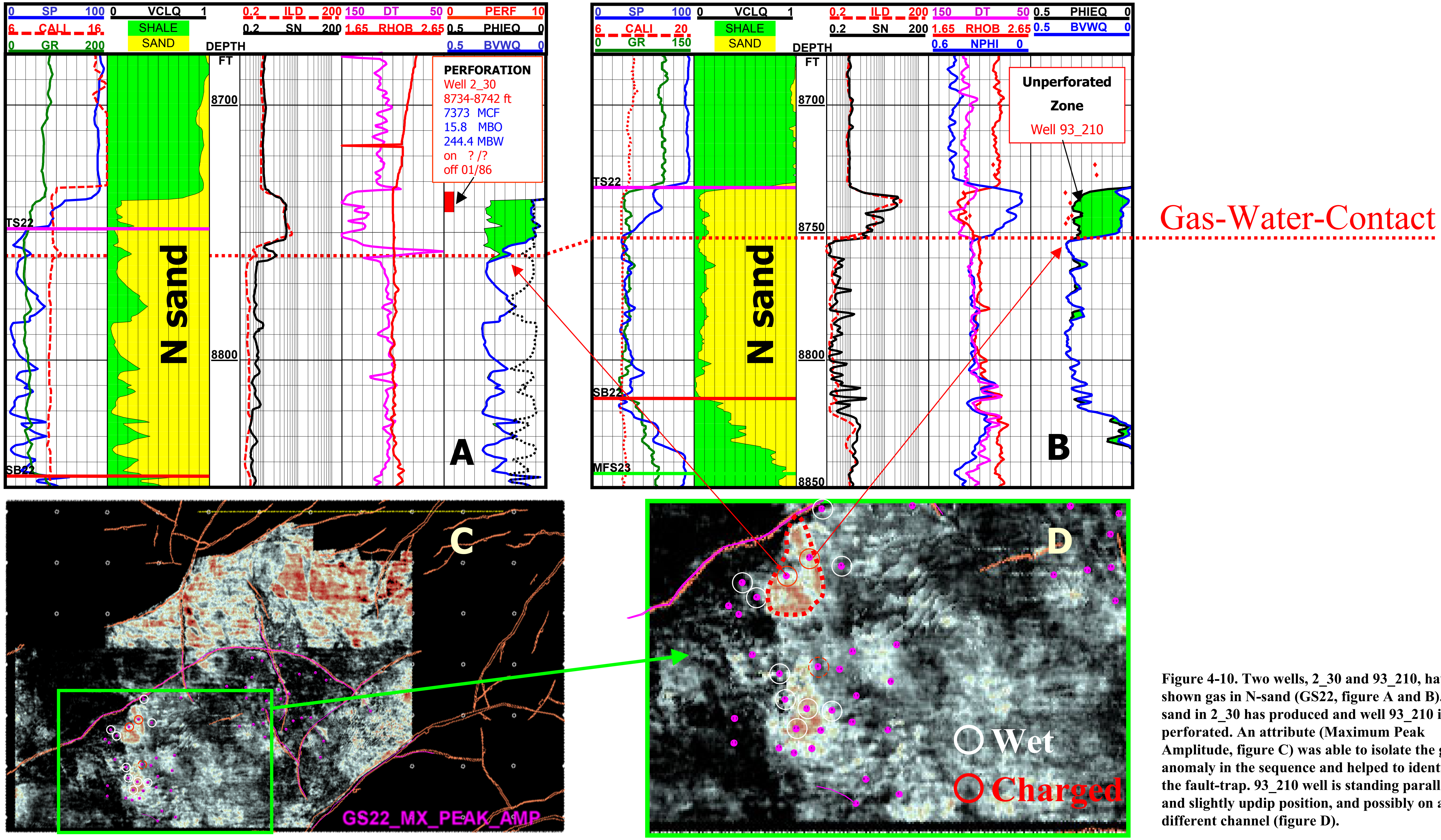

Figure 4-10. Two wells, 2_30 and 93_210, have shown gas in N-sand (GS22, figure A and B). N sand in 2_30 has produced and well 93_210 is not perforated. An attribute (Maximum Peak Amplitude, figure C) was able to isolate the gas anomaly in the sequence and helped to identify the fault-trap. 93_210 well is standing parallel and slightly updip position, and possibly on a different channel (figure D).

Genetic Sequence 18 (GS18; MFS18 - MFS19, M SAND interval)

Although GS18 is slightly above the Middle Miocene interval, it is included in the study because of its unique depositional features of fluvial entrenchment into the shelf mud and overlying transgressive deltaic deposits.

On the bottom, MFS19 (proportional slice 11) is entrenched by a large incision in the middle and a minor one on the west (**Figure 4-11a,b**). Both incisions become much wider at the south edge of the study area. These incisions are interpreted as incised valleys, and less confinement in the south is due to growth faults.

In map 9, it is also possible to identify a bird-foot-shaped pattern fed from the tip of incision at the downthrown side of the growth fault (in pink circle). At the NE corner, another incision occurred and leaves the area to east, indicating continuing incision on the shelf and deposition in the sub-basin. The system shows a strong N-NW to S-SE direction of incision and deposition.

Map 7 shows an E-W widespread depositional trend, contrary to the N-S confined trend of previous maps. Valleys are beginning to lose their shape and disappear. In the east half, including the detached delta, deposition has changed to a NE-SW direction. Valley abandonment, and new widespread, multi-angle and shifted deposition directions suggest rising sea level, and starting of a TST (Transgressive System Tract).

Deposition shifts from west to east (map 5), and the system is fed from the NE corner (outlined in blue). Thin semi-confined deposits are introduced along growth faults in the north. A detached delta (in yellow circle) is at approximately the same location but fed from the NE edge of the fault, also indicating source and deposition shift.

On map 3, sand deposits remain only in the NE corner. This sand, outlined with blue, actually migrated east from its original location in map 5.

Map 1 shows very little and diminishing deposition in the NE corner and new development in the middle. As the last map (map 1), the lack of sand deposition indicates that the system basically reached maximum transgression (MFS18). The stand-alone lobe in the map 1 is interpreted as the distal lobe of following highstand delta.

When the overall picture is considered with the seismic facies map (**Figure 4-12**), it is clearly demonstrated that the incised valley is stratigraphically older than those channels bifurcating to the west, contrary to Zeng et al. (2001). Most of the incised valley is represented by fourth and fifth wavelets (green and light blue, **Figure 4-13**). On the other hand, channels are represented by the third wavelet (yellow). Another advantage of seismic facies is that combinations of different facies types yield a more complete picture of the geology. The proximal part of those channels is dominated by facies seven, indicating shale or fine-grained thin sandstone. The overall shape suggests a back-stepping, Transgressive System Tract deltaic lobe.

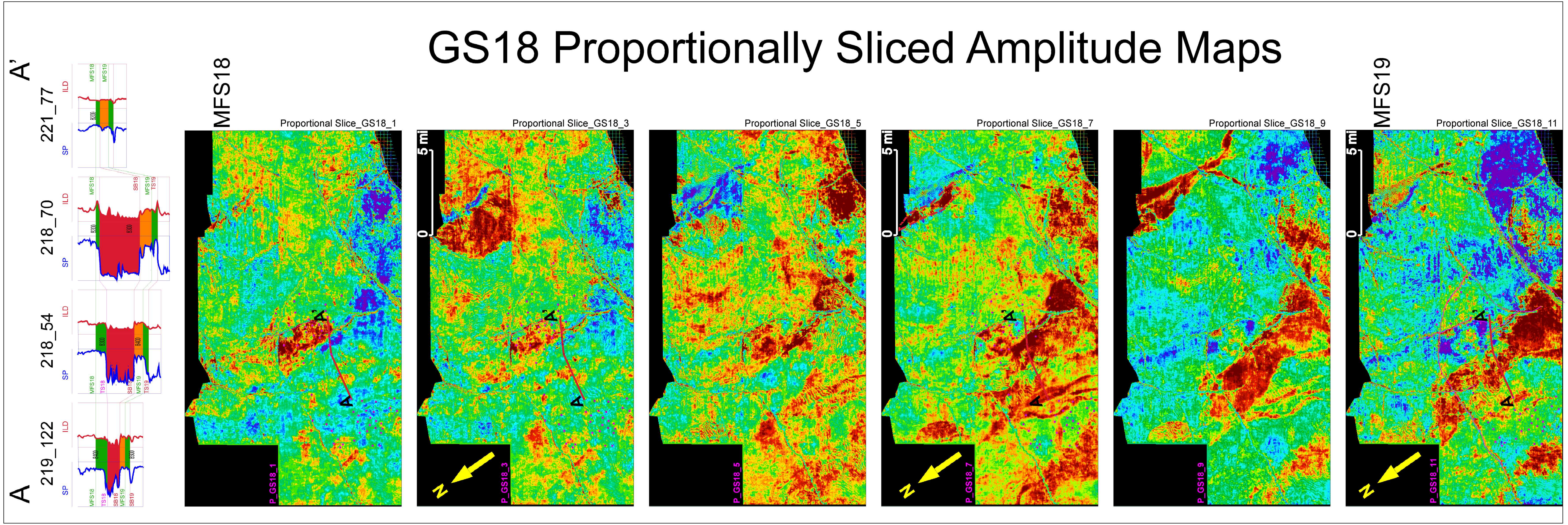

Figure 4-11a. Six intermediate proportional slices of GS18 (defined between MFS18 and MFS19) and log cross-section showing valley incision. Proportional slices allow visualizing the progress of individual geobodies, their vertical and lateral changes, and overall life cycle of genetic sequence

GS18 Proportionally Sliced Amplitude Maps

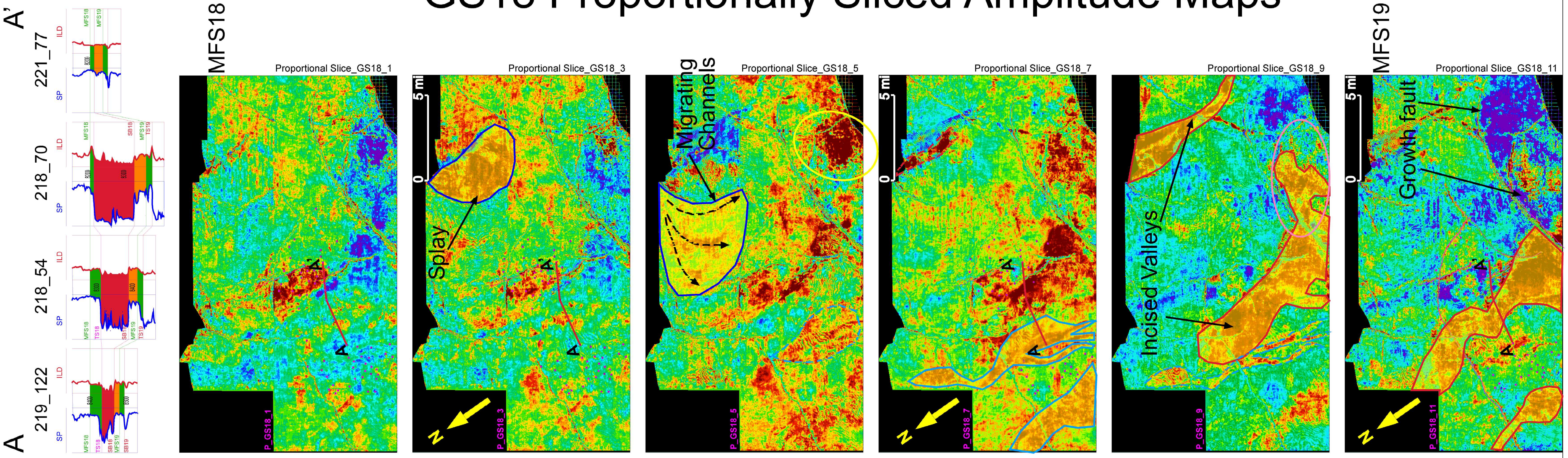

Figure 4-11b. An incised valley eroded MFS19 (map-11) and developed a small delta in the south side of growth faults (map-9). By map 7, sea level began to rise and valleys started to be replaced by semi-confined migrating channels and splays. Sand deposition started to diminish and restricted to the northeast (map-5 and 3). System reaches maximum transgression (FMS18) and little sand is deposited along secondary faults (map-1).

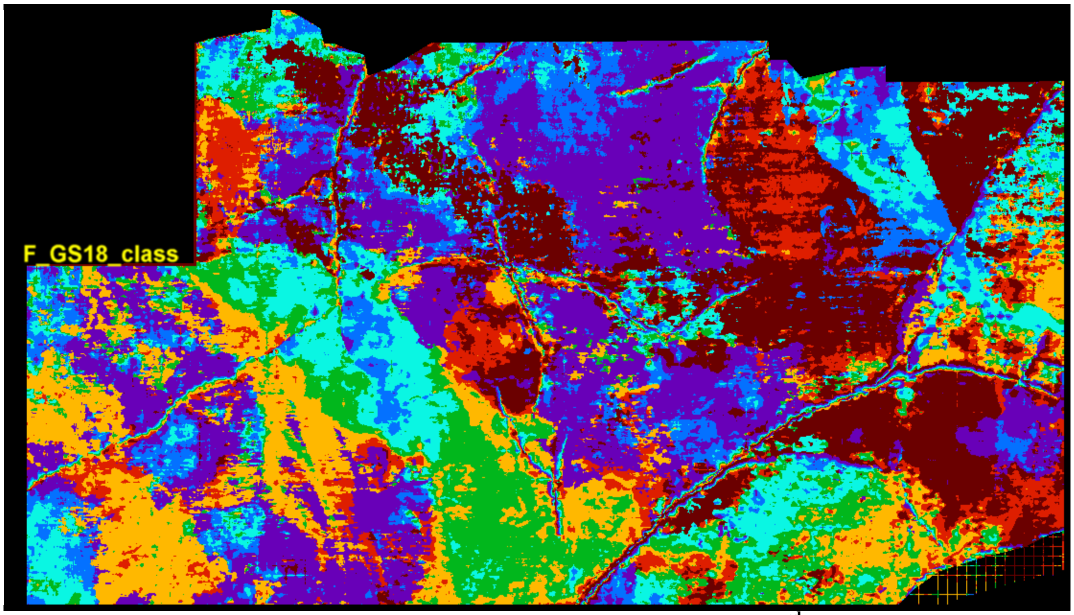

Figure 4-12. Seismic facies map of GS18. Channels are defined by 3rd wavelet, incised valley 4th and 5th, and unconfined deltaic sediments are mostly defined by 1st and 2nd. It is also possible to see a brown belt crossing the area from the left upper corner to right lower corner. This is a relict from the previous incised valley, GS19.

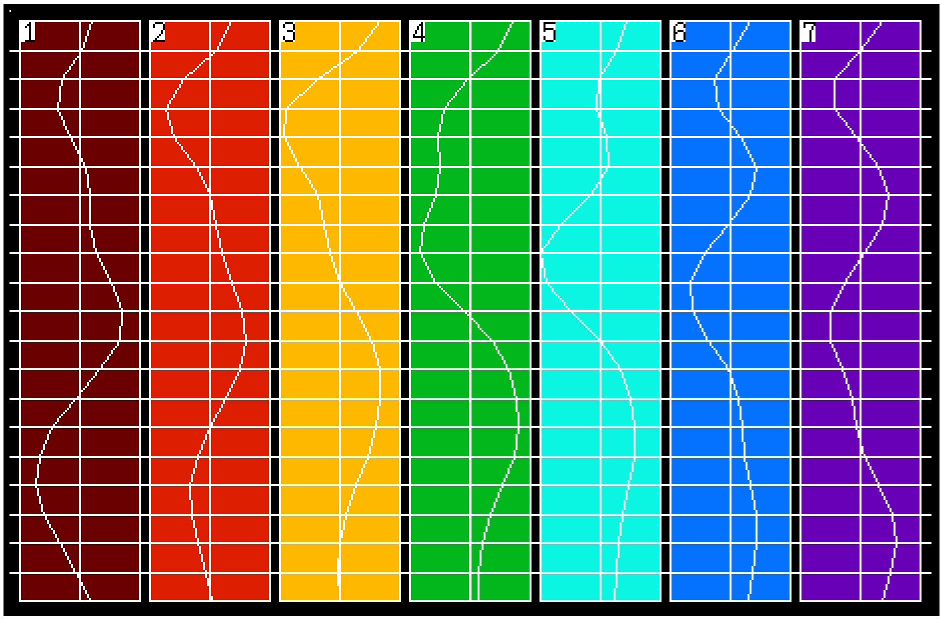

Figure 4-13. Seven representative color-coded wavelets of GS18.

Seismic Attributes

Seismic attribute maps of GS18 show similar sand trends to those observed in proportional slices. In addition, some of the maps are able to isolate the gas effect (**Figure 4_14**). The Maximum Trough Amplitude map shows the overall distribution of sandy facies and allows the interpretation of incised valleys and delta. When the extreme amplitudes are isolated, the gas-charged portion of incised valley is highlighted (Figure 4-14b).

Another beneficial application of this high-resolution mapping is the ability to study the individual sand packages, and trace small faults into shallower sections. Although diminishing, they have enough throw on them to create structural trap (4-14c). This particular sand is being drained by two other wells (58_218 and 99_221), but structural complexity of the area creates additional small closures (Figure 4-14c).

This closure is similar to the other two, which are being drained by wells 58_218 and 99_221. Gas water contact can be seen at well 58. If the prospect well is drilled, water will reach this closure sooner than it will reach others. The feasibility of the prospect will be very sensitive to the price of the gas, because the closure is rather thin and covers small area.

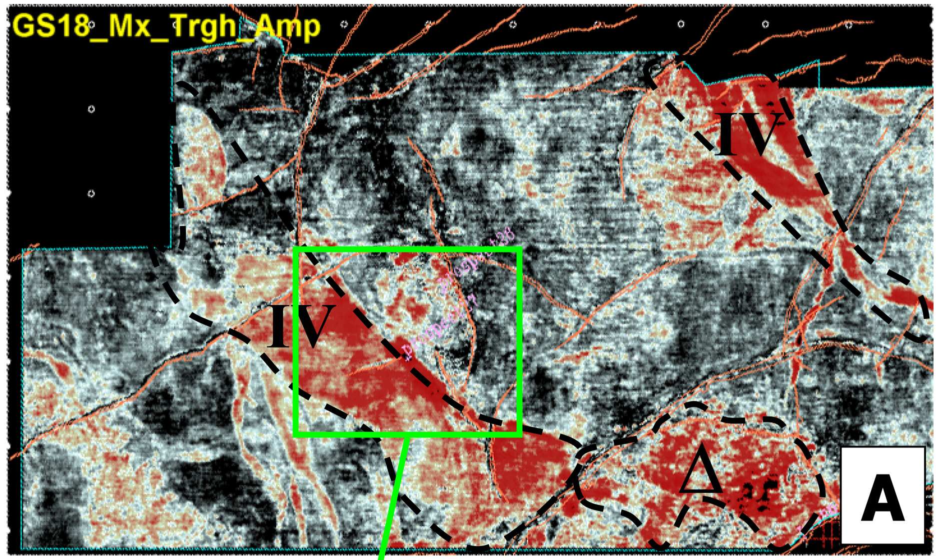

Maximum trough amplitude of GS18 shows incised valleys and delta.

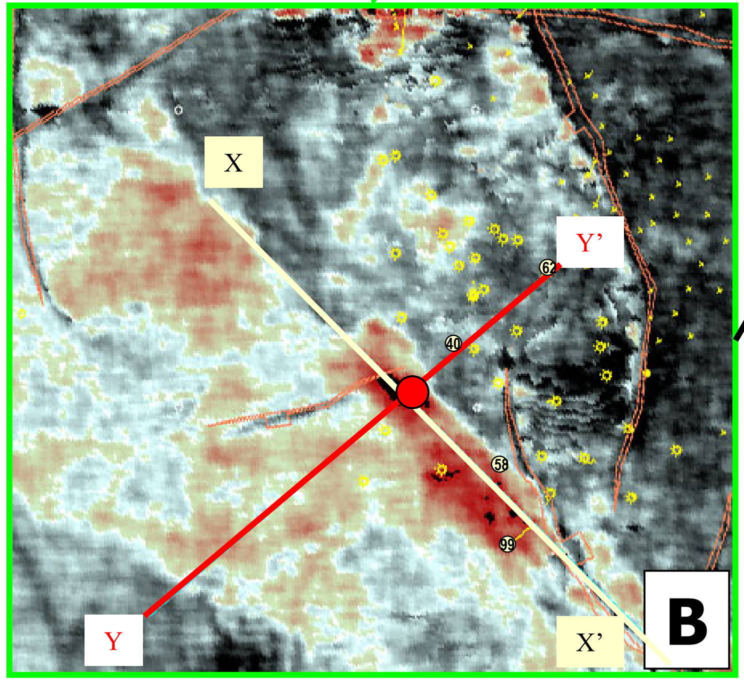

Extreme amplitudes are gained to isolate gas effect. A prospect is identified.

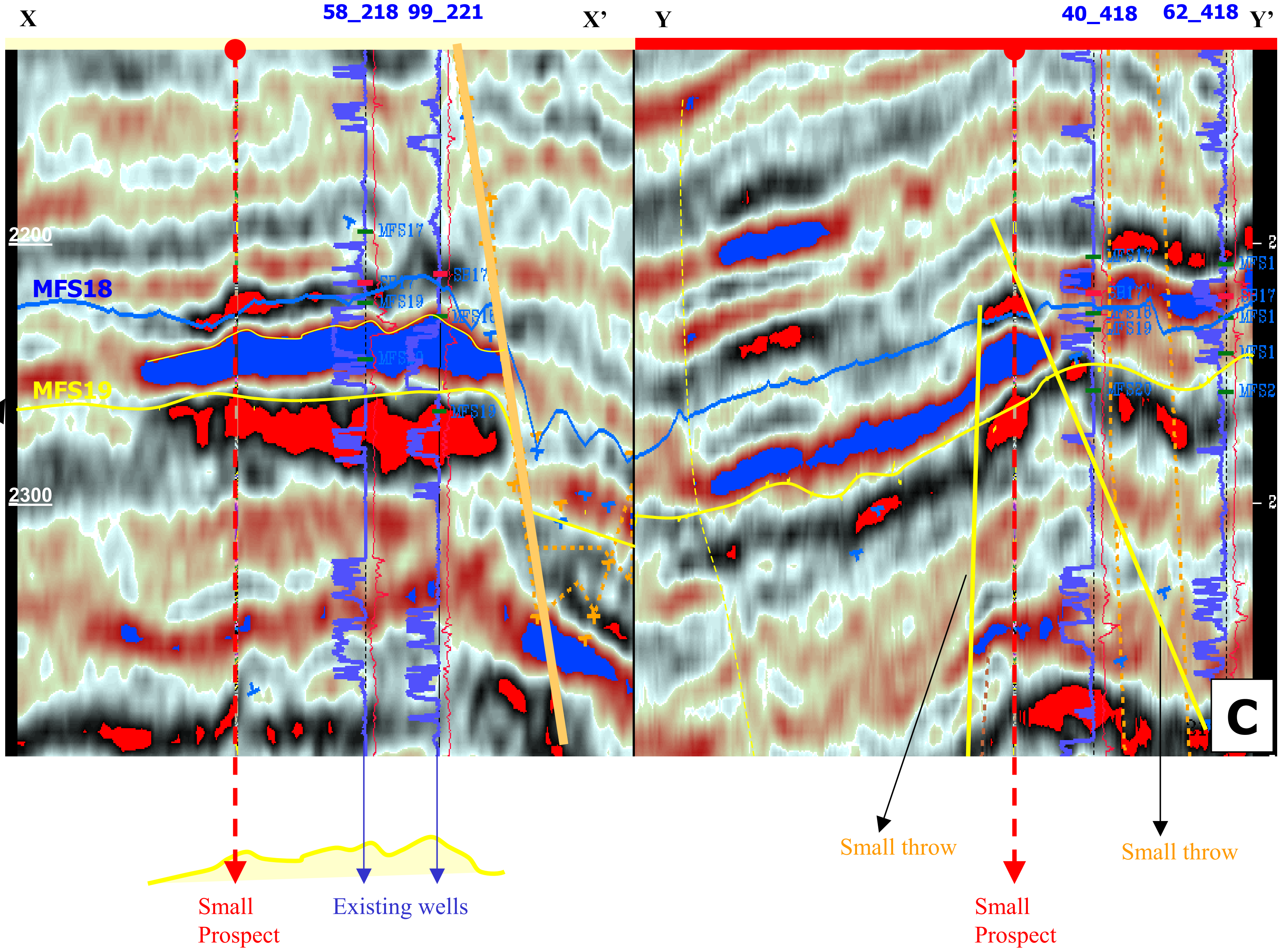

Figure 4-14. Attribute maps are used to identify lithology and fluid changes within the genetic sequence. Maximum Trough Amplitude differentiate the sand and shale; hot colors indicate sand and dark colors shale. Incised valleys, and the delta in the downthrown side of the growth fault can be interpreted easily (figure A). Extreme amplitudes are gained to isolate gas effect, and with cross-sections, a small prospect is identified.

QUANTIFICATION

The relationship between 3D seismic and well log data, and the effectiveness of the transformation have been key issues for the last 25 years. However, the methodology of transforming 3D seismic volume to petrophysical properties (mostly porosity, thickness, volume of shale) and/or geological features/facies has also become important (Ronen et al., 1994; Schultz et al., 1994a and b; Taner et al. 1994; De Groot, 1995; Vinson et al., 1996; Gastaldi et al., 1997; Kalkomey, 1997; Raeuchle et al., 1997; Russell et al., 1997; Hart and Balch, 2000; Walls et al., 2000; Wood et al., 2000; Hampson et al., 2001; Hart, 2002; Dorrington and Link, 2004).

Numerous types of Neural-Network (NN) structures have been proposed and tested for the quantification of reservoirs, by transformation of seismic data. After a few tests, probabilistic types of NN have been chosen for quantification, because compared to Multi Layer Feed Forward (MLFF) the PNN worked much faster and gave results with slightly better accuracy.

Transformation of seismic amplitude volume to petrophysical properties was established in two steps. First, with the help of Hampson-Russell^{TM} a series of volumetric seismic attributes was computed for each well bore (**Table 4-1**). A number of these attributes were then used to predict petrophysical properties using these equation below.

$$\begin{pmatrix}\phi_1\\ \phi_2\\ \phi.\\ \phi_n\end{pmatrix}\begin{matrix}=\\=\\=\\=\end{matrix}\begin{pmatrix}1 & A_1 & A_2 & A_3\\ 1 & A_1 & A_2 & A_3\\ 1 & A_1 & A_2 & A_3\\ 1 & A_n & A_n & A_n\end{pmatrix}\begin{pmatrix}w_1\\ w_1\\ w_1\\ w_1\end{pmatrix}\quad\begin{matrix}\phi = \text{porosity}\\ A = \text{attribute}\\ w = \text{weight}\\ \ \end{matrix}$$

One of the unknowns in this matrix is the weight, and the weights are computed by

$w = [M^T M]^{-1} M^T P$,

where T indicates transposed and –1 indicates inversed matrix, and $[M^T M]$ is called 'covariance matrix' (Russell et al., 1997).

The second unknown is the attributes to be included for the transformation. Individual attributes are ranked from best to worst in 'correlation coefficient', indicative of how well the attributes correlate with the targeted property.

$C_{AP} = \sigma_{AP} / \sigma_A \sigma_P$,

where C_{AP} is Correlation Coefficient, σ_{AP} is covariance between A and P, σ_A is standard deviation of A, σ_P is standard deviation of P, A is attribute, and P is the parameter (Russell et al., 1997).

After the ranking of correlation coefficients, a number of attributes are selected and included in the above matrix equation. The result is plotted and RMS (root mean square) error computed. Attributes are added one by one to reduce the RMS error. After a certain number of attributes, when the lowest error is reached, each new attribute starts to drive the RMS error higher. This indicates the optimum number of attributes is reached and others should be excluded from the multi-attribute analysis.

As an example of quantification, GS22 was selected, and 13 wells were used to train the NN for predicting VCL (Volume of Clay, look for detail in chapter 2), which is mainly a product of SP and GR curves. First, multi-attribute transforms have been used to predict VCL in 13 wells distributed over the study area (**Table 4-2**). Five attributes with lowest correlation errors were chosen and cross-validation was applied (**Figure 4-15 and Table 4-3**). Overall application correlation is 0.70, and cross-validation is 0.65.

Table 4-1. List of volume attributes created for each well. They are then ranked by correlation coefficient and highest ones are included in transformation.

1	Amplitude Envelope	13	Filter 25/30-35/40
2	Amplitude Weighted Cosine Phase	14	Filter 35/40-45/50
3	Amplitude Weighted Frequency	15	Filter 45/50-55/60
4	Amplitude Weighted Phase	16	Filter 55/60-65/70
5	Average Frequency	17	Instantaneous Frequency
6	Apparent Polarity	18	Instantaneous Phase
7	Cosine Instantaneous Phase	19	Integrate
8	Derivative	20	Integrated Absolute Amplitude
9	Derivative Instantaneous Amplitude	21	Quadrature Trace
10	Dominant Frequency	22	Second Derivative
11	Filter 5/10-15-20	23	Second Derivative Inst. Amp.
12	Filter 15/20-25-30	24	Time

Table 4-2. Thirteen wells used in multi-attribute analysis and PNN training. For better correlation, minor time shifts have been applied to individual wells.

#	Trained with the following wells:	Shift (millisecond)
1	210_197 Window 2320 To 2408 ms	0
2	210_95 Window 2320 To 2384 ms	-8
3	219_122 Window 2360 To 2432 ms	0
4	30_1 Window 2320 To 2384 ms	0
5	30_2 Window 2328 To 2400 ms	0
6	30_4 Window 2320 To 2392 ms	0
7	31_17 Window 2328 To 2424 ms	0
8	50_B1_(2) Window 2376 To 2456 ms	0
9	50_C3 Window 2376 To 2464 ms	-8
10	217_34 Window 2312 To 2400 ms	8
11	217_27 Window 2296 To 2392 ms	0
12	218_3 Window 2320 To 2384 ms	8
13	221_118 Window 2328 To 2416 ms	8

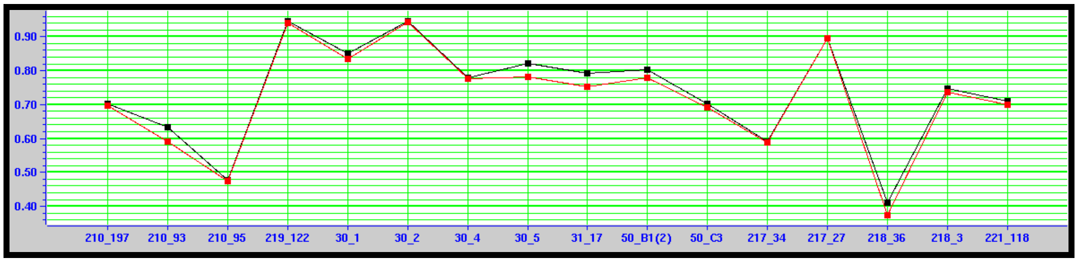

Figure 4-15. Correlation coefficients of multi-attribute transformation and cross validation by well. Application correlation is black and validation is in red.

Table 4-3. Attributes used in multi-attribute analysis and their weights (w). Each additional attribute reduces the error.

#	Target	Final Attribute	Training Error	Validation Error	Weight
1	VCLQ	Integrate	0.199228	0.202879	0.001969
2	VCLQ	Amplitude Envelope	0.193753	0.198082	-0.001489
3	VCLQ	Instantaneous Phase	0.190810	0.196430	0.000485
4	VCLQ	Filter 25/30-35/40	0.189490	0.196375	0.002002
5	VCLQ	Filter 35/40-45/50	0.187953	0.195886	-0.004801
6	VCLQ	constant = 0.763184			

Following the multi-attribute analysis, PNN has been set up and run using the same attributes with an 8 ms search window, which is also called ‘operating length’ (**Table 4-4**).

Table 4-4. Specification of the NN for predicting VCL.

Type Neural Network	Probabilistic
Calculated by	Emerge Version: 3
Multi-attribute transform	
Threshold	2
Standard Error	0.120249
Predicting: VCLQ [fraction]	
Using these attributes:	Integrate
	Amplitude Envelope
	Instantaneous Phase
	Filter 25/30-35/40
	Filter 35/40-45/50
The operator	
Length	8
Lag measured from center	0
Neural Network parameters:	
The network is not cascaded.	
The network is in mapping mode.	
Number of sigmas for training	40
Sigmas range	0.1 to 3
Number of conjugate-gradient iterations	200
The Training Error is:	**0.0916765 [fraction]**
The Validation error is:	**0.108552 [fraction]**

The analysis window has been narrowed down to a small interval in order to achieve higher correlation and to speed up the process. Additional 200 ms seismic data (100 ms above and below GS22) are included in the analysis.

Following multi-attribute analysis, PNN was trained with these 13 wells and 5 attributes. After training and cross-correlation, the correlation coefficient reaches up to 0.92 (**Figure 4-16**).

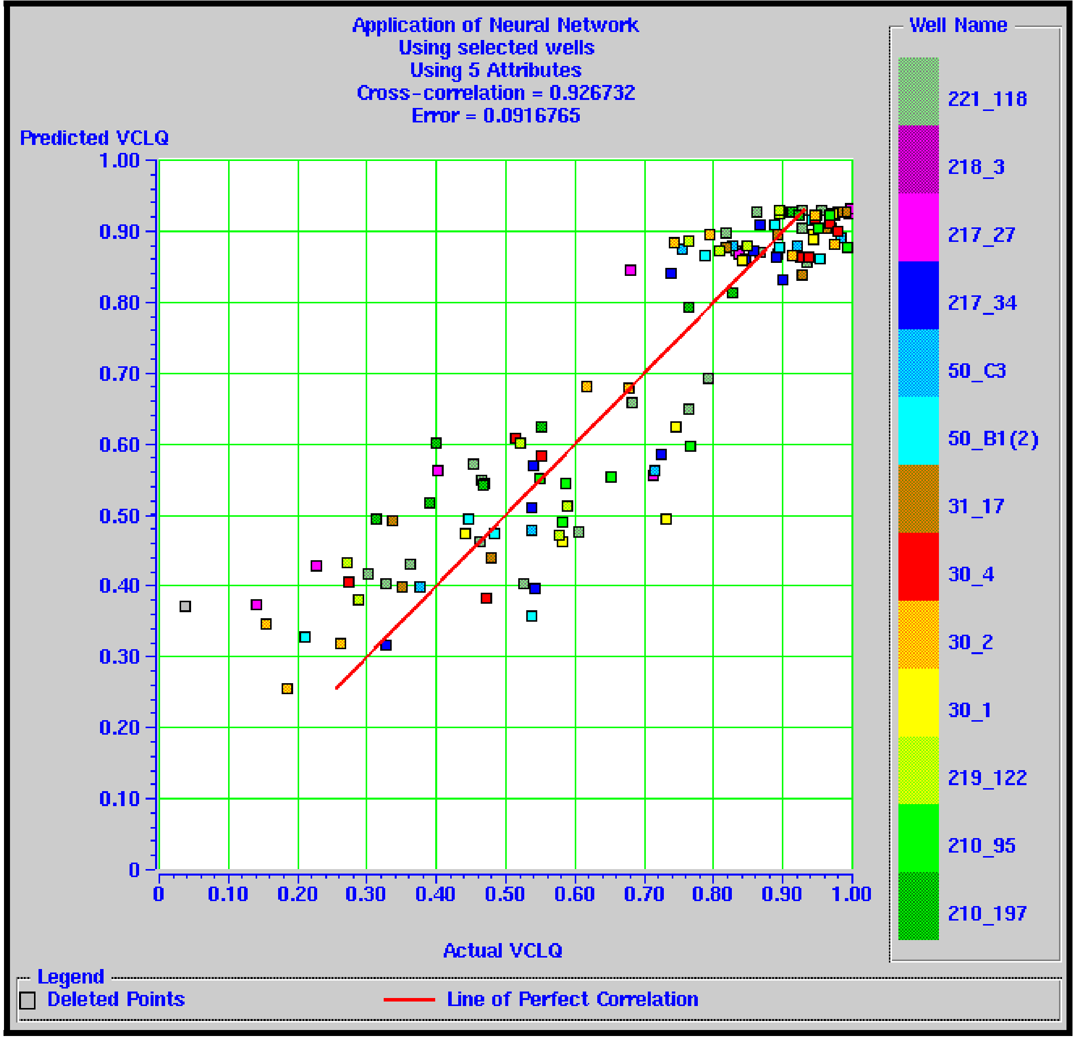

Figure 4-16. Cross-plot between actual VCL and predicted VCL after training. NN includes 5 attributes from multi-attribute analysis and improves correlation coefficient significantly.

Predicted and actual VCL numbers are very close for the shale, and they make a tight cluster, but there is some separation in the sand end. Predicted VCL is estimated slightly more than actual values for the sandy intervals.

Cross-validation of PNN also yields acceptable correlation between seismic and VCL, 0.89 (**Figure 4-17**). As a last step of transformation, this PNN was applied to GS22 (± 100 ms), and this portion of the seismic was converted into volume of clay (**Figure 4-18**). As an accuracy check, VCL_GS22 (GS22 of VCL volume) was sliced by 9 intermediate proportional slices and compared to amplitudes slices (**Figure 4-19**). Comparison between amplitude slice and VCL slice indicates a strong relationship between them. However, in the west and southeast sides of the area, the amplitude map indicates strong negative reflections, but the VCL map does not entirely concur. Instead, some minor shaly sand indicated by the VCL slice occurs in those areas. Thickness also plays a role, but could not be ruled out due to lack of well coverage in the area.

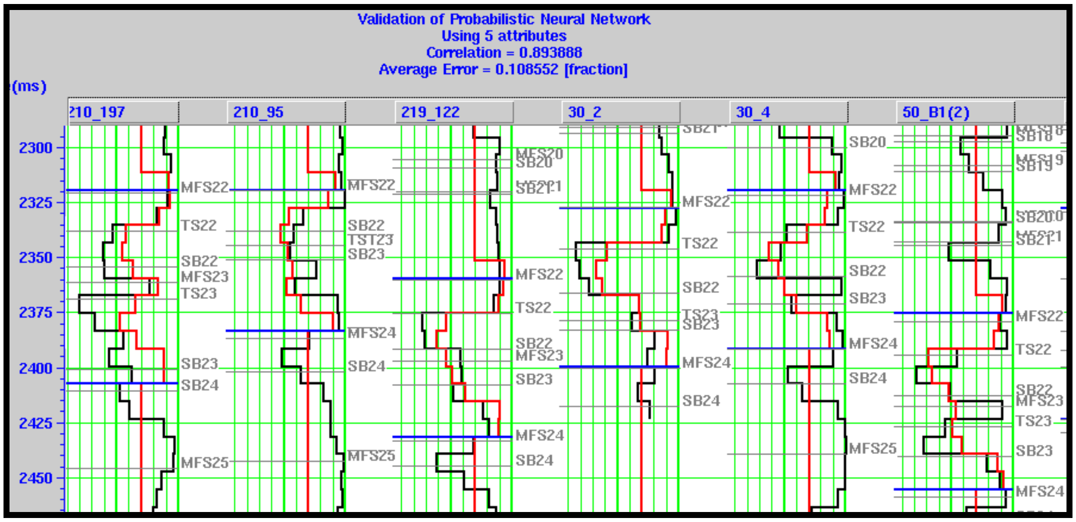

Figure 4-17. Some of the wells used in training/targeting VCL curve. Sequence surfaces (gray lines, ex. MFS22-MFS24) have been used to limit analysis window (between blue lines). Original logs (in black) and modeled logs (in red) show a consistent match.

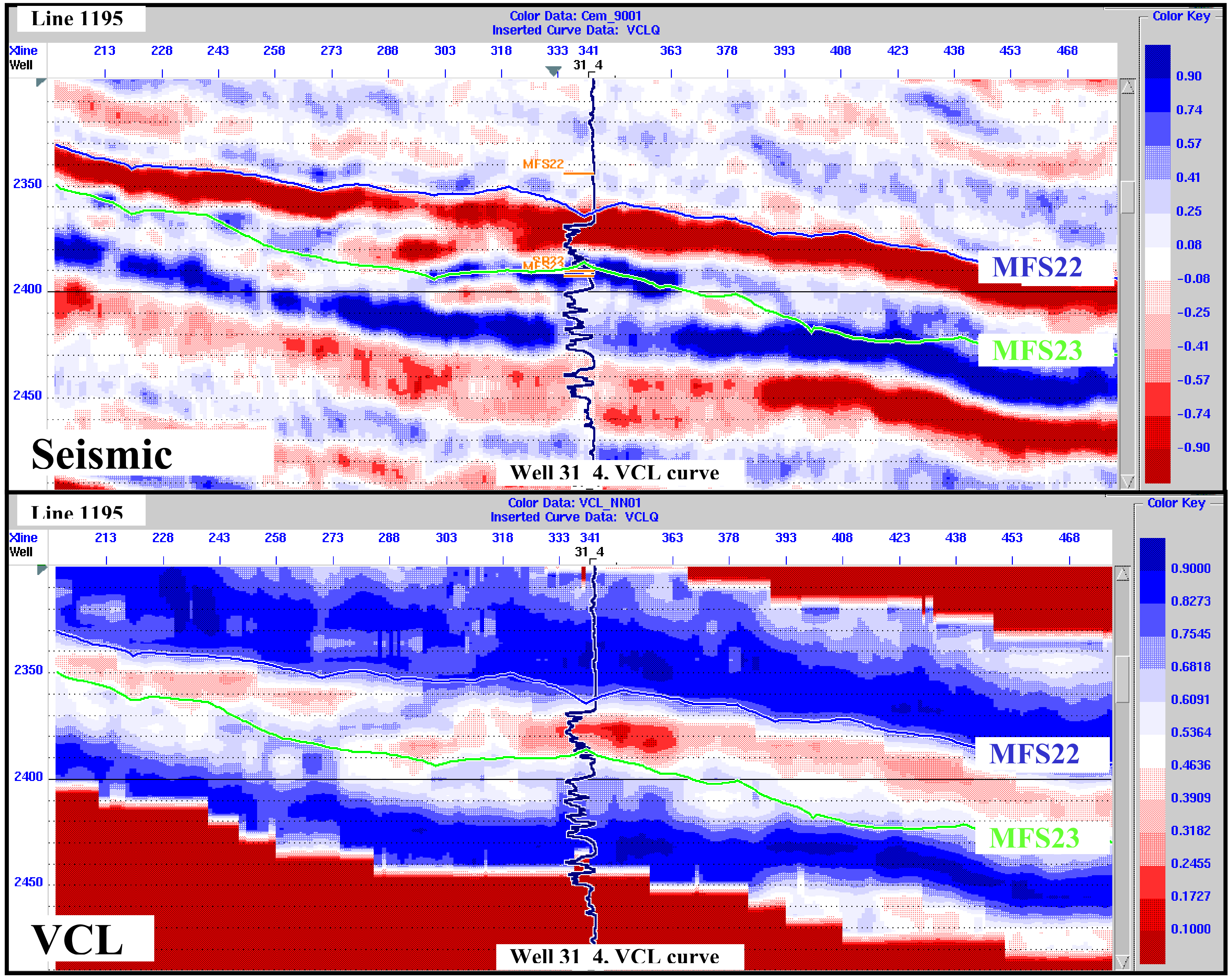

Figure 4-18. (Top) Seismic section (inline 1195) and GS22 (MFS22 and MFS23) at well 31_4, which was not used in training. (Bottom) Section of VCL in the same location (inline 1195). Only GS22 (± 100ms) has been transformed for better accuracy. VCL curve of well 31_4 matches very well with VCL volume. Also note degrading quality of transformation outside GS22.

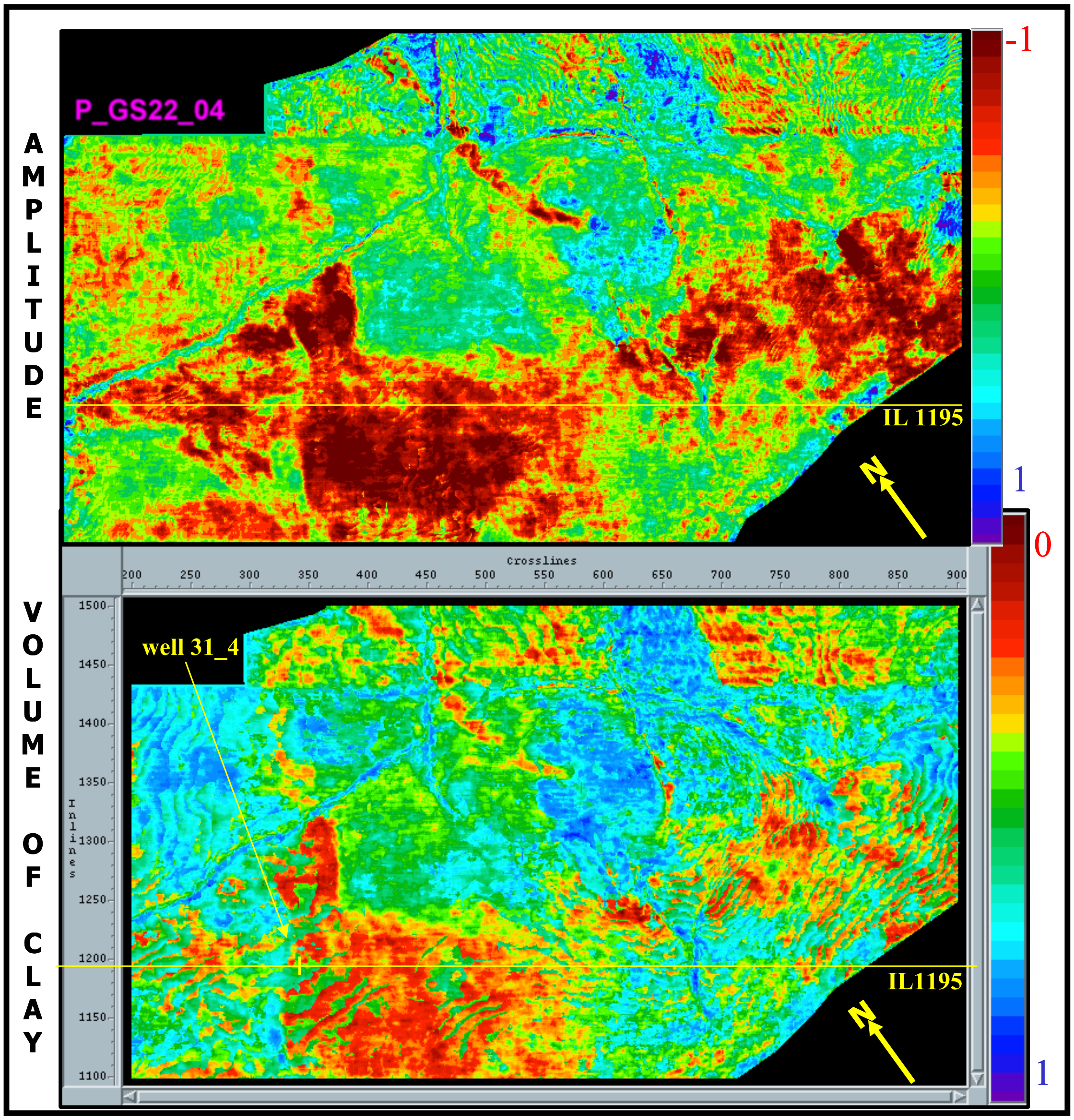

Figure 4-19. Comparison between amplitude slice and VCL slice. a) Seismic amplitude map of GS22. Troughs, negative amplitudes, correspond to sand. b) Porosity map of GS22. Hot colors correspond to clean rock. There is a considerable difference on the west and southeast side of the field, indicating thin, shaly sands can also yield brighter amplitudes.

Similar steps are also taken for transforming seismic data into PHIE (effective porosity). Transformation is prepared in the same way, but PHIE calculation from logs is inherently more complex than VCL. Effective porosity includes more than one type of measurement. These are neutron porosity, density, sonic, and if none of them is available, modified Phiamax (look for detail in chapter 2). In addition, the porosity curve is modified for the presence of clay content of the rock. Relationship between porosity and clay content is linear up to 50% of VCL. Beyond this value, the porosity curve is suppressed logarithmically (**Figure 4-20**).

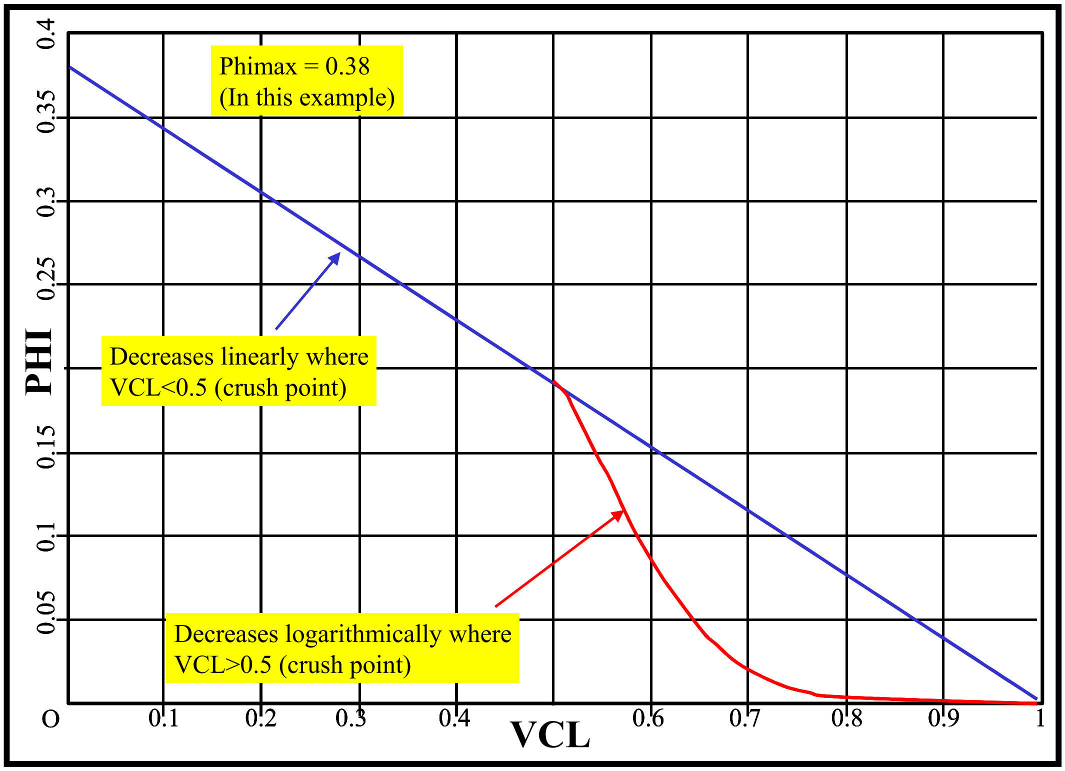

Figure 4-20. Modification of porosity curve. Porosity and VCL are inversely proportional and increasing clay content more than 50% accelerates reduction of porosity.

After multi-attribute analysis 5 attributes were selected and, using 10 wells, a series of neural network were trained. The most successful one was used for transformation (**Table 4-5 and 4-6**). Cross-correlation reached up to 0.83, but validation could only reach up to 0.66 (**Figure 4-21 and 4-22**).

Table 4-5. Specification of the NN for predicting PHIE.

Type Neural Network	Probabilistic
Calculated by	Emerge Version: 3
Multi-attribute transform	
Threshold	2
Standard Error	0.0628992
Predicting: PHIE [fraction]	
Using these attributes:	Integrate
	Time
	Quadrature Trace
	Amp. Wei. Cos. Phs.
	Amplitude Envelope
The operator	
Length	8
Lag measured from center	0
Neural Network parameters:	
The network is cascaded with the linear transform after applying a smoother of length: 50.	
The network is in mapping mode.	
Number of sigmas for training	25
Sigmas range	0.1 to 3
Number of conjugate-gradient iterations	500
The Training Error is:	**0.036263 [fraction]**
The Validation error is:	**0.0508319 [fraction]**

Table 4-6. Ten wells used in multi-attribute analysis and PNN training. For better correlation, minor time shifts have been applied to individual wells.

#	Trained with the following wells:	Shift (millisecond)
1	31_5 Window 2368 To 2432 ms	8
2	31_15 Window 2360 To 2448 ms	0
3	31_20 Window 2320 To 2400 ms	8
4	210_93 Window 2328 To 2944 ms	0
5	50_D2(7) Window 2328 To 2416 ms	8
6	50_F1 Window 2384 To 2464 ms	0
7	31_4 Window 2344 To 2432 ms	-8
8	218_47 Window 2296 To 2384 ms	8
9	218_65 Window 2136 To 2384 ms	8
10	31_17 Window 2328 To 2424 ms	0

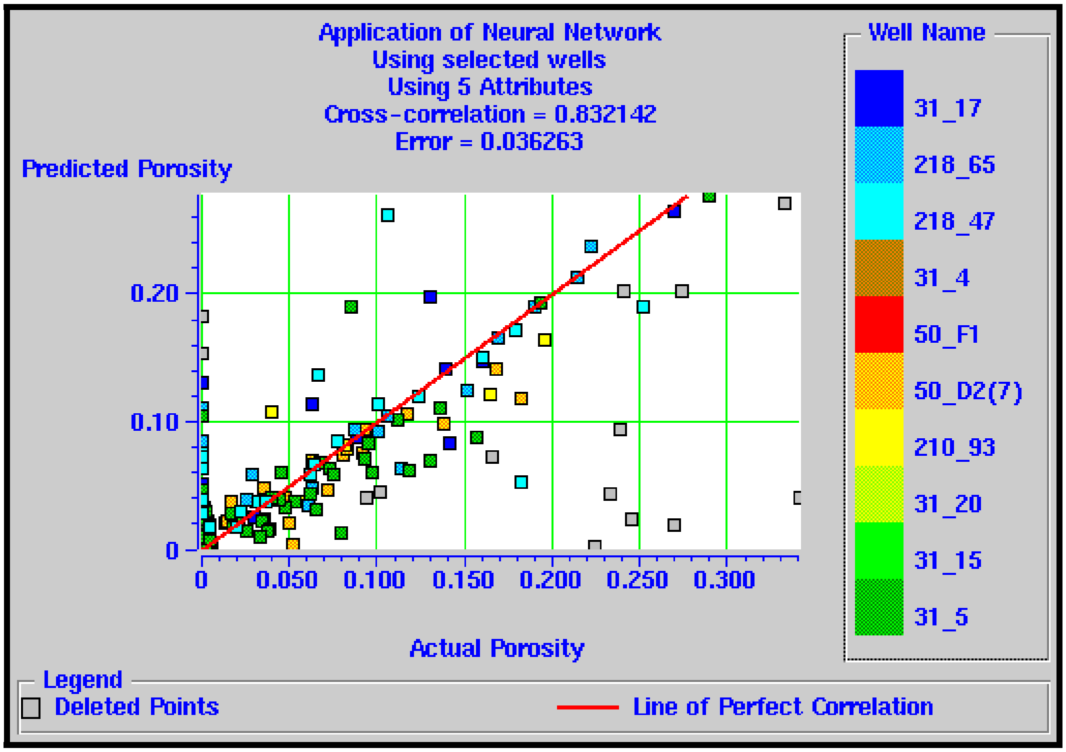

Figure 4-21. Training cross-correlation reached up to 0.83. NN failed to predict some of the very low porosity rocks, possibly thin and tight zones.

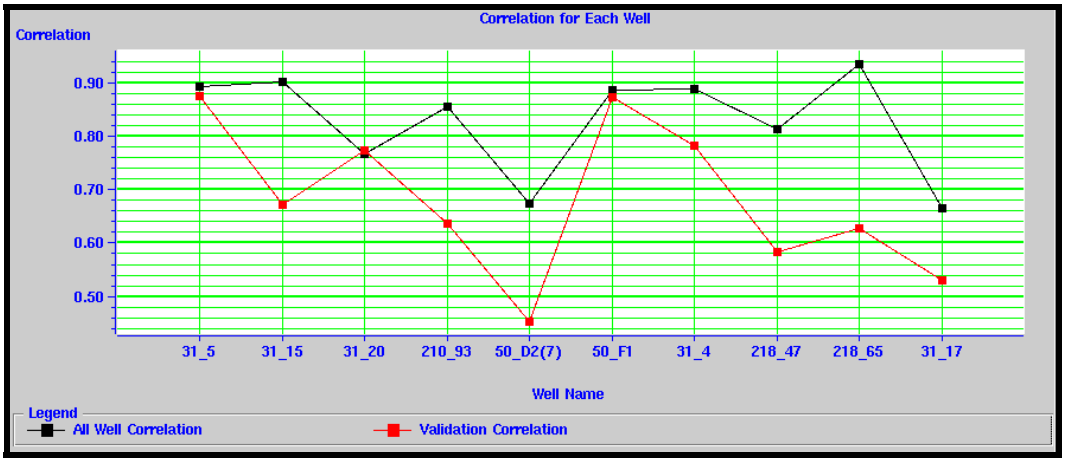

Figure 4-22. Correlation coefficients of NN and cross validation by well. Application correlation is in black and validation is in red. Validation could reach only 0.66.

Trained NN was applied to seismic data to transform into PHIE. Hundred millisecond seismic data above and below GS22 are also included (**Figure 4-23**). Sands in GS22 do not indicate much change in the amplitude and appear as a bright red zone, but the PHIE section indicates some variation.

NN was also able to predict porosity at well #6_31, which was not included in the training set. The tie between VCL curve and negative amplitudes in the seismic section is proven by the PHIE curve and by high porosity in the porosity section (Figure 20).

GS22 of porosity volume is also sliced proportionally and compared to amplitude slice (**Figure 4-24**). Amplitude and porosity maps display similar features, but in detail there are some differences, especially in the delta. Amplitude maps displaying higher values exist in different places on the delta, but the PHIE map displays higher values, mostly on the east flank of the delta.

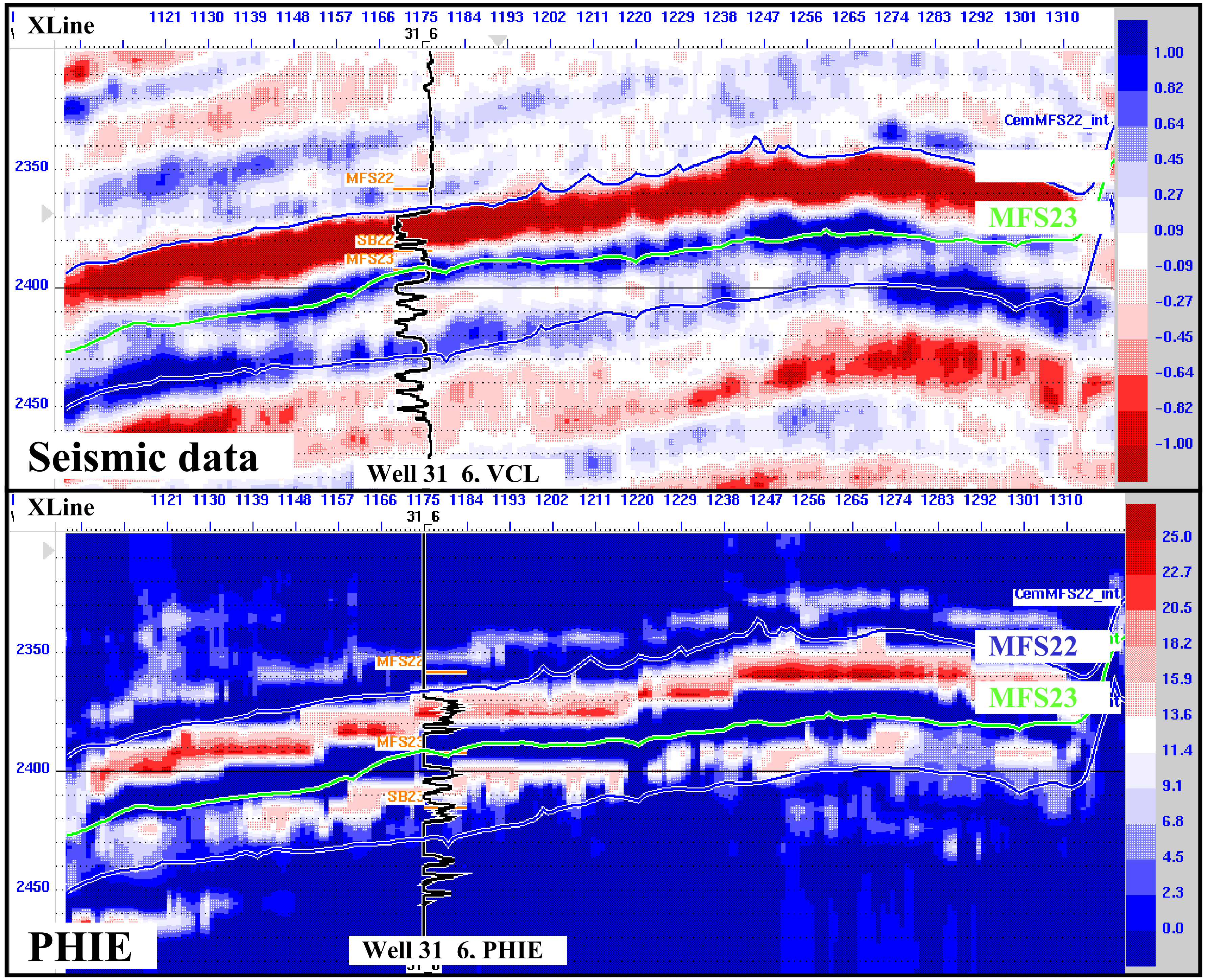

Figure 4-23. (Top) Seismic section (cross line 342) and GS22 (MFS22 and MFS23) at well 31_6, which was not used in training. (Bottom) Section of PHIE (effective porosity) in the same section (cross line 342). PHIE curve of well 31_6 matches very well with PHIE volume.

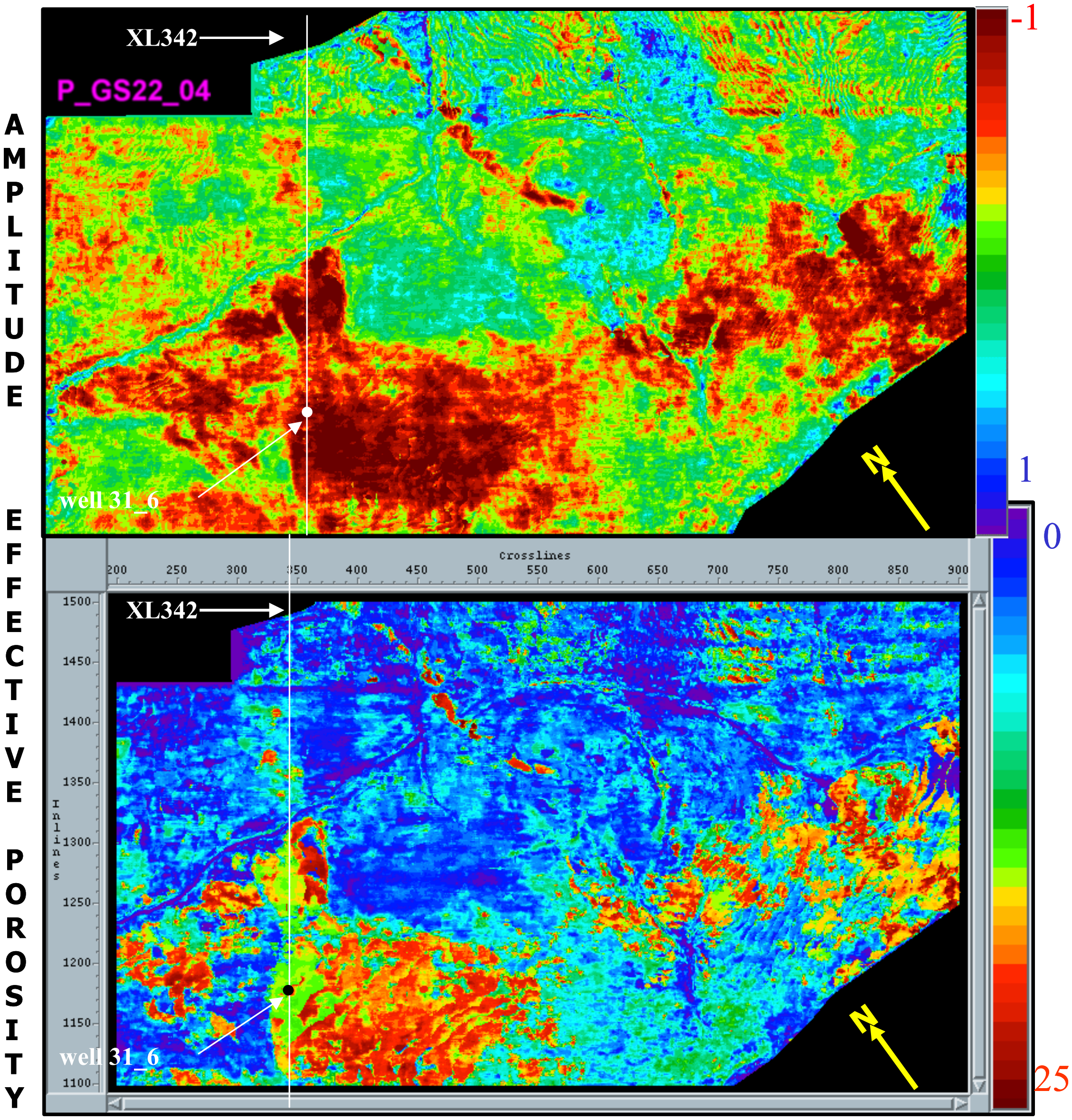

Figure 4-24. Comparison between amplitude slice and PHIE slice. Troughs, negative amplitudes, mostly correspond to clean rock, and hot colors correspond to high porosities. Although the amplitude map indicates high values on the both sides of the delta, the porosity map indicates higher values on the east side.

Both maps were able to catch the narrow channel in the north, which also verifies that NN was able to transform seismic data into effective porosity successfully.

Discussion, Summary and Conclusions

DISCUSSION

This study incorporates different types of measurements, data processing techniques, and analyses. In the process, two main assumptions are made. The first assumption is that those eleven proportional maps, created by two slices at the flooding surfaces and nine intermediate slices, are depicting time-correlative depositional features. In other words, individual slices do not cut time lines. In actuality, proportional slices cut time lines. Since the overall system is on the outer shelf and close to horizontal, slices divide the section as parallel as possible to timelines. In some cases, the upstream/proximal portion of the fluvio-deltaic system is imaged at one slice later/higher than the downstream/distal portion. In every analysis of genetic sequence and in this case, individual slices are not interpreted alone. On the contrary, they are interpreted with many slices at the same time in a comprehensive manner. Development of depositional elements can be traced over many slices, and their boundary relations can be established as well. This technique allows for the interpretation of not only the internal progress of a sequence, but also the continuous story of the sequences in the area. Sometimes proportional slices sample a wavelet in close points, where the tuning occurs, especially where two sand bodies get closer or touch in vertical space. In this situation, the only reliable tool is to look for the distribution of sand bodies in different slices, because they tend to display a different depositional orientation and distribution. They are not in tune in every part of the sequence and they separate vertically enough to be detected by different slices.

The second assumption is that attributes are indicative of lithology and porosity. As discussed in 'Quantification', there are not always clear physical evidence of relationship between attributes and petrophysical properties of the rocks. On the other hand, attributes show very high correlation coefficient with lithologic type and above medium correlation with effective porosity. In the identification and quantification, I used attributes cautiously by choosing only those that show a high correlation coefficient and by applying vigorous confirmation practices. Accurate integration of well logs and seismic also enabled a high degree of confidence for predicting lithology and porosity. Correlation between certain filtered frequency ranges and log properties could be explained by the fact that 'certain facies types are consistent in thickness and imaged by these frequency ranges the best'. It is also possible to assume further and suggest that 'these certain facies types have consistent effective porosity range and eventually indicate a relationship with attributes'.

SUMMARY

Two offshore fields, Starfak and Tiger Shoal, have produced more than 3.5 Tcf of gas and 50 MMbl of oil from more than 60 reservoirs, ranging from upper Lower Miocene to Pliocene. Compared to GOM fields, they are, especially the Tiger Shoal, one of the largest field in gas production, and moderate size in oil. In two fields, the Middle Miocene alone has produced 77% of all production

(Boe). Middle Miocene reservoirs have become the most important target for the advanced recovery, and the Lower Miocene emerged as new promising frontier with its large rollover structures, high rate gas production capacities, and royalty relief by the government.

Detailed analysis and careful integration of a 3D seismic data, petrophysical well logs, side-well core analysis, paleontological data, and hydrocarbon production information generated a high-resolution geological framework of Middle Miocene. Methodology used to create this framework is the key part of this process.

Paleontologic information from 13 wells and petrophysical well logs from 156 wells allowed identification of fourth-order flooding surfaces with accurate age constraints. The Middle Miocene in the area is more than 5000 ft thick and includes more than 24 fourth-order sequences. The overall section is regressive and deposition slowed down during third- and fourth-order flooding time.

Inventory of log and core data indicates that over the years the log quality and quantity has increased as more complete log suites and porosity logs were run. Side-well core data from 99 wells allowed building a porosity trend for the area, and provided a guide and an accuracy curve for petrophysical model.

A merged 3D seismic data (352 mi^2) and its attributes, well logs with paleontological data allowed interpretation of 24 fourth-order maximum flooding surfaces and generation of genetic sequences, defined by flooding surfaces. Study showed that quantification of reservoirs in fourth-order scale is possible but requires meticulous data preparation.

CONCLUSIONS

There are three main scientific contributions of this study. These are:

1. In order to achieve the characterization of a fourth-order sequence and its reservoir on a standard seismic data, a methodology, certain steps of data preparation and integration, is suggested. This is certainly not the only way to achieve fine scale characterization, but it is unique to achieve characterization with limited data sets.

Detailed analysis and careful integration of a 3D seismic data, petrophysical well logs, side-well core analysis, paleontological data, and hydrocarbon production information generated a high-resolution geological framework of the Middle Miocene. The thick Middle Miocene section is divided by flooding surfaces into genetic sequences, which are the building blocks of a high-resolution stratigraphic framework. There are 24 fourth-order genetic sequences in the Middle Miocene, defined on both well logs and seismic data. It is possible to construct depositional history of a basin with this technique. Each sequence provides an independent unit during stratigraphic interpretation and quantification.

2. Quantification of reservoirs can be done in the fourth-order scale. Building a high-resolution sequence stratigraphic framework and defining the fourth-order genetic sequences allows for quantification of reservoirs in detail.

The probabilistic neural network is successfully utilized to predict volume of clay values from the attributes of seismic data. The correlation coefficient during training reached up to 92 percent and dropped down to 89 percent in validation.

With the same method, PHIE (effective porosity) prediction yielded correlation coefficient only 83 percent in training, and 66 percent in validation. Since the effective porosity calculation includes different tool measurements and a series modification by other curves and by human judgment, it could not be predicted in high correlation. In future studies, prediction of sonic porosity and density porosity individually is recommended. As a second step effective porosity can be calculated from these two porosity data, but this process will involve many steps of attribute analysis and multi volumes of porosity.

3. Integration of petrophysical analysis, production information, and seismic data allows for identification the zones that are bypassed during the reservoir completions, known as unperforated productive zones, missed possibly due to digitizing problems, and new prospects.

In some of the wells, productive zones, which are drained by the offset wells, are physically higher but yet to be perforated (figure 4-10). This kind of completion problem is observed, where the second well drilled to drain the same or different deeper target, but also cuts the upper reservoir in shallower depth than the first well. These unperforated zones present great opportunity to increase production and efficiency.

In addition, quality of the log data plays an important role in reservoir completion and interpretation. Overlapping resistivity curves are sometimes digitized erroneously and high values are clipped. Quality checking of digital data and paper logs helped identification of many digitizing problems.

Benefits of integration at this scale are also achieved when it leads to anew prospect. Study showed that some infill drilling opportunities still exist, even if the fields are densely drilled (figure 4-14).

Some other specific conclusions that can be mentioned are:

4. Integration of sidewall core data with a porosity model allowed petrophysical analysis of the wells without porosity curves, and served as a quality and quantity indicator for the wells with porosity curves.

Phiamax (maximum expected porosity) proved itself to be valuable, because in Tiger Shoal field less than 17% of the wells have porosity logs in Middle Miocene. The effective porosity is required for the Swe (effective water saturation) calculations and identification of pay zones.

5. Most of the production comes from the LST (lowstand system tract). It is relatively confined, thicker, and sealed by TST and HST thick shales. Also LSTs have higher average porosity than TSTs and HSTs.

6. Spectral balancing of seismic data and integration with paleontologic information allowed detailed interpretation of fourth-order maximum flooding surfaces, which could not be identified on the standard 3D seismic data. With the help of age indicative foraminifers, nannofossils, and flora information, a high-

resolution, accurate stratigraphic division of Middle Miocene intervals was created. This is an improvement over slicing of a third-order interval, where slices cross time lines. However, since many fourth-order flooding surfaces are required, this is a much slower process. When the time is limited, it is more effective and efficient to slice the data in third-order and then focus in fourth-order zones.

7. There are two orders of growth faults identified in the area. First order growth faults (>500ft of maximum offset) are broadly arcuate and east-west trending. They primarily control the depositional system, and act as a shelf or depositional break. Many of the first-order faults have large rollover structures, especially in the Lower Miocene interval. Some of these have been tested successfully and are producing gas at very high rates.

   Second-order faults (<200, <500) are usually cut by the first-order faults in angle, and a combination of these present many structural traps, especially in Tiger Shoal.

8. Proportional slicing of fourth-order sequences generated a series of maps capturing the depositional history of the area. In addition, slicing allowed locating some of the sequence boundaries, which cannot be interpreted on the standard seismic profile.

9. Seismic facies maps, created specifically for the genetic sequences, sometimes lead to different conclusions about the depositional history than log interpretation. With help of proportional slices, seismic facies maps have given sequences the third dimension, which log sections always lack.

Contact relationship between individual facies and overall settings yield a more complete depositional picture than standard amplitude slices or attribute maps. Generally, specific types of wavelets in the facies maps allowed lithology predictions, especially when they are compared to amplitude slices and attribute maps, which are also created for the same specific sequences. In a number of the cases, it is possible to differentiate different sandy facies, for example; channel versus valley fill.

10. Depositional features imaged from proportional slices of amplitude and VCL/PHIE volumes are similar, but not identical. Both allow the visualization of changes of the depositional features in time, but it is possible to observe local differences in VCL and PHIE volumes.

References

Addy, S.K., 1998. Neural network classification method helps seismic interval interpretation. *Oil and Gas Journal, September 14, p. 47-59.*

Asquith, B.G., 1995. Log evaluation of shaly sandstones: A practical guide. *The AAPG continuing education course note series, no. 31, 59 p.*

Begg, S.H., Kay, A., Gustason, E.R., and Angert, P.F., 1994. Characterization of a complex fluvial-deltaic reservoir. *Society of Petroleum Engineers 69th annual technical conference, New Orleans, no. 28398, 375-384.*

Berggren, W. A., D. V. Kent, C. C. Swisher III, and M. –P. Aubry, 1995. A revised Cenozoic geochronology and chronostratigraphy, *in W. A. Berggren, D. V. Kent, M. –P. Aubry, and Jan Hardenbol, eds., Geochronology, time scales and global stratigraphic correlation: SEPM (Society for Sedimentary Geology) Special Publication No. 54, p. 129-212.*

Brown, R.R., 2001. Understanding seismic attributes. *Geophysics, v. 66, no. 1, p. 47-48.*

Chen, Q., and Sidney, S., 1997. Seismic attribute technology for reservoir forecasting and monitoring. *The Leading Edge, v. 16, no. 5, 8p.*

Countiss, M.L., 2002. Frequency-enhanced imaging of stratigraphically complex, thin-bed reservoirs: A case study from South Marsh Island, Block 128 Field. *Leading Edge, v. 21, no. 9, p. 826–836.*

Crawford, T. G., Bascle, B. J., Kinler C. J., Prendergast, M. T., and Ross, K. M., 2000. Outer continental shelf estimated oil and gas reserves, Gulf of Mexico, December 31, 1998: *U.S. Department of Interior, Minerals Management Service, OCS Report MMS 2000 – 069, 26 p.*

DeAngelo, M.V., and L.J. Wood, 2001. 3-D seismic detection of undrilled prospective areas in a mature province, South Marsh Island, Gulf of Mexico. *Leading Edge, v. 20, no. 11, p. 1282–1292.*

DeAngelo, M.V., Hentz, T.F., Wood, L.J., Zeng, H., and Barba, R.E., 2000. Targeting reserve-growth opportunities in the Northern Gulf of Mexico Basin: Transferring secondary gas recovery technology to the offshore environment. *Second year technical progress report to U.S. Department of Energy, Bureau of Economic Geology, Univ. of Texas at Austin, 167p.*

De Groot, P.F.M., 1999a. Volume transformation by way of neural network mapping. *EAGE 61st conference and technical exhibition, Finland.*

De Groot, P.F.M., 1999b. Seismic reservoir characterization using artificial neural networks. *19th Mintrop seminar, Muenster, Germany.*

De Groot, P.F.M., 1995. Seismic reservoir characterization employing factual and simulated wells. *Thesis, Delft University of Technology, 185 p. ISBN 90-407-1163-1*

Doraisamy, H., Vice, D.H., and Halleck, P.M., 2000. Detection of hydrocarbon reservoir boundaries using neural networks analysis of surface geochemical data. *AAPG Bulletin, v. 84, no. 12, p. 1893-1904.*

Dorrington, K. P., and Link, C.A., 2004. Genetic-algorithm/neural-network approach to seismic attribute selection for well-log prediction. *Geophysics, v. 69, no. 1, p. 212-221.*

Eschard, R., Lemouzy, P., Bacchiana, C., Desaubliaux, J., Parpant, J., and Smart, B., 1998. Combining sequence stratigraphy, geostatistical simulations, and production data for modeling a fluvial reservoir in the Chaunoy field (Triassic, France). *AAPG bulletin, v. 82, no. 4, p. 541-551.*

Fillon, R.H., Lawless, P.N., 2000. Lower Miocene-Early Pliocene deposystems in the Gulf of Mexico: Regional sequence relationships. *Gulf Coast Association of Geological Societies, transactions, v. 50 (L), p. 411-428*.

Fillon, R.H., and Lawless, P.N., and Lytton, R.G.III, 1997. Gulf of Mexico Oligocene-Miocene biostratigraphic and cycle chart: *Texaco E&P Inc. publication.*

Galloway, W.E., Curry, P.E.G., Li, X., and Buffler, R.T., 2000. Cenozoic depositional history of the Gulf of Mexico basin. *AAPG Bulletin, v. 84, no. 11, p. 1743-1774.*

Galloway, W. E., 1998. Depositional processes, regime variables, and development of siliciclastic stratigraphic sequences: Sequence Stratigraphy Concept and Applications: *Norwegian Petroleum Society (NPF), Special Publication, no. 8.*

Galloway, W.E., Bebout, D.G., Fisher, W.L., Dunlap, J.B. Jr., Castro, R.C., Rivera, J.E.L., Scott, T.M., 1991. *Cenozoic. In Amos Salvador, ed., the Gulf of Mexico basin: Geological Society of America, geology of North America, Boulder, Colorado, v. J, p. 245-324.*

Galloway, W.E., 1989. Genetic Sequences in Basin Analysis I: Architecture and Genesis of Flooding-Surface Bounded Depositional Units. *AAPG Bulletin, v. 73, no. 2, p. 125-142.*

Gastaldi, C., Biguenet, J.P., and DePazzis, L., 1997. Reservoir characterization from seismic attributes: An example from the Peciko field, Indonesia. *The Leading Edge, v. 16, no. 3, p. 263-266.*

Gazdag, J., and Sguazzero, P., 1984. Migration of seismic data by phase shift plus interpolation. *Geophysics, v. 49, no. 2, p. 124-131*.

Haldorsen, H.H., and Damsleth, E., 1993. Challenges in reservoir characterization. *AAPG bulletin, v 77, no. 4, p 541-551.*

Hampson, D.P., Schuelke, J.S., and Quirein, A., 2001. Use of multi-attribute transforms to predict log properties from seismic data. *Geophysics, v. 66, no. 1, p. 220-236.*

Haq, B.U., Hardenbol, and Vail, J.P.R., 1988. Mesozoic and Cenozoic chronostratigraphy and cycles of sea level change. *In Wilgus, C.K., Hastings, B.S., Kendall, C.G.S.C., Posamentier, R.C.A, Van Wagoner, J.C., Sea level Changes: an integrated approach. Society of economic paleontologists and mineralogist, special publication, v. 42, p. 71-108.*

Hart, B.S., 2002. Validating seismic attribute studies: Beyond Basics. *The Leading Edge, v. 21, no. 10, p. 1016-1021.*

Hart, B.S., and Balch, R.S., 2000. Approaches to defining reservoir physical properties from 3-D seismic attributes with limited well control: An example from the Jurassic Smackover Formation, Alabama. *Geophysics, 65, p. 368-376.*

Hart, B.S., 1999. Geology plays key role in seismic attribute studies. *Oil and Gas Journal, July 12, p. 78-80.*

Hart, G.F., Ferrell, R.E. Jr., Lowe, D.R., and Lenoir, A.E., 1989. Shelf sandstone of the Robulus L zone, offshore Louisiana. *GCSSEPM foundation, seventh annual research conference proceedings, April, p 117-141.*

Hentz, T.F. and Zeng, H., 2003. High-frequency Miocene sequence stratigraphy, offshore Louisiana: Cycle framework and influence on production distribution in a mature shelf province. *AAPG Bulletin, v. 87, no. 2 (February 2003), pp. 197–230.*

Hentz, T.F. and Wood, L.J., DeAngelo, M.V., Zeng, H., Holtz, M., Dutton, S.P., Chan, K.S., Rassi, C., Garcia, J., Kim, E.M., 2002. Targeting reserve-growth opportunities in the northern Gulf of Mexico basin: Transferring secondary gas recovery technology to the offshore environment. *Final report to U.S. Department of Energy, Bureau of Economic Geology, Univ. of Texas at Austin, 40p*.

Hentz, T. F., Zeng, Hongliu, Wood, L. J., Badescu, A. C., Rassi, Claudia, and Kiliç, C. O., 2001. Controls on hydrocarbon distribution within a sequence-stratigraphic framework: a case study from the Miocene of offshore Louisiana (abstract). *AAPG CD-ROM, AAPG Annual Meeting, Louisiana.*

Hentz, T.F., Zeng, Hongliu, and Kiliç, C.O., 2000. Sequence stratigraphy, depositional framework, and resource potential of mature gas reservoirs, Miocene of offshore Louisiana (abstract). *AAPG Annual Meeting*.

Hentz, T.F., Zeng, H., Wood, L.J., Kiliç, C.O., Yeh, J.S., Skolnakorn, J., and DeAngelo, M., 1999. Targeting reserve-growth opportunities in the northern Gulf of Mexico basin: Transferring secondary gas recovery technology to the offshore environment. *First year technical progress report to U.S. Department of Energy, Bureau of Economic Geology, Univ. of Texas at Austin, 40p*.

Hirsche, K., Hirsche, J.P., Mewhort, L., and Davis, R., 1997. The use and abuse of geostatistics. *The Leading Edge, v. 16, no. 3, 6 p.*

Kalkomey, C. T., 1997., 1997. Potential risks when using seismic attributes as predictors of reservoir properties. *The Leading Edge, v. 16, no. 3, p 247-251.*

Kiliç, C.O., 1998, Applying Artificial Neural Network Technology in Reservoir Characterization Studies (Master Thesis). *The University of Texas, at Austin, Department of Geological Sciences.*

Landmark, 1996. PostStack/PAL user guide.

Lawless, P.N., Fillon, R.H., and Lytton, R.G.III, 1997. Gulf of Mexico Cenozoic biostratigraphic, lithostratigraphic, and sequence stratigraphic event chronology. *Gulf Coast Association of Geological Societies, transactions, v. 47, p. 271-282.*

Lei, L.K., McPherson, J.G., Kan, Y., 1999. Integration of 3D seismic attributes with core and wireline log data for detailed modeling of Cretaceous fluvial reservoirs. *The Leading Edge, v. 18, no. 6, p. 730-738.*

Linari, V., Santiago, M., Pastore, C., Azbel, K., Poupon, M., 2003. Seismic facies analysis based on 3D Multiattribute volume classification, La Palma Field, Maracaibo, Venezuela. *The Leading Edge, v. 22, no. 1, p 32-56.*

Lore G.L., Ross, K.M., Bascle, B.J., Dixon, L.D., Klazynski, R.J., 1999. Assessment of conventional recoverable hydrocarbon resources of the Gulf of Mexico and Atlantic outer continental shelf as of January/1/1995: *U.S. Department of Interior, Mineral Management Service, Gulf of Mexico OCS Region, Office of Resource Evaluation, OCS Report MMS 99-0034, CD-ROM.*

Love, KM, Strohmenger, C., Woronow, A., and Rockenbauch, K., 1997. Predicting Reservoir quality Using linear regression models and neural networks. *AAPG memoir 69, p. 47-60.*

Mawdsley, M.J., Eamer, A.L., and Zaitlin, B.A., 1997. Pitfalls in seismic definition of incised valley reservoirs: A case study from the Lower Cretaceous glauconitic formation in South Central Alberta. *The Leading Edge, v. 16, no. 9, 3p.*

McBride, E.F., Land, L.S., Diggs, T.N., and Mack, L.E., 1988. Petrography, stable isotope geochemistry and diagenesis of Miocene sandstones, Vermilion block 31, offshore Louisiana. *Gulf Coast Association of Geological Societies Transactions, v. 38, p. 513-523.*

Mitchum, R.M., J.B. Sangree, P.R. Vail, and W.W. Wornardt, 1993, Recognizing sequences and systems tracts from well logs, seismic data, and biostratigraphy: examples from the late Cenozoic of the gulf of Mexico, *in Paul Weimer and Henry Posamentier, eds., Siliciclastic sequence stratigraphy: recent developments and applications: AAPG Memoir 58, p. 163 – 197.*

Mitchum, R. M., and J. C. Van Wagoner, 1991. High-frequency sequences and eustatic cycles in the Gulf of Mexico basin, *in J. M. Armentrout and B. F.*

Perkins, eds., Sequence stratigraphy as an exploration tool: concepts and practices in the Gulf Coast: Gulf Coast Section of the Society of Economic Paleontologists and Mineralogists, Eleventh Annual Research Conference Proceedings, p. 257 – 267.

MMS, 2003a. Deep shelf gas may be more abundant in Gulf than earlier forecast, probability estimate increases by 175%: *U.S. Department of Interior, Minerals Management Service, Release no. 3012, 3p.*

MMS, 2003b. Gulf of Mexico deep shelf gas shelf update: *U.S. Department of Interior, Minerals Management Service, Report MMS 2003-026, 8p.*

MMS, 2001. The promise of deep gas in the Gulf of Mexico: *U.S. Department of Interior, Mineral Management Service, OCS Report MMS 2001-037.*

Nehring, R., 2000. The past and the future of the Gulf of Mexico OCS Shelf. *Gulf Coast Association of Geological Societies Transactions, v. L, p. 193-201*

Nur, A., Dvorkin, J., and Galmudi, D., 1998. Critical porosity: A key to relating physical properties to porosity in rocks. *The Leading Edge, v. 17, no. 3, p. 357-362.*

Pennington, W.D., 2001. Reservoir geophysics. *Geophysics, v. 66, no. 1, p. 25-30.*

Pennington, W.D., 1997. Seismic petrophysics: An applied science for reservoir geophysicist. *The Leading Edge, v. 16, no. 3, p. 241-244.*

Picou, E. B., Perkins, B. F., Rosen, N. C., and Nault, M. J. (eds.), 1999. Gulf of Mexico basin biostratigraphic index microfossils: a geoscientist's guide. Foraminifers and nannofossils, Oligocene through Pleistocene: Gulf Coast Section of the Society of Economic Paleontologists and Mineralogists Foundation, Part I & 2, 215 p. and 3 charts.

Pocknall, D. T., Geen, A. F., and Wood, L. J., 1998. Depositional facies in the Pliocene–Pleistocene section, offshore eastern Trinidad*, in Paul, T., ed., Transactions of the 14th Caribbean Geologic Conference, Port-of-Spain, unpaginated.*

PostStack/PAL User Guide. 1996. Landmark Graphics Corporation.

Raeuchle, S.K., Hamilton, D.S., Uzcategui, M., 1997. Integrating 3-D seismic imaging and seismic attribute analysis with genetic stratigraphy:

Implications for infield reserve growth and field extension, Budare field, Venezuela. *Geophysics, v. 62, no. 5, p. 1510-1523.*

Rainwater, E.H., 1964. Regional stratigraphy of the Gulf of Coast Miocene. *Gulf Coast Association of Geological Societies Transactions, v. 14, p. 81-124.*

Ronen, S., Schultz, P.S., Hattori, M., and Corbett, C., 1994. Seismic-guided estimation of log properties: Part 2, using artificial neural networks for nonlinear attribute calibration. *The Leading Edge, v. 13, no. 6, p. 674-678.*

Russell, B., Hampson, D., Schuelke, J., and Quirein, J., 1997. Multiattribute seismic analysis. *The Leading Edge, v. 16, no. 10, 5p.*

Schultz, P.S., Ronen, S., Hattori, M., and Corbett, C., 1994a. Seismic-guided estimation of log properties: Part1, A data-driven interpretation methodology. *The Leading Edge, v. 13, no. 5, p. 674-678.*

Schultz, P.S., Ronen, S., Hattori, M., and Corbett, C., 1994b. Seismic-guided estimation of log properties: Part3, A controlled study. *The Leading Edge, v. 13, no. 7, p. 674-678.*

Slatt, R.M., and Galloway, W.E., 1992. Geological heterogeneities. *AAPG special publication, p. 278-281.*

Stratimagic, 1999. Stratimagic user guide.

Taner, M. T., Schuelke, J.S., O'Doherty, R. and Baysal, E., 1994. Seismic attributes revisited. *Soc. of Exploration Geophysics, 64th ann. international meeting, p. 1104-1106.*

Taner, M.T., Koehler, F., and Sheriff, R.E., 1979. Complex seismic trace analysis. *Geophysics, 44, no. 6, p. 1041-1063.*

Tinker, S.W., 1996. Building the 3-D Jigsaw Puzzle: Applications of sequence stratigraphy to 3-D reservoir characterization, Permian Basin. *AAPG Bulletin, v. 80, no. 4, p. 460-485.*

Tyler, N., 1991. Architectural controls on the recovery hydrocarbons from sandstone reservoirs. *In Miall, A.D., and Tyler N., The three dimensional architecture of terrigenous clastic sediments and its implication for hydrocarbon discovery and recovery: Society of Economic Paleontologists and Mineralogist, Concepts in Sedimentology and Paleontology, v. 3, p. 1-5.*

Tyler, N., 1988. New oil from old fields. *Geotimes, July 1988, p. 8-10*.

Van Wagoner, J. C., R. M. Mitchum, K. M. Campion, and V. D. Rahmanian, 1990. Siliciclastic sequence stratigraphy in well logs, cores, and outcrops: concepts for high-resolution correlation of time and facies. *AAPG, Methods in Exploration Series, No. 7, 55 p*.

Vinson, T.E., Standley, P.G., Jager, G., and Kidd, G.D., 1996. Recent enhancement for 3D seismic interpretation: Visualization, image processing and attribute analysis. *28th Annual Offshore Technology Conference, Houston, TX. OTC 7956, p. 35-54.*

Walls, J.D., Taner, T.M., Taylor, G., Smith M., Carr, M., and Derzhi, N., 2000. Seismic reservoir characterization of a mid-continent fluvial system using rock physics, poststack seismic attributes and neural networks, a case history. *Soc. of Exploration Geophysics, 70th annual meeting, Calgary, Canada.*

Wood, L.J., Zeng, H., DeAngelo, M.V., Hentz, T.F., Holtz, M.H., Chan, K., Badescu, A., Kilic, C., Rassi, C., and Zhou, D., 2001. Targeting reserve-growth opportunities in the northern Gulf of Mexico basin: Transferring secondary gas recovery technology to the offshore environment. *Third year technical progress report to U.S. Department of Energy, Bureau of Economic Geology, Univ. of Texas at Austin*.

Wood, L.J., Pecuch, D., Schulein, B., and Helton, M., 2000. Seismic attribute and sequence stratigraphic integration methods for resolving reservoir geometry in San Jorge Basin, Argentina. *The Leading Edge, v. 19, no. 9, p. 952-962.*

Zeng, H., Tucker, F.H., and Lesli, J.W., 2001. Stratal slicing of Miocene-Pliocene sediments in Vermilion Block 50-Tiger Shoal Area, offshore Louisiana. *The Leading Edge, v 20, no4, p 408-418*.

Zeng, H.L., and Kerans, C., 2003. Seismic frequency control on carbonate seismic stratigraphy: A case study of the Kingdom Abo sequence, west Texas. *AAPG bulletin, v. 87, no. 2, p. 273-293*.

Zeng, H.L., T.F. Hentz, and L.J. Wood, 2000. Three-dimensional seismic facies imaging by stratal slicing of Miocene–Pleistocene sediments in the greater Vermilion Block 50-Tiger Shoal field area, offshore Louisiana (abs.): *AAPG Annual Meeting Program, v.9, p. A165*.

Vita

Cem Okan Kılıç was born on November 12, 1971, in İstanbul, Turkey to Vicdan and Orhan Kılıç. After graduating from the Izmit Technical High School in Izmit, he attended the University of Istanbul where, in 1993, he received a Bachelor of Science in Geology. In January 1995, he was awarded a full master scholarship to study petrophysics by the Ministry of Turkey. In the fall of 1996 he moved to Austin, Texas, and in December 1998 he received a Master of Science in Geology from The University of Texas at Austin. In the fall of 1999 he enrolled in the doctoral program at The University of Texas at Austin.

Permanent address:
Agah Ates Mah. Zambak Sk. No:9
41800, Hereke, Kocaeli, Turkey

This dissertation was typed by the author.